24th Annual Fall Field *Frolic*

Department of Geological Sciences
California State University, Northridge
August 30 to September 5, 2006

THE COLORADO PLATEAU: TO THE STABLE CRATON AND BACK!!!

Itinerary:

Wednesday – CAMP at Virgin River Gorge with possible stop at Valley of Fire.

Thursday – (a) overview of Virgin River Gorge, (b) Hurricane fault, (c) Bryce Canyon, CAMP at North Rim of Grand Canyon.

Friday – (a) North Rim Grand Canyon, (b) Lees Ferry, (c) Grand Falls, (d) Sunset Crater, CAMP near Flagstaff

Saturday – (a) Lava tube, (b) Meteor Crater, CAMP near Flagstaff

Sunday – (a) Peach Springs tuff, (b) Sacramento Mtns overview

Trip Leaders: Yule, Vazquez, Liggett, and Miranda

Figure 9–11. Topography of the Basin and Range Province, western United States, part of a shaded-relief image prepared by Thelin and Pike (1991) by digitizing elevation values at intervals of 805 m and illuminating the resulting digital elevation model from the west-northwest, 25° above the horizon. North is approximately toward the top of page. Vertical exaggeration 2×. Black area at upper right is Great Salt Lake; flat area farther north is Snake River Plain (cf. Fig. 9–12). Basin and Range Province extends from Wasatch fault, east of Great Salt Lake, to eastern front of Sierra Nevada (lower left corner). Albers Equal-Area Conic Projection.

Comp overview of Colo/Bo/R Margin

Geological Society of America Centennial Field Guide—Cordilleran Section, 1987

10

Virgin River Gorge; Boundary between the Colorado Plateau and the Great Basin in northwestern Arizona

R. L. Langenheim, Jr., Department of Geology, 245 NHB, 1301 West Green Street, University of Illinois, Urbana, Illinois 61801
M. K. Schulmeister, Illinois State Water Survey, 101 Island Avenue, Batavia, Illinois 60510

LOCATION

The Virgin River Gorge and one of its tributaries are traversed by I-15 between milepost 12, about 13 mi (21 km) east of Mesquite, Nevada, and Milepost 28, about 12 mi (19 km) west of St. George, Utah (Fig. 1). Geologic features are readily observable from the road and from a scenic viewpoint in the Virgin River Canyon Recreation Area, which is entered from an interchange between mileposts 18 and 19. The site is in the northern half of the Purgatory Canyon, Arizona, 7½-minute Quadrangle and in the northeastern quarter of the Littlefield, Arizona, 15-Minute Quadrangle.

SIGNIFICANCE

The Virgin River crosses the boundary between the Colorado Plateau and the Basin and Range physiographic province in a deep gorge separating the Beaverdam Mountains and Virgin Mountains (Fig. 1). Little-deformed, nearly flat-lying rocks of the westernmost plateau are well exposed east of the "Narrows." The gorge cuts across a broad anticline broken by numerous basin-and-range–type faults. The Grand Wash fault, the western boundary of the Colorado Plateau, is not obvious from the road, but is well exposed. The Beaver Dam–Virgin Mountain block is separated from the intermountain valley containing Beaverdam Wash and the Virgin River by a major range-front fault at the lower end of the Narrows. Late Cambrian through Middle Permian rocks exposed in the gorge (Fig. 1) are characteristic of the transition from miogeosynclinal deposition, dominant to the northwest, and platform deposits on the plateau to the east. In addition, the Narrows is a fine example of the results of accelerated erosion that accompanied elevation of the Colorado Plateau and extensional deformation in the Basin and Range during the late Tertiary and Quaternary. Ancient channel and terrace deposits are prominent in the gorge. Classic alluvial fans, basin-filling deposits, and caliche crusts border the west face of the Beaver Dam-Virgin Mountains and the intermontane valley to the west.

SITE DESCRIPTION

Late and Middle Cambrian Bonanza King Dolomite, Dunderberg Shale, and Nopah Dolomite, Late Devonian Muddy Peak Limestone, Mississippian Monte Cristo Group, and Mississippian-Pennsylvanian Callville Limestone crop out along the road in the Narrows between milepost 12.8 at the western end of the gorge and milepost 17.3, where the Sullivans Canyon and Cedar Wash faults cross the highway (Fig. 1).

The Cambrian Bonanza King Dolomite and Nopah Dolomite crop out in steep rounded cliffs and benches and the intervening Dunderberg Shale forms the most prominent of the benches between mileposts 13.5 and 16.8 (Figs. 1, 2). The Bonanza King Dolomite in the vicinity of the gorge is brown-weathering, fine- to medium-grained dolomite with 33 ft (9 m) of interbedded limestone and dolomite resting on a notably glauconitic layer near the top (Steed, 1980). The glauconitic layer forms a notable bench and is exposed in a road cut at milepost 15.8. The Dunderberg Shale, thinly interbedded green shale and dolomite, is cleanly exposed in roadcuts near mileposts 13.9 and 16.8. The Nopah Dolomite is mostly very fine-grained, light-gray dolomite, and weathers somewhat ligher brown than the underlying Bonanza King Dolomite.

Cambrian rocks of the Virgin Gorge are at the southeastern limit of characteristic Middle and Late Cambrian miogeosynclinal or carbonate platform deposits. The same formations crop out in the Mormon Mountains, the first range to the northwest, where the mostly Middle Cambrian Bonanza King Dolomite is 1,914 ft (580 m) thick and the Late Cambrian Nopah Dolomite is 627 ft (190 m) thick (Wernicke and others, 1984). Farther northwest, these units are two or three times as thick. Cambrian rocks to the east on the platform differ greatly; they consist of the basal Tapeats Sandstone, a middle Bright Angel Shale, and an upper argillaceous Muav Limestone along the Grand Canyon (McKee and Resser, 1945). The Grand Canyon rocks, however, are all older than those in the Virgin Gorge; late-Middle Cambrian and Late Cambrian rocks have been removed by erosion at the canyon.

The hiatus at the post-Nopah Dolomite unconformity in the Virgin Gorge is represented by some of the uppermost Nopah Dolomite, the Ordovician Pogonip Dolomite, Eureka Quartzite, Ely Springs Dolomite, and, probably, part of the basal Devonian sequence in the Mormon Mountains—more than 1,221 ft (370 m) of rock (Wernicke and others, 1984). Farther west, in the Arrow Canyon Range, 649.5 ft (197 m) of Silurian Laketown Dolomite and Early and Middle Devonian Piute Formation intervene between the Ely Springs Dolomite and Late Devonian rocks. All of these rocks are absent along the Grand Canyon to the southeast.

Late Devonian Muddy Peak Limestone crops out in the slope of ledges and cliffs just below the high, sheer cliffs of the Monte Cristo Group on the north wall of the Narrows between mileposts 13.5 and 16.8 (Figs. 1, 2, 3). On the south wall of the canyon the Muddy Peak Limestone outcrop, as well as that of the Monte Cristo Group, is visible from the road between milepost 13.5 and 14.3. The lower part of the Muddy Peak Limestone is

3

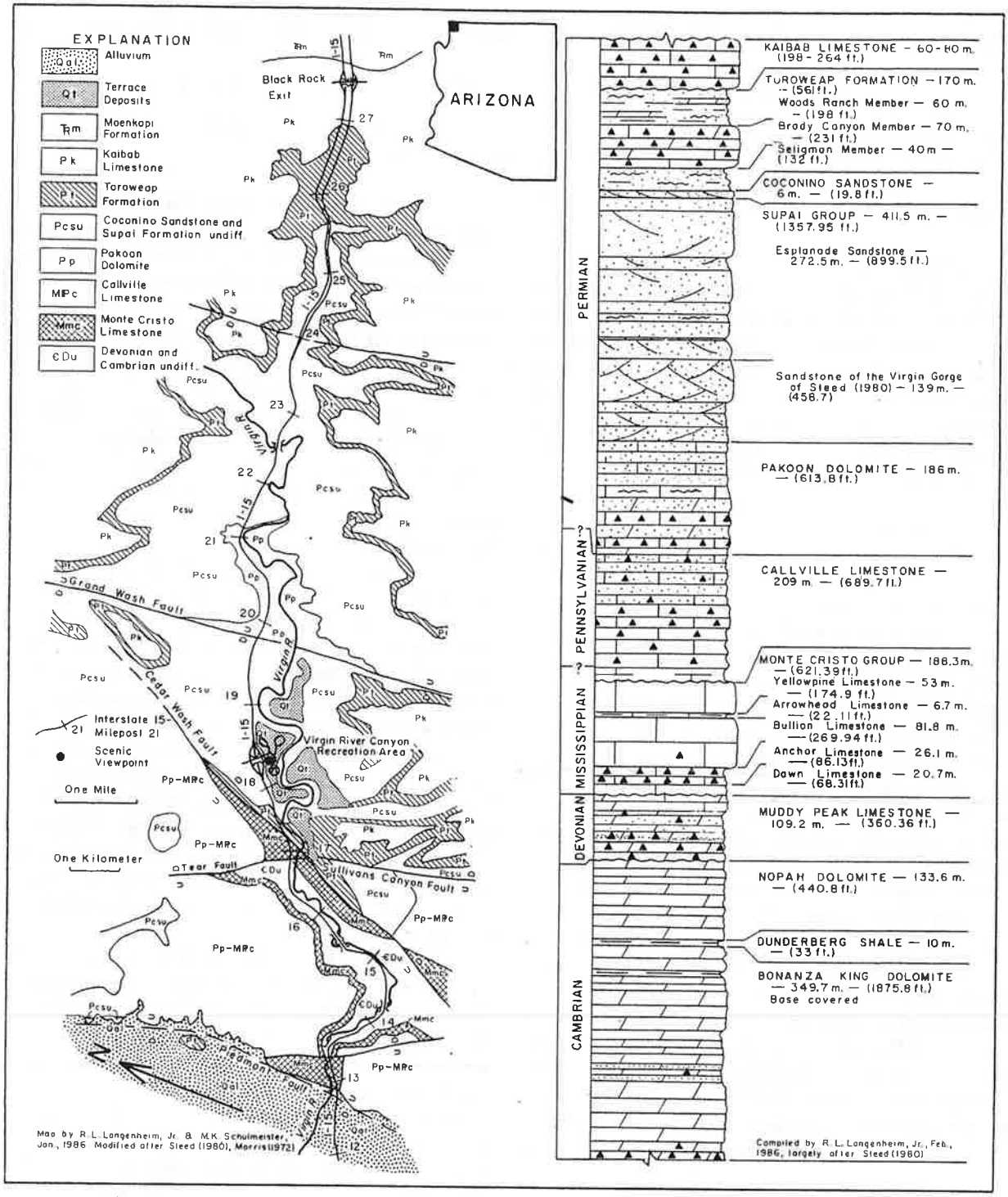

Figure 1. Geologic map and columnar section of rocks exposed along I-15 between mileposts 12 and 27, Arizona.

almost entirely medium-grained dolomite, but includes fairly prominent nodular layers of flint and rusty-weathering quartzite (Steed, 1980). The flint and quartzite distinguish the formation from the underlying Nopah Dolomite. The upper part of the Muddy Peak Limestone is lighter colored, includes substantial amounts of limestone, and is, in part, fine grained (Steed, 1980).

Devonian rocks thin on the platform to the southeast and only scattered remnants of Temple Butte Limestone occur in the eastern part of the Grand Canyon. To the northwest, Devonian rocks thicken substantially and Early and Middle Devonian sed-

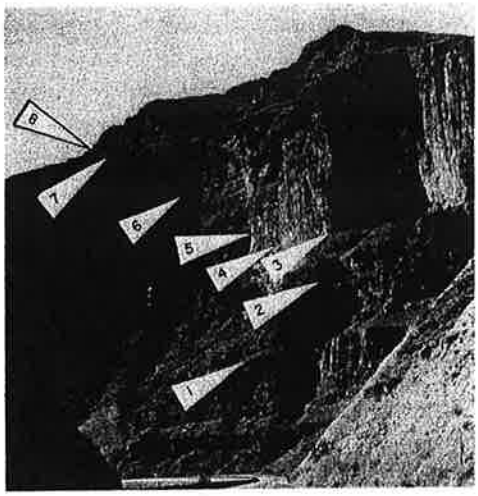

Figure 2. Late Cambrian through Early Pennsylvanian rocks, view down the canyon from milepost 17. 1 = bench formed by Dunderberg Shale, 2 = base of Muddy Peak Limestone, 3 = base of Dawn Limestone, 4 = base of Anchor Limestone, 5 = base of Bullion Limestone, 6 = Arrowhead Limestone, 7 = base of Callville Limestone, and 8 = top of shaley basal part of Callville Limestone.

Figure 3. View west-southwest across the Cedar Wash fault from "Scenic Viewpoint" in the Virgin River Recreation Area. The Esplanade Sandstone, Coconino Sandstone, and the Brushy Canyon and Seligman Members of the Toroweap Formation are exposed in the foreground and in the prominent butte in the middle of the picture. Cliffs behind are on the upthrown block of the Cedar Wash fault and expose Cambrian through Mississippian rocks. The Callville Limestone and Permian rocks crop out along the skyline. 1 = base of Toroweap Formation. The Coconino Sandstone is the thin, white, cliffy ledge just below the contact. 2 = base of Monte Cristo Group, 3 = base of shaley bench in lowermost Callville Limestone, and 4 = base of ledge and cliff sequence in the Callville Limestone. Smooth slopes rising to the top of the ridge on the right include Pakoon Dolomite and Supai Group outcrops.

iments are also present. Wernicke and others (1984) reported 726 ft (220 m) of Sultan Limestone in the Mormon Mountains, and Langenheim and others (1962) cited 1970 ft (597 m) of Devonian rocks in the Arrow Canyon Range.

The Early and Middle Mississippian Monte Cristo Group crops out in a high, sheer cliff that rises precipitously above the ledge and slope exposures of the Muddy Peak Limestone (Figs. 1, 2, 3). The Yellowpine, Arrowhead, and Bullion Limestones are cleanly exposed in a roadcut from milepost 12.8 through 13.4. Prominent coral biostromes crop out in the vicinity of milepost 13. The lowermost Dawn Limestone is dominantly medium- to coarse-grained limestone with minor interbedded dolomite (Steed, 1980). The formation is chert free, and rests unconformably on the underlying Muddy Peak Limestone. The Anchor Limestone is sharply delineated by abundant nodular chert interbedded with fine- to coarse-grained bioclastic limestone. The chert weathers dark brown or black, and the unit forms either an indentation in the Monte Cristo cliff or a minor bench. The overlying Bullion Limestone is predominantly very thick-bedded, coarse-grained, bioclastic limestone and comprises most of the sheer cliff. The Arrowhead Limestone is composed of thin nodular bioclastic limestone beds separated by shale breaks. It is readily identified from a distance because it crops out as a light-colored, narrow stripe two-fifths of the way down the brown, sheer cliff. The uppermost formation of the Monte Cristo Group, the Yellowpine Limestone, is thick-bedded, medium- to coarse-grained limestone in the lower half and very fine-grained, somewhat thinner bedded limestone in the upper portion. The formation makes up the upper two-fifths of the sheer cliff and is abruptly succeeded by bench-forming basal Callville Limestone.

The Dawn Limestone correlates with the Whitmore Wash Member of the Redwall Limestone on the platform to the southeast. The Anchor Limestone correlates with the Thunder Springs Member, the Bullion Limestone with the Mooney Falls Member, and the Arrowhead and Yellowpipe Limestones with the Horseshoe Mesa Member. These units are strikingly uniform and continuous across the miogeosynclinal-platform boundary, in marked contrast to patterns in the pre-Mississippian sequence and in the Carboniferous and pre-Toroweap Limestone rocks above the Monte Cristo or Redwall Limestone. The Redwall Limestone thins from about 490.5 ft (148.6 m) in the eastern Grand Canyon (McKee and Gutschick, 1969) and the Monte Cristo Group thickens to 924 ft (280 m) in the Mormon Mountains (Wernicke and others, 1984).

The Late Mississippian and Pennsylvanian Callville Limestone is not exposed at the roadside, but crops out above the Monte Cristo Group north of the highway from the lower entrance of the Narrows to the Cedar Wash fault (Fig. 1), and south of the highway from the lower entrance of the Narrows to milepost 14.4. The basal 62.7 ft (19 m) of the Callville Limestone crops out in a well-defined bench separating the cliff of the Monte Cristo Limestone from the markedly cyclic low cliff and bench succession above. This covered slope is underlain by interbedded thin limestone and argillaceous beds (Steed, 1980). Very fine-grained limestone, with chert in nodules and nodular layers, in-

Hurricane Valley Rd Stop #1 Dozy Fault systems Jorge - Volcanic centers - aligned w/ faults

JOURNAL OF GEOPHYSICAL RESEARCH, VOL. 108, NO. B4, 2199, doi:10.1029/2001JB000682, 2003

Comparison of geodetic and geologic data from the Wasatch region, Utah, and implications for the spectral character of Earth deformation at periods of 10 to 10 million years

Anke M. Friedrich,[1] Brian P. Wernicke, and Nathan A. Niemi[2]
Division of Geological and Planetary Sciences, California Institute of Technology, Pasadena, California, USA

Richard A. Bennett and James L. Davis
Smithsonian Astrophysical Observatory, Harvard University, Cambridge, Massachusetts, USA

Received 22 June 2001; revised 2 June 2002; accepted 21 November 2002; published 15 April 2003.

[1] The Wasatch fault and adjacent fault zones provide an opportunity to compare present-day deformation rate estimates obtained from space geodesy with geologic displacement rates over at least four temporal windows, ranging from the last millennium up to 10 Myr. The three easternmost GPS sites of the Basin and Range Geodetic Network (BARGEN) at this latitude define a ~130-km-wide region spanning three major normal faults extending east-west at a total rate of 2.7 ± 0.4 mm/yr, with an average regional strain rate estimated to be 21 ± 4 nstrain/yr, about twice the Basin and Range average. On the Wasatch fault, the vertical component of the geologic displacement rate is 1.7 ± 0.5 mm/yr since 6 ka, <0.6 mm/yr since 130 ka, and 0.5–0.7 mm/yr since 10 Ma. However, it appears likely that at the longest timescale, rates slowed over time, from 1.0 to 1.4 mm/yr between 10 and 6 Ma to 0.2 to 0.3 mm/yr since 6 Ma. The cumulative vertical displacement record across all three faults also shows time-variable strain release ranging from 2 to 4 mm/yr since 10 ka to <1 mm/yr averaged over the past 130 kyr. Conventional earthquake recurrence models ("Reid-type" behavior) would require an accordingly large variation in strain accumulation or loading rate on a 10-kyr timescale, for which there appears to be no obvious geophysical explanation. Alternatively, seismic strain release, given a wide range of plausible constitutive behaviors for frictional sliding, may be clustered on the 10-kyr timescale, resulting in the high Holocene rates, with comparatively low, uniform strain accumulation rates on the 100-kyr timescale ("Wallace-type" behavior). The latter alternative, combined with observations at the million-year timescale and the likelihood of a significant contribution of postseismic transients, implies maxima of spectral amplitude in the velocity field at periods of ~10 Myr (variations in tectonic loading), ~10 kyr (clustered strain release), and of 100 years (postseismic transients). If so, measurements of strain accumulation and strain release may be strongly timescale-dependent for any given fault system. *INDEX TERMS:* 1208 Geodesy and Gravity: Crustal movements—intraplate (8110); 1243 Geodesy and Gravity: Space geodetic surveys; 7209 Seismology: Earthquake dynamics and mechanics; 8107 Tectonophysics: Continental neotectonics; 8109 Tectonophysics: Continental tectonics—extensional (0905); *KEYWORDS:* geodetic, geologic, fault slip rate, normal fault, timescale, earthquake cycle

Citation: Friedrich, A. M., B. P. Wernicke, N. A. Niemi, R. A. Bennett, and J. L. Davis, Comparison of geodetic and geologic data from the Wasatch region, Utah, and implications for the spectral character of Earth deformation at periods of 10 to 10 million years, *J. Geophys. Res.*, *108*(B4), 2199, doi:10.1029/2001JB000682, 2003.

1. Introduction

[2] Geodetic data and geological displacement rate data are the observational basis for physical models of the earthquake deformation cycle and the assessment of seismic hazards. In the simplest model, the elastic strain energy accumulated across locked faults is periodically released during earthquakes of relatively uniform slip and recurrence interval, each of which releases the strain energy accumulated since the last earthquake (Figure 1a) [*Reid*, 1910; *Savage and Burford*, 1973; *Scholz*, 1990]. In this model, far-field displacement, which is proportional to strain accumulation, occurs at a uniform rate and is equal to the displacement rate recorded by earthquakes on the fault.

[1]Now at Institute of Geosciences, Potsdam University, Golm, Germany.
[2]Now at Institute for Crustal Studies, University of California, Santa Barbara, California, USA.

0148-0227/03/2001JB000682$09.00

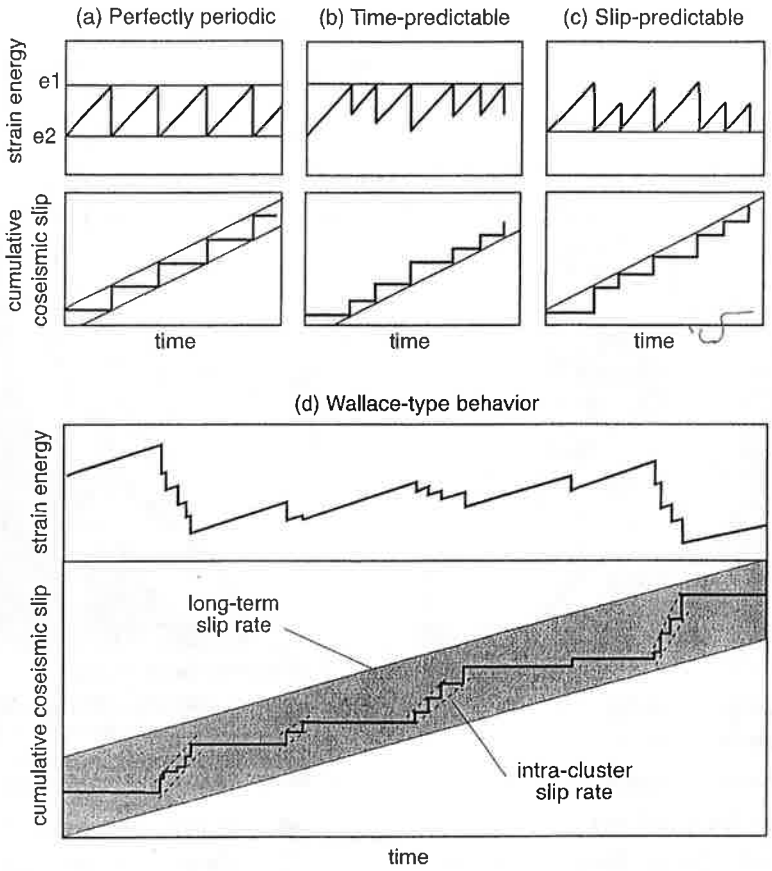

Figure 1. Strain release models for earthquakes (Figures 1a–1c are redrawn after *Scholz* [1990]). (a) Perfectly periodic model [*Reid*, 1910], (b) time-predictable model where the size of the last earthquake predicts the time of the next earthquake [*Shimazaki and Nakata*, 1980], and (c) slip-predictable model where the time since the last earthquake predicts the size of the next earthquake [e.g., *Shimazaki and Nakata*, 1980]. (d) Clustered strain release and uniform, low strain accumulation, modified after *Wallace* [1987]. See color version of this figure in the HTML.

This model was modified to account for the fact that the interseismic interval and the size of earthquakes on a particular fault are not perfectly periodic [e.g., *Shimazaki and Nakata*, 1980]. One variant is the "time-predictable" model where each event occurs when a critical amount of strain energy has accumulated (Figure 1b). In this model, the slip rate and the size of the last earthquake predict the time, but not the size, of the next earthquake. Another variant is the "slip-predictable" model where for any given event, all strain energy accumulated since the last earthquake is released. In this model, the slip rate and the time since the last earthquake are combined to predict the size, but not the time, of the next event (Figure 1c).

[3] In terms of both earthquake physics and hazards analysis, models such as these beg the question [*Wallace*, 1987; *Ward*, 1998]: Is the strain release rate of some small number of earthquakes equal to the long-term strain accumulation rate applied to faults? All three models assume a constant rate of far-field displacement and strain accumulation, and therefore predict that well-constrained slip histories, determined over several earthquake cycles, will agree with contemporary interseismic measurements of far-field displacement. The question is complicated, however, by the fact that it is not clear to what degree both strain accumulation and release are influenced by local stress diffusion within a viscous or viscoelastic substrate due to each event [e.g., *Foulger et al.*, 1992; *Hager et al.*, 1999; *Kenner and Segall*, 2000; *Wernicke et al.*, 2000]. Here we evaluate these issues through comparison of recently acquired geodetic data with displacement rates derived from paleoseismic and other geologic data for the Wasatch and related faults, which are among the best characterized Quaternary fault systems in the world [e.g., *Machette et al.*, 1992a].

[4] For the Wasatch and a number of other fault zones, an important consideration in comparing deformation rates on different timescales is that strain release may occur during "clusters" of earthquakes, wherein recurrence intervals are as much as an order of magnitude shorter than during quiescent periods between clusters [*Wallace*, 1987; *Swan*, 1988; *Sieh et al.*, 1989; *McCalpin and Nishenko*, 1996; *Grant and Sieh*, 1994; *Marco et al.*, 1996; *Zreda and Noller*, 1998; *Rockwell et al.*, 2000]. Clustering is consistent with the time-predictable and slip-predictable behavior. However, because slip per event for most well-documented fault segments does not appear to be highly variable [e.g., *Schwartz and Coppersmith*, 1984], these models require

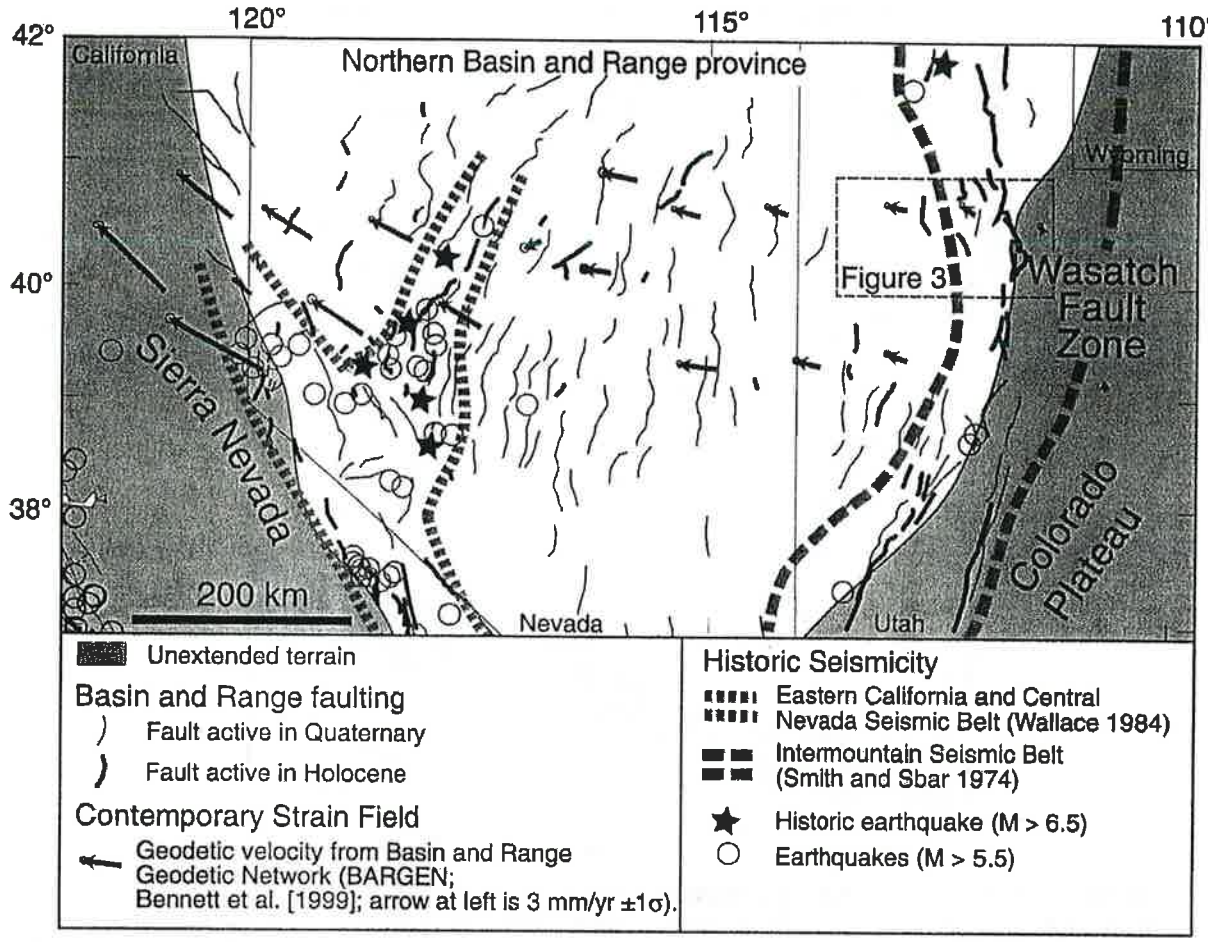

Figure 2. Simplified tectonic map of the northern Basin and Range province, located between the Sierra Nevada and the Colorado plateau. The BARGEN geodetic velocities [e.g., *Bennett et al.*, 1999] and the distribution of active normal faults and historic earthquakes are shown. See color version of this figure in the HTML.

that strain accumulation (via changes in either the far-field or local processes mentioned above) would vary markedly, on the same timescale as the clusters. In this event, at any given time strain accumulation inferred from geodesy and strain release inferred from paleoseismology should be the same. On the other hand, far-field strain accumulation may be constant, generally being lower than seismic strain release rates during clusters, and higher in between clusters. In this case, strain release would bear no relation to either a critical level of strain energy required for slip (time-predictable model), nor the amount of strain energy accumulated since the previous earthquake (slip-predictable model) (Figure 1d) [*Wallace*, 1987].

[5] The Wasatch fault zone is ideally suited for comparisons of strain accumulation and release because the slip histories of most or all segments of the fault are well known, and there are good constraints on the longer term slip history [e.g., *Machette et al.*, 1992a, 1992b; *McCalpin and Nishenko*, 1996; *McCalpin and Nelson*, 2000; *Parry and Bruhn*, 1987; *Ehlers et al.*, 2001]. In this paper we present new geodetic data from the Basin and Range Geodetic Network (BARGEN) from 1996 to 2000 across the eastern Basin and Range-Colorado Plateau transition region at the latitude of Salt Lake City and compare them with a synthesis of published geological displacement rates across the same region at the 1-kyr, 100-kyr, 1-Myr, and 10-Myr timescales.

2. Neotectonic Setting

[6] The northern Basin and Range province, bounded on the west by the Sierra Nevada and on the east by the Colorado Plateau (Figure 2), is a wide (~750 km) region of extended continental crust. Extension initiated in the Oligocene and peaked during mid to late Miocene time (~15–10 Ma [*Stockli*, 2000]) with a maximum displacement rate near 20 mm/yr [*Wernicke and Snow*, 1998], resulting in the formation of range front faults spaced ~30 km apart, separating ~15-km-wide basins from mountain ranges. Since ~10 Ma the overall rate of deformation has slowed to about half the maximum value and includes a major component of right-lateral shear along the western margin of the province [*Bennett et al.*, 1998, 1999; *Thatcher et al.*, 1999].

[7] Most range-bounding faults in Nevada and western Utah have been active in Quaternary time [*Dohrenwend et al.*, 1996; *Hecker*, 1993]. Regions of modern seismicity, however, are restricted to three narrow belts, the Eastern

Displacement rates on the Toroweap and Hurricane faults: Implications for Quaternary downcutting in the Grand Canyon, Arizona

Cassandra R. Fenton* Department of Geology and Geophysics, University of Utah, Salt Lake City, Utah 84112, USA
Robert H. Webb U.S. Geological Survey, 1675 W. Anklam Road, Tucson, Arizona 85745, USA
Philip A. Pearthree Arizona Geological Survey, 416 W. Congress Street, Tucson, Arizona 85701, USA
Thure E. Cerling Department of Geology and Geophysics, University of Utah, Salt Lake City, Utah 84112, USA
Robert J. Poreda Department of Earth and Environmental Sciences, University of Rochester, Rochester, New York 14627, USA

ABSTRACT

The Toroweap and Hurricane faults, considered to be the most active in Arizona, cross the Uinkaret volcanic field in the western Grand Canyon. These normal faults are downthrown to the west, and the Colorado River crosses these faults as it flows west in the Grand Canyon. Cosmogenic ^{3}He (^{3}He$_c$) dates on basalt flows and related landforms are used to calculate vertical displacement rates for these faults. The two faults cross unruptured alluvial fans dated as 3 ka (Toroweap) and 8 ka (Hurricane), and 10 other landforms that range in age from 30 to 400 ka are displaced. Middle and late Quaternary displacement rates of the Toroweap and Hurricane faults are 70–180 and 70–170 m/m.y., respectively. On the basis of these rates, the combined displacement of 580 m on these faults could have occurred in the past 3 to 5 m.y. All ^{3}He$_c$ dates are younger than existing K-Ar dates and are consistent with new ^{40}Ar/^{39}Ar dates and existing thermoluminescence (TL) dates on basalt flows. These different dating techniques may be combined in an analysis of displacement rates. Downcutting rates for the Colorado River in the eastern Grand Canyon (400 m/m.y.) are at least double the downcutting rates west of the faults (70–160 m/m.y.). Faulting probably increased downcutting in the eastern Grand Canyon relative to downcutting in the western Grand Canyon during the late Quaternary.

Keywords: cosmogenic elements, Colorado River, normal faults.

INTRODUCTION

The Hurricane and Toroweap faults are the most active faults in northwestern Arizona (Jackson, 1990; Stenner et al., 1999). These north-south–trending normal faults cross the southwestward-flowing Colorado River near river miles 179 and 191 (Fig. 1A) and are in the structural transition zone between the Great Basin and Colorado Plateau physiographic provinces (Stenner et al., 1999). The faults are downthrown to the west and have a combined vertical displacement of 580 m in Paleozoic rocks (Fig. 1B). Quaternary landforms in the Uinkaret volcanic field have been displaced by Toroweap and Hurricane faults. Dates of volcanism near the rim of the Grand Canyon range from 1 ka (Fig. 1A) to 3.7 Ma at Mount Trumbull (Wenrich et al., 1995), although most lava flows are younger than 600 ka (Dalrymple and Hamblin, 1998). At various times basalt flows have dammed the Colorado River (Hamblin, 1994).

Previous estimates of displacement rates on the Toroweap fault are 20 m/m.y., 56 m/m.y., and 110 m/m.y. in the time periods from 10 Ma to 600 ka, 600 to 40 ka, and 40 to 3 ka, respectively (Jackson, 1990). Holmes et al. (1978) reported displacement estimates of 60 to 75 m/m.y. for the interval 300 to 200 ka. Jackson inferred that either the rate of displacement increased significantly during the Quaternary or that faulting began more recently than previously thought. Previous estimates for the displacement rate on the Hurricane fault from 200 to 90 in the vicinity of Grand Canyon range from 30–70 m/m.y. (Pearthree et al., 1983) to 125–250 m/m.y. (Holmes et al., 1978).

In this paper we report new displacement rates based on ^{3}He$_c$ ages for surfaces younger than 400 ka crossed by the Toroweap and Hurricane faults. We linearly extrapolate these rates to estimate that the combined total vertical displacement on both faults could have occurred in the past 3 to 5 m.y. We suggest that these displacement rates probably differentially affected downcutting rates of the Colorado River in the eastern versus western Grand Canyon.

AGE DATING OF BASALT FLOWS AND ASSOCIATED LANDFORMS

The age of volcanism in the Uinkaret volcanic field has been previously estimated using K-Ar (Dalrymple and Hamblin, 1998) and thermoluminescence (TL) dating (Holmes et al., 1978). K-Ar dating in this volcanic field is known to be problematic owing to excess ^{40}Ar incorporated into large phenocrysts from the magmatic environment (Damon et al., 1967) and abundant glassy groundmass (Dalrymple and Hamblin, 1998). ^{39}Ar/^{40}Ar dating is more precise than K-Ar analysis and has been used to accurately date young basalt flows (Laughlin et al., 1994). However, hydration and alteration of abundant glassy groundmass in Uinkaret basalts can contribute atmospheric Ar to analyses and can cause large uncertainties in ^{39}Ar/^{40}Ar ages. In the Uinkaret volcanic field, ^{3}He$_c$ dating provides an alternative to K-Ar dating and, in certain cases to ^{39}Ar/^{40}Ar dating, particularly for relatively young (<200 ka) basalt flows with abundant olivine and/or pyroxene phenocrysts (Fenton et al., 2001). Samples collected from the Uinkaret volcanic field were analyzed in accordance with techniques described in Cerling et al. (1999).

Most of the ^{3}He$_c$ ages on surfaces in the Uinkaret volcanic field differ significantly from existing K-Ar ages (Table 1; for details see Table DR1[1]). Damon et al. (1967) reported a K-Ar age of 10 ka for Vulcan's Throne (Fig. 1A), noting that it is only an order of magnitude estimate because of a high atmospheric Ar correction. We believe our ^{3}He$_c$ age of 73 ± 4 ka is fairly accurate, although it is a minimum age because Vulcan's Throne, a cinder cone, is more erodible than nearby basalt flows. Damon (quoted in Hamblin, 1994) reported a K-Ar age of 993 ± 97 ka for Hamblin's (1994) Whitmore Dam basalt, but Dalrymple and Hamblin (1998) concluded that this date may not be reliable, on the basis of stratigraphic relations.

Fenton et al. (2001) concluded that their Whitmore Cascade basalt is correlative with the Whitmore Dam basalt (Fig. 1A) and reported a ^{3}He$_c$ age of 177 ± 9 ka for the flow. This age is bracketed by TL dates of the same flow (Table 1; Holmes et al., 1978). The Whitmore Cascade contains abundant glass that may contribute to an anomalously old K-Ar

*E-mail: crfenton@mines.utah.edu.

[1]GSA Data Repository item 2001119, ^{3}He$_c$ exposure ages of landforms in the Uinkaret volcanic field, is available on request from Documents Secretary, GSA, P.O. Box 9140, Boulder, CO 80301-9140, editing@geosociety.org, or at www.geosociety.org/pubs/ft2001.htm.

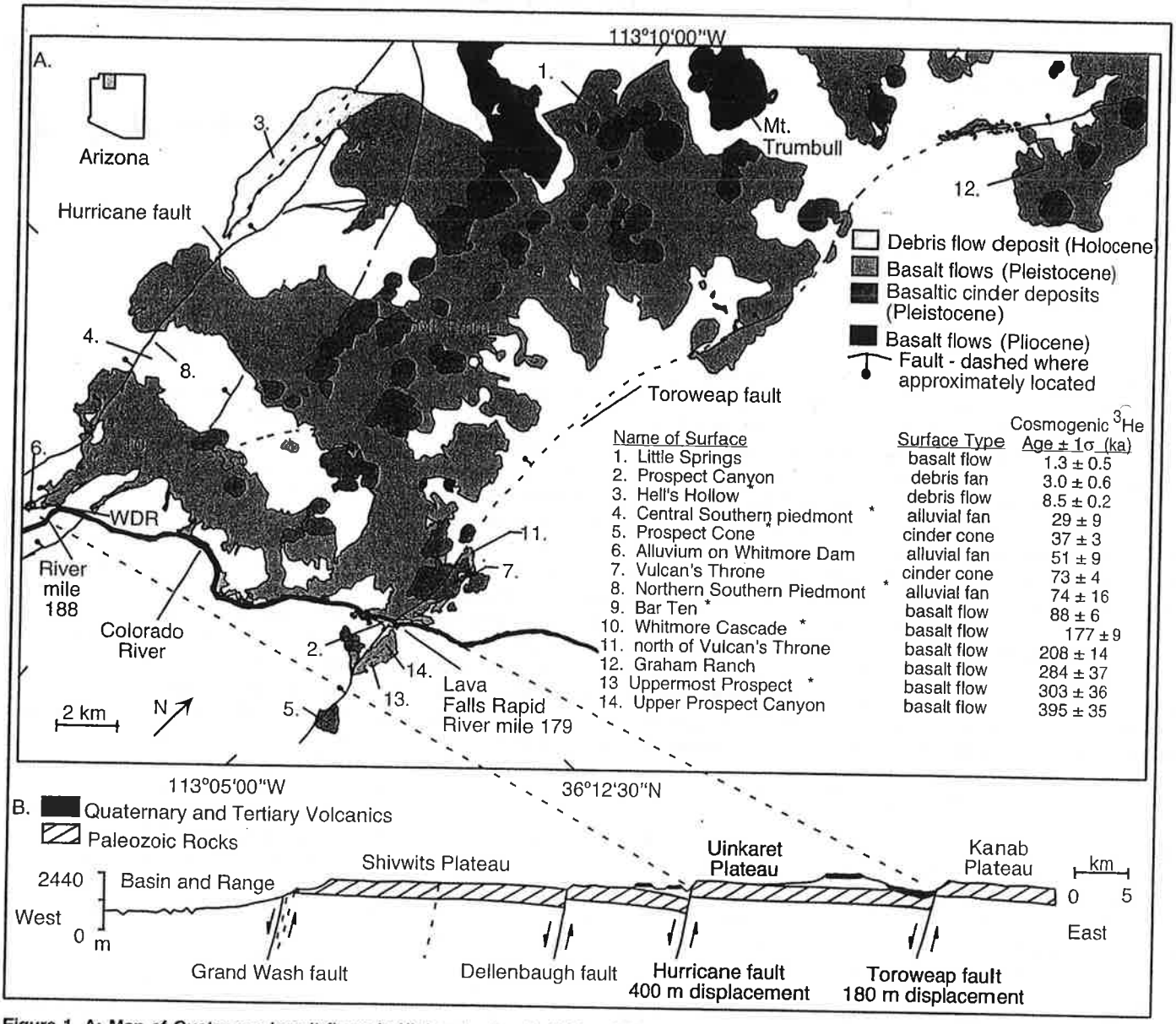

Figure 1. A: Map of Quaternary basalt flows in Uinkaret volcanic field and Hurricane and Toroweap faults, western Grand Canyon, Arizona (adapted from Wenrich et al., 1997). Details of analyses in Table DR1 (see text footnote 1). Hurricane and Toroweap faults do not displace Hell's Hollow and Prospect Canyon debris flows, respectively. Little Springs basalt flow (Billingsley, 1997) is not crossed by either fault, but is reported to show range in age of volcanic activity in region. Names with asterisk are informal. WDR—Whitmore Dam remnant (Hamblin, 1994). B: East-west cross section of western Grand Canyon from Grand Wash fault to Toroweap fault (adapted from Jackson, 1990).

age. ^3He_c ages of the Whitmore Cascade and Bar Ten basalt flows are consistent with middle to late Quaternary age $^{39}Ar/^{40}Ar$ and TL age estimates of these flows (Table 1). Large analytical uncertainties render the $^{39}Ar/^{40}Ar$ ages essentially useless in calculating late Quaternary slip rates.

Three basalt flows with the oldest ^3He_c ages are found along the Toroweap fault. A lava flow adjacent to and north of Vulcan's Throne has identical TL and ^3He_c ages of 201 ± 14 ka and 208 ± 14 ka, respectively (Table 1). The K-Ar (500 ± 47 ka; Dalrymple and Hamblin, 1998) and ^3He_c (395 ± 35 ka) ages of Hamblin's (1994) Upper Prospect basalt flow overlap within two standard deviations (Table 1). The ^3He_c age may be younger due to minimal flow-surface weathering. In contrast, the K-Ar age may be older because of the presence of excess Ar. The Graham Ranch flow in Toroweap Valley (Fig. 1A) has reported K-Ar and TL ages of 635 ± 24 ka (Jackson, 1990) and 284 ± 48 ka (Holmes et al., 1978). We obtained a ^3He_c age of 284 ± 37 ka for that flow. The ^3He_c age of the Graham Ranch flow may be younger than the reported K-Ar age because the flow is weathered, but it is likely that the ^3He_c and TL ages are more accurate than the K-Ar age.

TOROWEAP AND HURRICANE FAULTS

An alluvial fan at the mouth of Prospect Valley (Fig. 1A) composed of debris-flow deposits delineates the Holocene displacement history on the Toroweap fault. The debris flow covering the surface was emplaced 3.0 ± 0.6 ka, and the fault does not rupture this surface (Cerling et al., 1999). An estimated displacement of 2.2 m occurred during a magnitude 7 earthquake on the Toroweap fault at 3.1 ± 1.6 ka, on the basis of morphologic fault-scarp analysis in Prospect Valley, south of the Colorado River (Jackson, 1990). This earthquake must have occurred before 2.4 ka, the minimum age of the surface of the fan.

Using ^3He_c ages of volcanic landforms along the Toroweap fault and published displacements (Jackson, 1990; Wenrich et al., 1997), we estimate a range in displacement rates of 70–180 m/m.y. for the past 300 k.y.

TABLE 1. DISPLACEMENT RATES FOR THE TOROWEAP AND HURRICANE FAULTS

Fault	Site	Average ^3He_c age $\pm 1\sigma$* (ka)	K-Ar or $^{39}Ar/^{40}Ar$ age (ka)	TL age (ka)	Displacement (m)	Average Displacement rate (m/m.y.)
Toroweap	Prospect Canyon debris fan	3.0 ± 0.6	—	—	0	0
Toroweap	Prospect Cone	37 ± 3	—	—	7	180
Toroweap	Vulcan's Throne	73 ± 4	10	—	5	70
Toroweap	Basalt flow north of Vulcan's Throne	208 ± 14	—	201 ± 34	14	70
Toroweap	Graham Ranch basalt flow	284 ± 37	635 ± 24	284 ± 48	36	130
Toroweap	Upper Prospect basalt flow	395 ± 35	500 ± 47	—	46	120
Hurricane	Hell's Hollow debris flow	8.5 ± 0.2	—	—	0	0
Hurricane	Northern alluvial fan of southern piedmont	74 ± 16	—	—	7	90
Hurricane	Central alluvial fan of southern piedmont	29 ± 9	—	—	3	100
Hurricane	Alluvium overlying Whitmore Dam remnant	51 ± 9	—	—	4*	80
Hurricane	Bar Ten basalt flow	88 ± 6	190 ± 390†	108 ± 29	10 ± 3	110
Hurricane	Whitmore Cascade basalt flow (north end)	177 ± 9	220 ± 120† 150 ± 220†	203 ± 24 88 ± 15	15 ± 3	80
Hurricane	Whitmore Cascade basalt flow (south end)	177 ± 9	220 ± 120† 150 ± 220† 993 ± 97	203 ± 24 88 ± 15	12	70

Note: Rates calculated using average ^3He_c ages of displaced lava flows, cinder cones, and alluvial deposits in the Uinkaret volcanic field. Details of analysis in Table 2 (see text footnote 1). —= no date. Documented K-Ar and TL (thermoluminescence) ages are listed for comparison and are referenced in the text. Displacements other than those produced by the authors are referenced in the text. Uppermost Prospect flow is not listed in this table because the vertical displacement of this flow has not been measured.

*Scarp profile measured by authors using laser range finder and displacement calculated using far-field slopes.

†$^{39}Ar/^{40}Ar$ ages analyzed at the New Mexico Geochronological Research Laboratory; Samples 97-AZ-318-WDA and 97-AZ-321-WCB were collected from the Whitmore Cascade and sample 97-AZ-329-BT came from the Bar Ten basalt flow. Large uncertainties likely result from alteration of glass in the groundmass.

for the Toroweap fault (Table 1). Two cinder cones—Prospect Cone and Vulcan's Throne—are displaced 7 and 5 m, respectively (Table 1). If we use ^3He_c ages of 37 ± 3 and 73 ± 4 ka for Prospect Cone and Vulcan's Throne (Fig. 1A), the displacement rates are 180 and 70 m/m.y., respectively. The basalt flow dated at 208 ± 14 ka (^3He_c) and located north of Vulcan's Throne has a displacement of 13–15 m (Jackson, 1990), yielding a vertical slip rate of 70 m/m.y.

If we use a displacement of 36 m and a K-Ar age of 635 ka, the Graham Ranch basalt flow has a minimum displacement rate of 56 m/m.y. (Jackson, 1990). Using the same displacement and our minimum ^3He_c age of 284 ± 37 ka, we calculate a maximum displacement rate of 130 m/m.y. Huntoon (1977) mentioned a 46 m displacement on "older lava flows that fill Prospect Valley" ~2.5 km south of the Colorado River. On the basis of field evidence, we conclude that Huntoon's flow is Hamblin's Upper Prospect Canyon flow (Fig. 1A), which has a cosmogenic ^3He age of 395 ± 35 ka; the displacement rate is 120 m/m.y., which agrees with a linear displacement rate (Fig. 2). Jackson (1990) concluded that the displacement rate on the Toroweap fault increases from 56 m/m.y. to 110 m/m.y. ca. 40 ka. Our data show that the displacement rate on the Toroweap fault has been linear over the past 400 k.y. (Fig. 2).

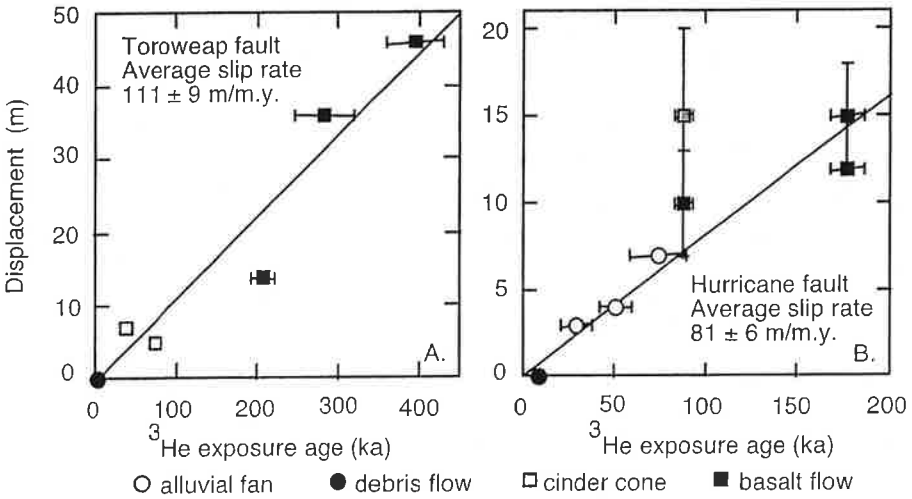

Figure. 2. Vertical displacement rates of (A) Toroweap and (B) Hurricane faults based on ^3He_c ages of displaced landforms in Uinkaret volcanic field. Average slip rates on faults, 111 ± 9 m/m.y. for Toroweap and 81 ± 6 m/m.y., for Hurricane, are based on linear regressions (R^2 = 0.966 and 0.970 for Toroweap and Hurricane faults). Gray square in B is maximum average displacement on Bar Ten flow. It is not included in average slip rate of Hurricane fault (see text for details).

On the Hurricane fault, alluvial fans provide data on displacements <100 k.y. old. The Hell's Hollow debris flow, which is not ruptured, yielded a ^3He_c age of 8.5 ± 0.2 ka, providing a datum on the age of youngest displacement (Fig. 1A). Our age agrees with morphologic analyses of fault scarps that suggest that the youngest displacement in Whitmore Wash, which resulted in 2–3 m of offset, occurred between 5 and 15 ka (Pearthree et al., 1983). A suite of alluvial fans, called the southern piedmont by Stenner et al. (1999), lies between the Bar Ten and Whitmore Cascade lava flows (Fig. 1A). Varnished basalt boulders in the alluvium yielded average ^3He_c ages of 74 ± 16 and 29 ± 9 ka for the northern and central fans, respectively, in the piedmont. These surfaces are displaced 7 and 3 m by the Hurricane fault (Stenner et al., 1999), and the resulting displacement rates are 90 and 100 m/m.y. Alluvium overlying Hamblin's (1994) Whitmore Dam remnant at the mouth of Whitmore Canyon (Fig. 1A) has a 4 m displacement (Table 1), and varnished basalt boulders yield a ^3He_c age of 51 ± 9 ka for a displacement rate of 80 m/m.y.

In Whitmore Canyon, the Bar Ten basalt flow, which has an ^3He_c age of 88 ± 6 ka, has an average vertical displacement of 15 ± 6 m (Stenner et al., 1999; Fig. 2). The flow surface is steep and irregular, and the displacement varies by at least 100% in short distances along strike. The higher displacements may reflect buried bedrock scarps over which the Bar Ten basalt flowed. Excluding the highest two or three scarps results in estimated displacements of 12 ± 4 and 10 ± 3 m for the Bar Ten flow; given the agreement in linear displacement of nearby alluvial fans and in the Whitmore Cascade (Fig.

2), we believe the lesser of the displacement values of 10 m on the Bar Ten flow is more reasonable. If this figure is used, the displacement rate is 110 m/m.y.

The Whitmore Cascade has an average total displacement of 15 ± 3 m at the north end of the basalt flow (Stenner et al., 1999) and a displacement of 12 m near the Colorado River (Wenrich et al., 1997). Given an average ^3He_c age of 177 ± 9 ka, the displacement rate for this basalt flow is between 70 and 80 m/m.y. Using these age and displacement data, we estimate a late Quaternary displacement rate for the Hurricane fault of between 70 and 170 m/m.y., but it is likely that the displacement rate is between 80 and 110 m/m.y. (Fig. 2). We conclude that the displacement rates for the Toroweap and Hurricane faults have been linear for the past 400 k.y. and 200 k.y., respectively, and we find no evidence to support Jackson's (1990) conclusion that displacement rates have increased in the past 40 k.y.

The Toroweap fault has 150–265 m of total vertical displacement along its length (Jackson, 1990); displacement in the vicinity of the Grand Canyon is 180 m (Wenrich et al., 1997). The total vertical displacement on the Hurricane fault is 400 m at the Colorado River (Wenrich et al., 1997), but published maps show the fault concealed by a 600 ka lava flow (Hamblin, 1994). Our field inspection indicates that the Hurricane fault lies east of the path mapped by Wenrich et al. (1997) and that the fault does not directly interact with the lava flow on the south side of the Colorado River. Instead, there is substantial Quaternary displacement in an alluvial fan just south of the river in 192 Mile Canyon. The displacement south of the river indicates that the Hurricane fault crosses the Colorado River with possibly the same activity it shows north of the river (Fig. 2B).

The Hurricane and Toroweap faults have a combined vertical displacement of 580 m. This is 68% of the depth of the Inner Gorge from Toroweap Overlook to Lava Falls Rapid (850 m) just upstream of the Toroweap fault. By extrapolation of the displacement rates (Fig. 2) on both faults through the Quaternary, we calculate that the Toroweap and Hurricane faults could have accommodated all of their vertical displacement in the past 1.5 and 5 m.y., respectively. Billingsley and Workman (2000) reported that all of the faults on the Uinkaret plateau probably became active at 3.5 to 2 Ma and that extension on the Hurricane fault began after emplacement of the Bundyville basalt (3.6 ± 0.18 Ma). Thus, the fault may have decelerated from approximately 115 m/m.y. to 80 m/m.y. between 3.5 Ma and 180 ka. The combined Quaternary vertical displacement on both faults is 380 m (45% the depth of the Inner Gorge), suggesting that 65% of the combined displacement on the Toroweap and Hurricane faults may have occurred in the past 2 m.y.

IMPLICATIONS FOR QUATERNARY DOWNCUTTING OF THE COLORADO RIVER

Displacements on the Toroweap and Hurricane faults probably induced differential downcutting rates of the Colorado River in the Grand Canyon east versus west of the faults. Vertical displacements on these faults result in local base-level fall, as evidenced by the west sides of these faults being downdropped relative to the eastern Grand Canyon. A river responding to base-level fall will incise upstream to reduce the gradient to its previous level and it can maintain a steady longitudinal profile as long as stream power of the river is large enough to allow downcutting to occur at a rate equal to that of the uplift (Merritts et al., 1994). The Colorado River has sufficient power to quickly downcut through material (Lucchitta et al., 2000) that is uplifted during individual fault movements of 3 m or less, and we would expect no discrete knickpoints in the channel profile related to faulting. Thus, the effects of this downcutting would be expressed in increased downcutting rates on the Colorado River and its tributaries in the eastern Grand Canyon, and perhaps an overall increase in the steepness of hillslopes in that part of the Grand Canyon.

Quaternary displacement on the Hurricane and Toroweap faults can help account for variations in downcutting rates reported for various locations in the Grand Canyon. Lucchitta et al. (2000) estimated downcutting rates of 70–160 m/m.y. and 400 m/m.y. for the Grand Canyon west and east, respectively, of these faults for the past 500–600 ka. Therefore, the fluvial incision rate in the eastern Grand Canyon is at least double that west of the faults, and displacement across the Toroweap and Hurricane faults is probably responsible for this difference. These faults likely played a major role in the development of the eastern Grand Canyon. Obviously, variations in lithology through the Grand Canyon influence the morphology of the canyon, but we propose that much of the development of the narrow, steep-sided Inner Gorge of the Grand Canyon just upstream of the Toroweap fault has been driven by displacement on these faults.

ACKNOWLEDGMENTS

Clair Roberts, Ben Passey, Dave Marchetti, Heidi Stenner, Jeanne Klawon, Tom Biggs, Jon Pelletier, Andy Hunt, Joel Pederson, and George Billingsley helped with field work, laboratory analyses, and technical discussions. David Fastovsky and Thomas Gardner critically reviewed the manuscript. Funding was provided by the National Science Foundation, U.S. Geological Survey, Geological Society of America, and Sigma Xi. We thank the Grand Canyon Monitoring and Research Center for logistical support.

REFERENCES CITED

Billingsley, G.H., 1997, Geologic map of the Mount Logan Quadrangle, northern Mohave County, Arizona: U.S. Geological Survey Open-File Report 97-426, scale 1: 24 000, 21 p. text.

Billingsley, G.H., and Workman, J.B., 2000, Geologic map of the Littlefield 30′ × 60′ Quadrangle, Mohave County, northwestern Arizona: U.S. Geological Survey Geologic Investigations Map I-2628, 1 sheet, scale 1:48 000, 25 p. text.

Cerling, T.E., Webb, R.H., Poreda, R.J., Rigby, A.D., and Melis, T.S., 1999, Cosmogenic ^{3}He ages and frequency of late Holocene debris flows from Prospect Canyon, Grand Canyon, U.S.A.: Geomorphology, v. 27, p. 93–111.

Dalrymple, G.B., and Hamblin, W.K., 1998, K-Ar of Pleistocene lava dams in the Grand Canyon in Arizona: National Academy of Science Proceedings, v. 95, p. 9744–9749.

Damon, P.E., Laughlin, A.W., and Percious, J.K., 1967, The problem of excess argon-40 in volcanic rocks, *in* Proceedings of the symposium Radioactive Dating and Methods of Low-Level Counting, Monaco, 1967: Vienna, International Atomic Energy Agency, 24 p.

Fenton, C.R., Webb, R.H., Cerling, T.E., Poreda, R.J., and Nash, B.P., 2001, Cosmogenic ^{3}He ages and geochemical discrimination of lava-dam outburst-flood deposits in western Grand Canyon, Arizona, *in* House, K., et al., eds., Ancient floods and modern hazards, principles and applications of paleoflood hydrology: Washington, D.C., American Geophysical Union, Water Science and Application Series, v. 4 (in press).

Hamblin, W.K., 1994, Late Cenozoic lava dams in the western Grand Canyon: Geological Society of America Memoir 183, 135 p.

Holmes, R.D., Best, M.G., and Hamblin, W.K., 1978, Calculated strain rates and their implications for the development of the Hurricane and Toroweap faults, Utah and northern Arizona: U.S. Geological Survey Technical Report Summaries, Earthquake Hazards Reduction Program, v. VII, p. 44–50.

Huntoon, P.W., 1977, Holocene faulting in the western Grand Canyon, Arizona: Geological Society of America Bulletin, v. 88, p. 1619–1622.

Jackson, G.W., 1990, Tectonic geomorphology of the Toroweap fault, western Grand Canyon, Arizona: Implications for transgression of faulting on the Colorado Plateau: Arizona Geological Survey Open-File Report, v. 90-4, p. 1–66.

Laughlin, A.W., Poths, J., Healey, H.A., Reneau, S., and WoldeGabriel, G., 1994, Dating of Quaternary basalts using the cosmogenic ^{3}He and ^{14}C methods with implications for excess ^{40}Ar: Geology, v. 22, p. 135–138.

Lucchitta, I., Curtis, G.H., Davis, M.E., Davis, S.W., and Turrin, B., 2000, Cyclic aggradation and downcutting, fluvial response to volcanic activity, and calibration of soil-carbonate stages in the western Grand Canyon, Arizona: Quaternary Research, v. 53, p. 23–33.

Merritts, D., Vincent, K.R., and Wohl, E.E., 1994, Long river profiles, tectonism, and eustasy: A guide to interpreting fluvial terraces: Journal of Geophysical Research, v. 99, p. 14 031–14 050.

Pearthree, P.A., Menges, C.M., and Mayer, L., 1983, Distribution, recurrence, and possible tectonic implications of late Quaternary faulting in Arizona: Arizona Bureau of Geology and Mineral Technology Open-File Report 83-20, 51 p.

Stenner, H.D., Lund, W.R., Pearthree, P.A., and Everitt, B.L., 1999, Paleoseismologic investigations of the Hurricane fault in northwestern Arizona and southwestern Utah: Arizona Geological Survey Open-File Report 99-8, 137 p.

Wenrich, K.J., Billingsley, G.H., and Blackerby, B.A., 1995, Spatial migration and compositional changes of Miocene-Quaternary magmatism in the western Grand Canyon: Journal of Geophysical Research, v. 100, p. 10 417–10 440.

Wenrich, K.J., Billingsley, G.H., and Huntoon, P.W., 1997, Breccia-pipe and geologic map of the northeastern part of the Hualapai Indian reservation and vicinity, Arizona: U.S. Geological Survey Miscellaneous Investigations Map I-2440, scale 1:48 000, 19 p. text.

Manuscript received January 4, 2001
Revised manuscript received June 29, 2001
Manuscript accepted July 20, 2001

Printed in USA

Geological Society of America
Field Guide 6
2005

Paleoseismology and geomorphology of the Hurricane Fault and Escarpment

Lee Amoroso
U.S. Geological Survey, 2255 North Gemini Drive, Flagstaff, Arizona 86001, USA

Jason Raucci
Department of Geology, Northern Arizona University, Flagstaff, Arizona 86011, USA

ABSTRACT

The Hurricane Fault is one of the longest and most active late Cenozoic normal faults in southwestern Utah and northwestern Arizona. This fault shows evidence of tectonic activity during the late Tertiary and Quaternary, neotectonism involving the Hurricane Fault as well as the Toroweap Fault imply encroaching Basin and Range extension onto the Colorado Plateau. Paleoseismology investigations suggest that the Hurricane Fault poses a seismic hazard to the southwestern Utah area. During the trip, we will examine evidence of late Pleistocene and earliest Holocene(?) surface-rupturing faulting along the Shivwits and Whitmore Canyon sections of the fault. The Hurricane Fault separates the Uinkaret and Shivwits plateaus and displacement along the fault produced the spectacular Hurricane Escarpment. We will see late Quaternary landforms related to back-wasting and mass movement along the Hurricane Escarpment and look at evidence of the style and age estimates of late Pleistocene fan deposition.

Keywords: Hurricane Fault, paleoseismology, neotectonism, alluvial fan, colluvium.

INTRODUCTION

The Hurricane Fault (Fig. 1) is the longest and most active of the late Cenozoic down-to-the-west normal faults in southwestern Utah and northwestern Arizona. The Hurricane Fault crosses the Arizona Strip between the Utah border and Grand Canyon in close proximity to St. George, Utah (Fig. 1). Although the Arizona portion of the Hurricane Fault crosses sparsely populated terrain, much of populous southwestern Utah lies within 75 km of the Shivwits section. Two significant, historic seismic events have occurred in the region. An ~M6 earthquake occurred in the Pine Valley, Utah, area in 1902 (Williams and Tapper, 1953). A M5.8 earthquake in the St. George area in 1992 caused minor structural damage in southwestern Utah, triggered a large landslide near the entrance to Zion National Park 45 km from the epicenter (Christensen, 1995), and caused numerous rockfalls along the Hurricane cliffs (G.H. Billingsley, 2000, personal commun.).

Several recent paleoseismic investigations have addressed the potential for larger earthquakes than those of the historic record. These workers have suggested that the threshold magnitude for surface rupture along faults within the Intermountain Seismic Belt (ISB; Fig. 1) in Utah is $6 < M < 6.5$ (Arabasz et al., 1992; Doser, 1985; Smith and Arabasz, 1991). Fault scarps and other evidence of Quaternary faulting suggest that there is potential for $M > 7$ earthquakes along the Hurricane Fault (Stewart et al., 1997; Stenner and Pearthree, 1999; Amoroso et al., 2004). This field trip guide introduces evidence for late Quaternary ruptures on the Hurricane Fault in Arizona, considers the neotectonics implications, and places the late Quaternary deformation within the context of the encroachment of Basin-and-Range style

Amoroso, L., and Raucci, J., 2005, Paleoseismology and geomorphology of the Hurricane Fault and Escarpment, *in* Pederson, J., and Dehler, C.M., eds., Interior Western United States: Geological Society of America Field Guide 6, p. 449–477, doi: 10.1130/2005.fld006(20).

13

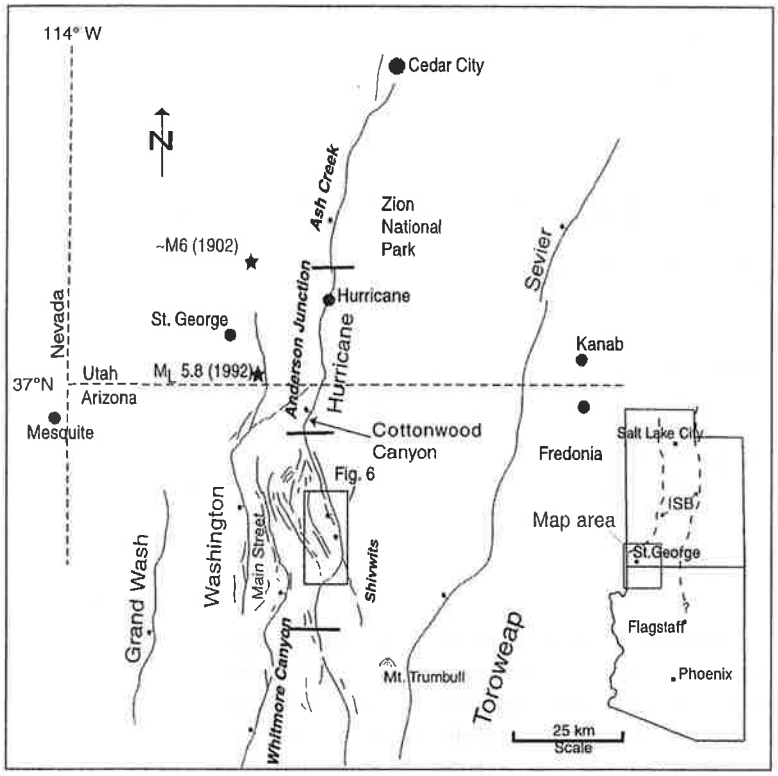

Figure 1. (A). Quaternary normal faults in northwestern Arizona and southwestern Utah, compilation adapted from Scarborough et al. (1986), Hecker (1993), and Pearthree and Bausch (1999). Significant recent earthquake epicenters (stars) and the sections (bold font) of the Hurricane Fault (Pearthree, 1998) are shown. Cottonwood Canyon, the site of recent seismic hazard assessment work on the Hurricane Fault in Arizona, is located north of the Shivwits-Anderson Junction boundary (Stenner et al., 1998). The Intermountain Seismic Belt (ISB) is a zone of earthquake activity extending through the Intermountain West from northwestern Montana south to Utah, southern Nevada and northern Arizona. The approximate boundaries of the ISB are shown in the inset.

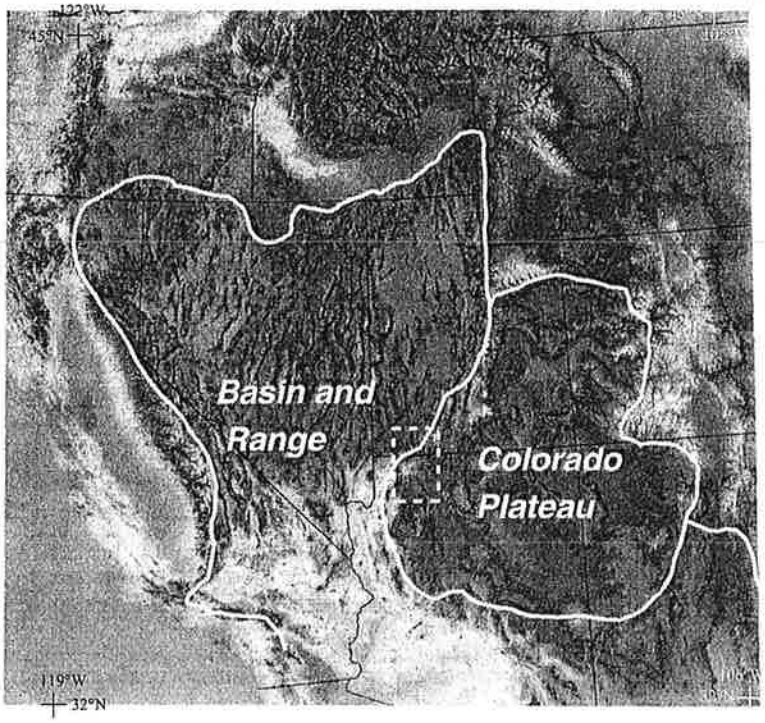

Figure 2. Digital elevation model/hillshade map of the southwestern United States showing the Colorado Plateau and Basin and Range physiographic provinces. The dashed white box shows the extent of Figure 1.

in the Fossil Mountain Member of the Kaibab Formation. Lower slopes on the cliffs consist of the Woods Ranch and Seligman Members of the Toroweap Formation, which bracket the cliff-forming Brady Canyon Member. Coarse, very poorly sorted colluvium covers much of the slope-forming units, especially the Seligman Member. Because of the structural complexity of the Hurricane Fault zone immediately across the valley from this vantage point, you may see all or parts of this sequence repeated several times.

Most of the Shivwits segment is a large structural embayment between two prominent convex fault bends. On the hanging wall at the northern end of the Shivwits segment, you can see a prominent east-sloping butte (mentioned at road-log mile 39.3), where beds of the Triassic Moenkopi Formation are capped with late Tertiary basalt and all are tilted toward the Hurricane Fault. This butte is at a major convex bend in the trace of the Hurricane Fault similar to the State Line geometric bend (Stewart and Taylor, 1996). Immediately northeast of our overlook, the gravel road of the Navajo Trail can be traced up to the Hurricane Escarpment, where it ascends the surface of a ruptured relay ramp between overlapping strands of the Hurricane Fault. The Grandstand, seen south of the Navajo Trail, is a zone of multiple fault strands associated with a left stepover. To the southeast, we can see the Moriah Knoll basalt where it flowed across the escarpment (Fig. 6). This is discussed at Stop 2.

Neotectonics of the Hurricane Fault

The Hurricane Fault provides excellent exposures of displaced Quaternary alluvium and basalt flows for the evaluation of seismic hazard and discerning its neotectonic history. Lund and Everitt (1999) and Stenner and Pearthree (1999) all have identified displaced basalt and alluvium that indicate that the Hurricane Fault has been active throughout the Quaternary. Paleoseismic investigations of the Anderson Junction section (Fig. 1) discovered evidence of several Pleistocene and Holocene surface-rupturing earthquakes. Stenner and others identified a latest Pleistocene to early Holocene surface-rupturing most-recent event (MRE) at Cottonwood Canyon on the Anderson Junction section (just south of the Utah border, Fig. 1) with 0.6 m of vertical displacement (Stenner et al., 1998). Further trenching investigations at Rock Canyon, 4 km north of Cottonwood Canyon, revealed that the last three events had variable amounts of slip per event (Stenner et al., 2003). The MRE had an estimated 0.3–0.4 m net vertical slip, whereas the penultimate and pre-penultimate events together had ~2.7–3.7 m of vertical slip. Possible scenarios to explain the lower MRE offset at Cottonwood and Rock Canyons include the rupture of the Shivwits that propagated north into the adjacent southern Anderson Junction sections, or a separate rupture in the boundary between the two sections. The size of older fault scarps at Cottonwood and Rock canyons, along with estimates of earthquake recurrence intervals (5–100 ka) in the Basin and Range province (Stenner et al., 1998), suggest that larger slip-per-event (more than 0.6 m) is typical along this part of the Hurricane Fault.

A paleoseismic investigation here along the Shivwits section of the Hurricane Fault revealed evidence of surface-rupturing late Quaternary events (Amoroso et al., 2004). Mapping did not show any evidence of surface rupture of Holocene deposits; the only convincing evidence of tectonic displacement was found in late to middle(?) Pleistocene alluvial fans. Results using displacement of the Moriah Knoll basalt (Fig. 7), topographic profiling, surface dating, morphologic modeling of fault scarps, and observations

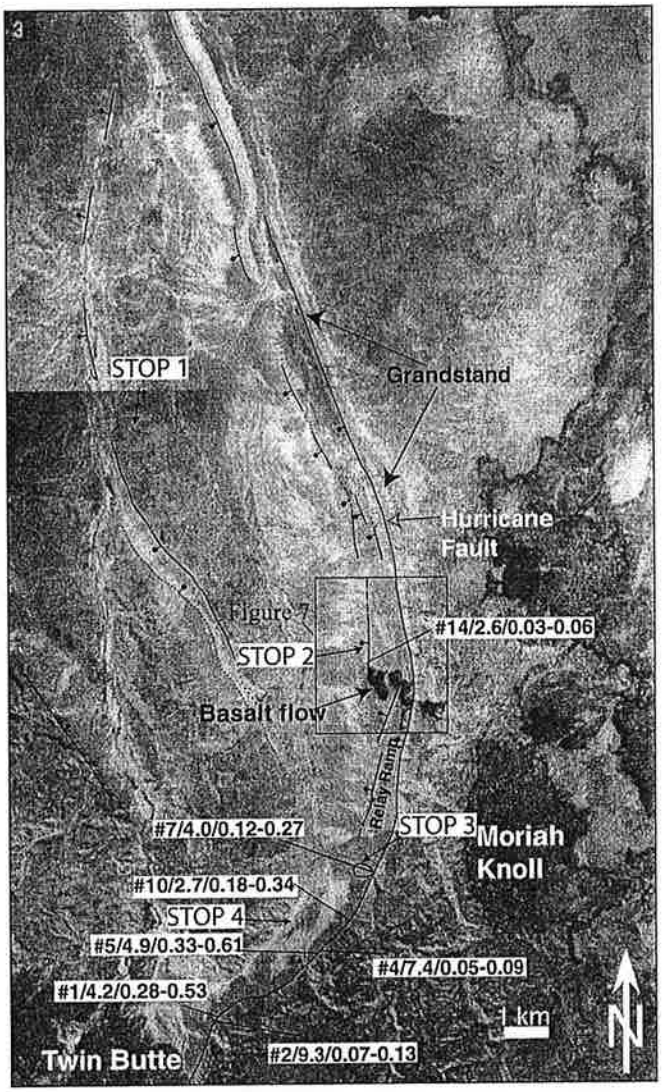

Figure 6. Mosaic of NASA high-altitude aerial photography of the central part of the Shivwits section of the Hurricane Fault showing fault traces, slip-rate estimates, and field trip stops. The fault strands are from Billingsley (1994a and 1994b) and field reconnaissance. Faults are dashed where approximate or inferred, dotted where concealed. The relay ramp, south of the basalt flow, is evidence that fault linkage had occurred on this portion of the fault (Peacock and Sanderson, 1994). Shown is a compilation of the vertical surface displacement observations (the format is profile #/surface offset in m/slip-rate range in mm/yr). Profile #7 is the Boulder Fan (outlined) trench site. The basalt flow displaced by the Hurricane Fault originated from Moriah Knoll.

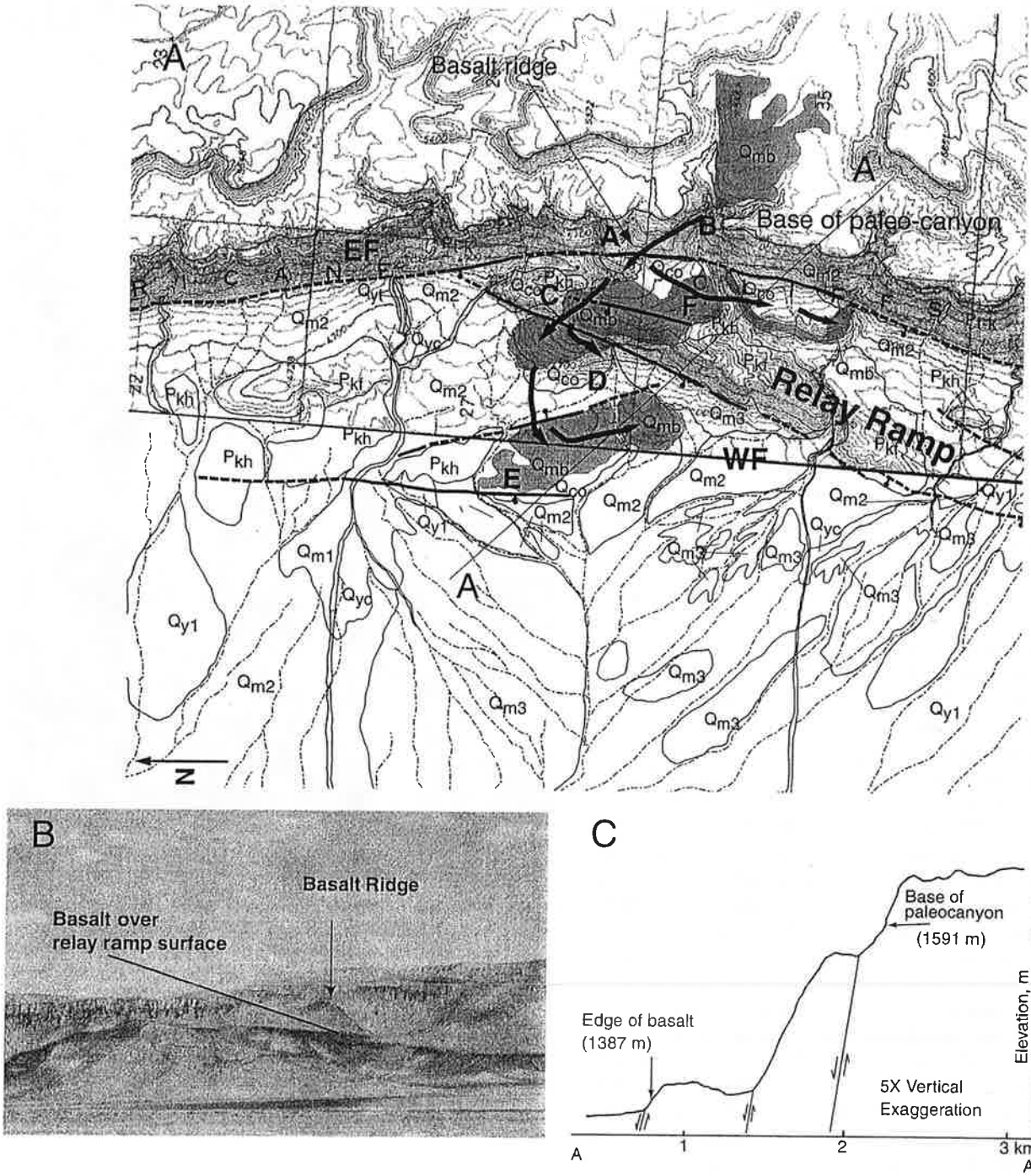

Figure 7. (A) Geologic map showing the relation of the faults to the Moriah Knoll basalt (Qmb) and the mapped flow directions (heavy black arrows). Mapped surficial units: Pkh, Harrisburg Member of the Kaibab Formation; Pt-k, Permian Toroweap and Kaibab Formations undifferentiated; Qm1–3, from mid to late Pleistocene alluvium; Qy1, Holocene alluvium; Qco, Quaternary colluvium. The basalt flowed through a paleo-canyon, crossed the fault, and covered the relay ramp surface between the escarpment and the Pkf western ridge of the relay ramp until the ridge was overtopped and the basalt flowed further northwest (B). The basalt flow directions, estimated from flow thickness, are shown by heavy black arrows. A–A′ is the location of the cross-section C. The letters on the map (A through F, EF, WF) refer to locations discussed in the text. (B) Photograph looking NE toward the Hurricane Cliffs, note the relay ramp and basalt flow that crossed the escarpment, flowed across the relay ramp, to the valley floor. (C) Cross section A–A′ showing the estimation of maximum vertical displacement of the Moriah Knoll basalt.

STOP at overlook and talked about the grand Staircase we could see Permian → Paleocene ≈ 200 mys

Field Guide to Permian Rocks of Grand Canyon and Sedona Areas, North-Central Arizona

Ronald C. Blakey *Department of Geology, Northern Arizona University, Flagstaff, AZ 86011*

Larry T. Middleton *Department of Geology, Northern Arizona University, Flagstaff, AZ 86011*

INTRODUCTION AND REGIONAL SETTING

Permian rocks of the southern Western Interior of the United States occupied the west-central margin of the supercontinent Pangea (Fig. 1) in an area that was part of a vast arid climate zone (Parrish and Peterson, 1988). The culmination of the assembly of Pangea resulted in the extensive Marathon-Ouachita-Appalachian mountain chain 800 km south and southeast of the study area. Stresses from continental collisions caused fracturing and local uplift of the North American craton including the Ancestral Rocky Mountains (Kluth and Coney, 1981), adjacent to and east of the study area (Fig. 2). Meanwhile, the long-established passive margin of western North America was evolving into the active Cordilleran margin. Thus, the southern Western Interior formed a southwest-tapered extension of cratonic North America bordered to the southeast, south, and west by active tectonic terranes and to the east by uplift on the craton. The field area escaped strong tectonism but was the site of minor tectonic and epeirogenic movements in the form of upwarps/arches and intervening basins (Armin, 1987). Late Paleozoic glacially controlled eustatic cycles (Ross and Ross, 1988) were superimposed on this complex tectonic and arid climatic regime.

The arid climate and abundant clastic sediment sources contributed to the widespread eolian deposition. Eolian deposits formed in environments that ranged from eolian sand sheets and coastal dune fields to vast coastal and inland ergs (eolian sand seas). Tectonic and eustatic controls strongly influenced the details of eolian sediment dispersal, distribution, geometry, and preservation (Blakey, 1988; 1996; Blakey et al., 1988). Eolian deposits are intimately interbedded with fluvial, sabkha, coastal-plain, and shallow marine deposits.

Permian rocks of the field area (Fig. 3), though sparsely fossiliferous and subject to abrupt facies changes, have been correlated in moderate detail based on locally excellent and continuous exposures and detailed stratigraphic analysis (Figs. 4,5). The correlations and nomenclature presented in this paper follow those of Blakey (1988), Blakey et al. (1988), Blakey and Knepp (1989), and Blakey (1990a).

Blakey (1996) recognized and correlated four widespread and prominent unconformities (Fig. 6). The unconformities are given letter designations as follows: P-O (base of Permian), P-sc (base of Schnebly Hill Formation or Coconino Sandstone), P-tw (base of Toroweap Formation or White Rim Sandstone), P-k (base of Kaibab Formation).

Modern sedimentological studies have been published on each of the Permian deposits in the study area. A summary of these studies and their interpretations is briefly summarized in Figure 6.

PERMIAN ROCKS IN GRAND CANYON

Permian strata are exposed throughout Grand Canyon and, and with coeval strata in the Sedona - Oak Creek Canyon area, record a complex interplay of eolian, fluvial, and nearshore marine processes. The Permian succession comprises the Esplanade Sandstone of the Supai Group, Hermit Formation, Coconino Sandstone, and the Toroweap and Kaibab Formations. The latter forms the prominent cap rock throughout Grand Canyon. This part of the field trip will focus on the Coconino, Toroweap, and Kaibab formations. We will examine sedimentological characteristics of each unit and discuss their significance with respect to depositional settings and regional paleogeography. Each of the units exhibit major features that developed in response to regional climatic, eustatic, and tectonic events.

17

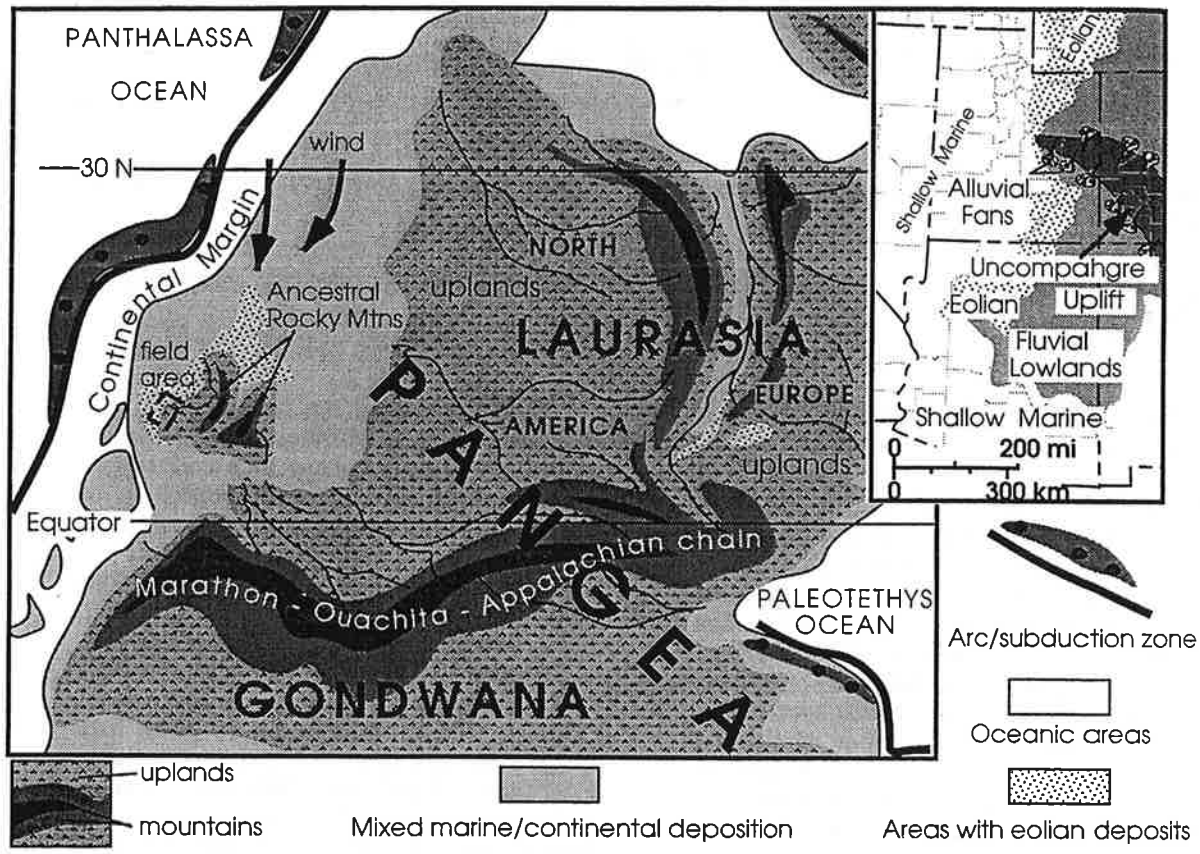

Figure 1. Generalized Permian paleogeographic and tectonic map of North America.

Esplanade Sandstone

The Esplanade Sandstone of the Supai Group crops out throughout Grand Canyon where it forms a prominent cliff beneath the less resistant Hermit Formation and in western Grand Canyon forms broad platforms, hence the name esplanade (Fig. 7). Although the thickness of the Esplanade varies throughout the Grand Canyon, the unit averages about 280 ft (92 m) thick (McKee, 1982).

In the Grand Canyon the basal third of the formation comprises slope-forming, fine-grained units that are overlain by a thick, cliff-forming, sandstone-dominated sequence (Fig. 8). The basal slope-forming sequence is heterogeneous, consisting of reddish, thinly bedded sandstones, mudstones and subordinate carbonates. The prominent cliff-forming sandstone contains abundant sedimentary structures including upward-coarsening ripple laminae, avalanche deposits (sand-flow strata) and small-large-scale trough and planar-tabular cross stratification that indicate a complex depositional arena.

The depositional settings in which the Esplanade accumulated include both nearshore marine and continental environments (McKee, 1982). The slope-forming basal part of the Esplanade likely was deposited in shallow shelf areas, although little work has been done on the unit . Stratification styles within the upper cliff-forming sandstone, however, strongly indicate deposition in eolian settings (Blakey, 1990a). These include the upward-coarsening laminae that are the products of wind ripple migration (Hunter, 1977), presence of down-foreset tapering of sand flows, that represent avalanche deposits, and rare suspension-deposited laminae (grain fall deposits). Other features such as wavy laminae and disrupted laminae suggest periodic flooding and reworking of these windblown deposits. Thus, the upper sandstones in the Esplanade likely record deposition in a coastal dune complex that experienced episodic flooding of dune and interdunal areas. An increase in plant fragments and vertebrate tracks and trails in outcrops in central parts of the Grand Canyon (McKee, 1982) and also in Marble Canyon likewise attest to deposition in

Marilyn told us about nocturnal giraffes.

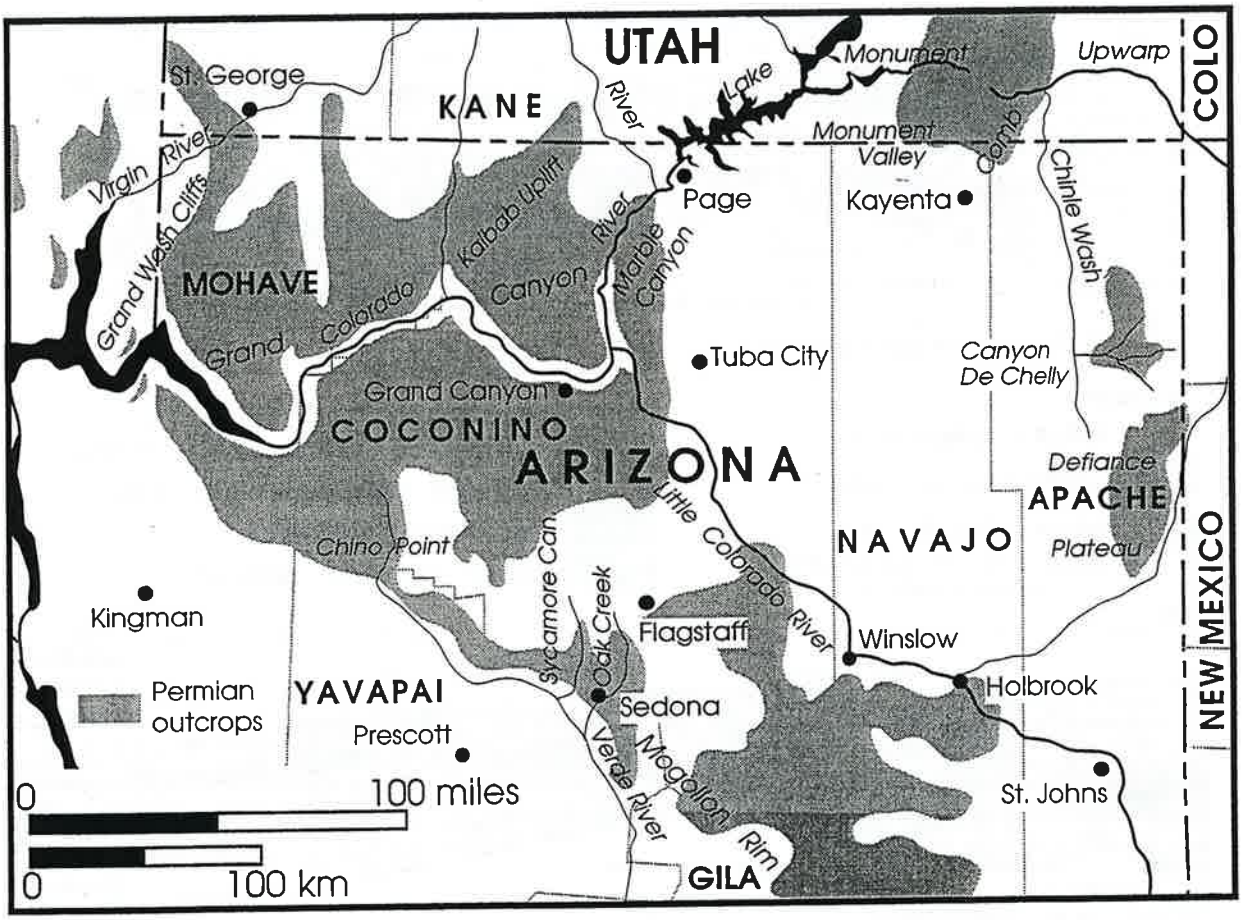

Figure 3. Permian outcrops (gray) in northern Arizona

westward thickening with sections in western Grand Canyon up to 1000 feet (300 m) thick (Beus, 1987).

In the Grand Canyon the Hermit comprises red-brown mudstones and subordinate, intercalated, thin-bedded sandstone (McKee, 1982). Deposition occurred in broad, shallow channels that likely were ephemeral to well established, channelized high sinuosity streams. The ephemeral nature of many channel complexes is indicated by the presence of planar bedded sandstone and presence of rip-up, intraformational mudstone clasts. Presence of large-scale inclined strata containing both trough and ripple cross stratification indicate that some of the Hermit stream systems were localized incised, of high sinuosity, and perennial. The latter represent the deposits of side and point bars. The best examples of these are seen in the Sedona area (Day 2). Many of the channelized sandstone deposits contain pedogenetically modified overbank fine-grained siliciclastics and carbonates. The carbonates occur as discrete nodules at the base of many sandstones and reflect prolonged periods of channel stability and a semi-arid environment. There are numerous intraformational carbonate conglomerates in the Hermit Formation composed of carbonate clasts that indicate the erosion of bank-margin calcic paleosols. These will be best be seen in the stops in the Oak Creek Canyon. Few other indicators of arid climatic conditions have been reported from the Hermit Formation. Blakey (1990b), however, reports wind ripple laminae from sandstones near the base of the Hermit Formation, indicating the onset of increasingly arid environments.

The upper contact of the Hermit with the Coconino Sandstone in Grand Canyon is sharp and represents a prolonged hiatus in deposition and also erosion preceding the southward incursion of the Coconino sand sea.

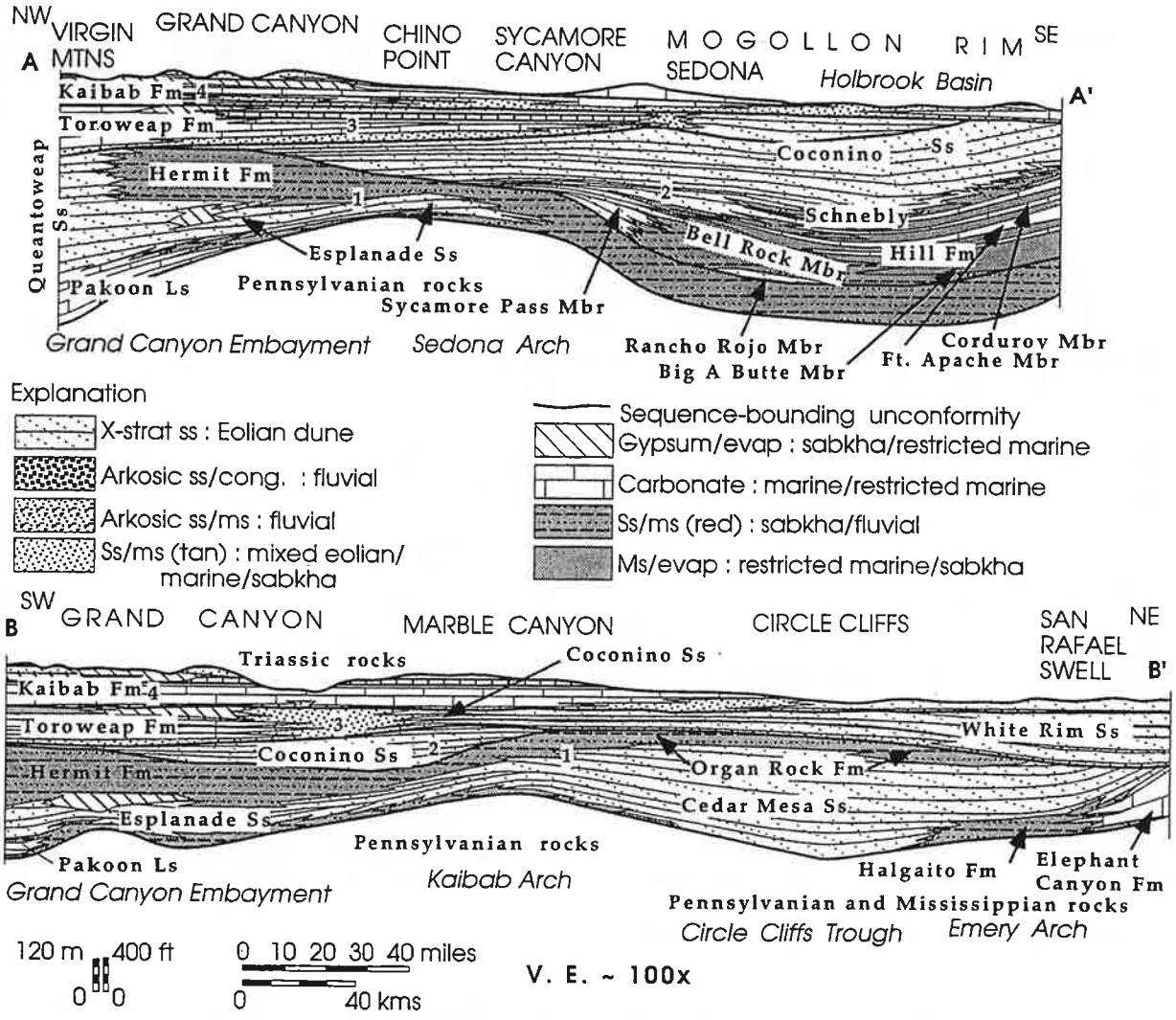

Figure 4. Stratigraphic cross sections of Permian strata on Colorado Plateau. Numbers 1 - 4 refer to sequences and locations of cross sections are shown on Figure 2.

Coconino Sandstone

One of the most distinctive units in the Grand Canyon is the early Permian (Leonardian) Coconino Sandstone (Fig. 10). Extraordinary exposures occur throughout the Grand Canyon region and extend into central Arizona (Fig. 11). The large-scale cross stratified sandstone is easily identifiable along the canyon walls and forms a pronounced marker horizon in the Permian succession. Regional stratigraphic relationships have been established by McKee (1933), Blakey and Knepp (1989), Blakey et al. (1988), and Blakey (1996). Surprisingly, comparatively few sedimentologic analyses have been conducted (McKee, 1933; Middleton et al., 1990).

Thickness of the Coconino is variable across the outcrop belt, thinning to the west in Grand Canyon and thickening to the south in the Sedona - Oak Creek Canyon area. The Coconino is 600 feet (180 m) thick in the eastern part of Grand Canyon thinning to 65 feet (20 m) near Lake Mead and to 60 feet (18 m) in Marble Canyon. The Coconino pinches out near the Arizona - Utah border. Along the Mogollon Rim in the Sedona area the formation is at least 1000 feet (305 m) thick (McKee, 1933). The increase in thickness of the Coconino to the south is related to increased rates of subsidence but also might reflect intertonguing of the Toroweap Formation with the Coconino.

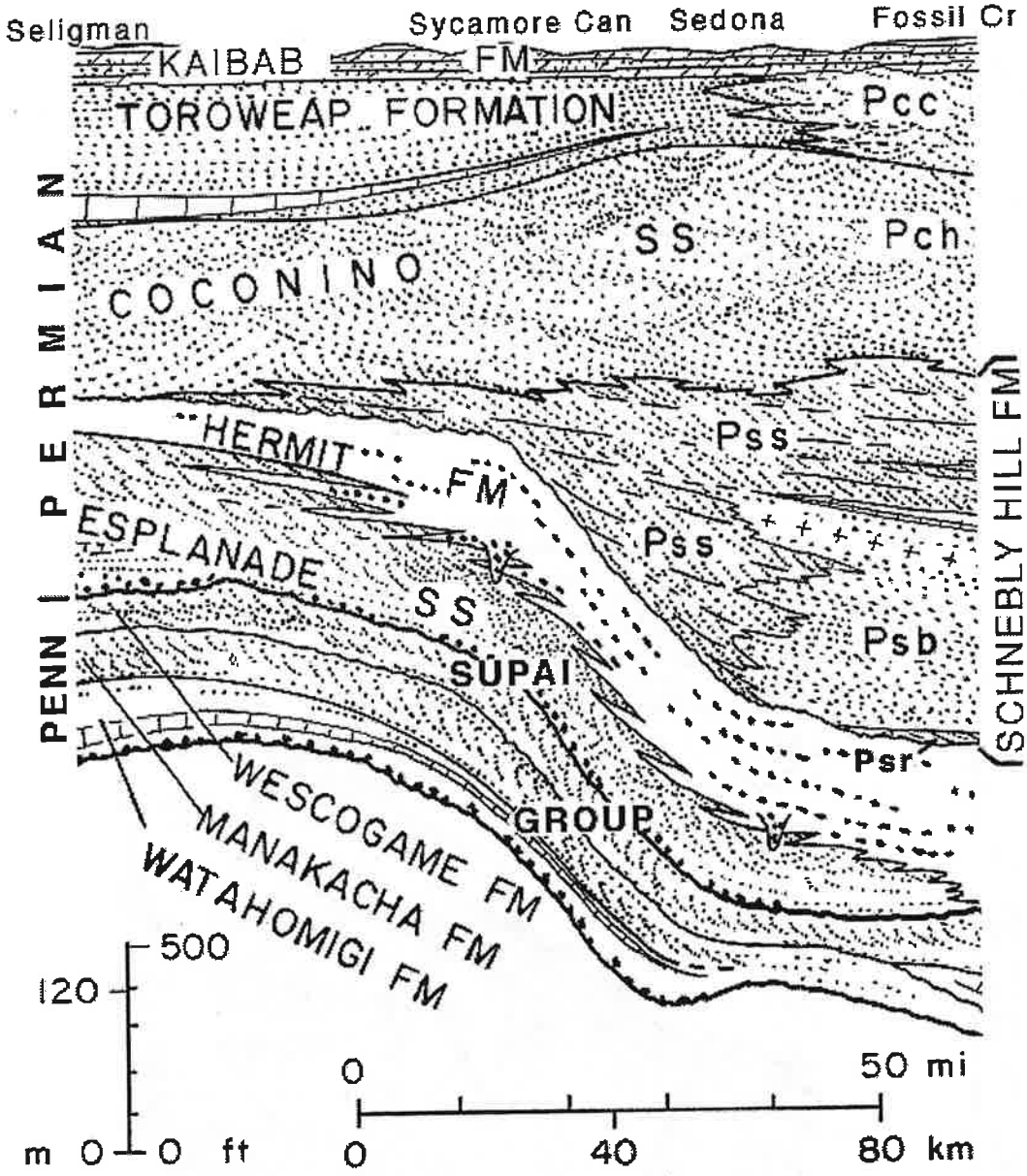

Figure 5. Lithologic and thickness relations of Penn-Permian strata in north-central Arizona.

Facies changes in both formations are similar and hence differentiation between the two is difficult. Blakey and Knepp (1989) proposed that these thickness variations are controlled to some extent by regional tectonic elements most notably the Sedona Arch and Holbrook basin (Fig. 2). An eolian origin for the Coconino Sandstone has been supported by sedimentologic and stratigraphic analyses (McKee 1933; Middleton et al., 1990). Middleton et al. (1990) provide a comprehensive discussion of the depositional systems. The Coconino is composed of well rounded and well sorted, fine- to medium-grained sand. Mineralogically, the unit is a quartz arenite with minor amounts of potassium feldspar. Although this degree of textural and mineralogic maturity is attainable in high energy, nearshore environments, facies sequences and regional stratigraphic patterns indicate that the Coconino represents a widespread sand sea or erg; the first major sand sea to develop during the Phanerozoic on the

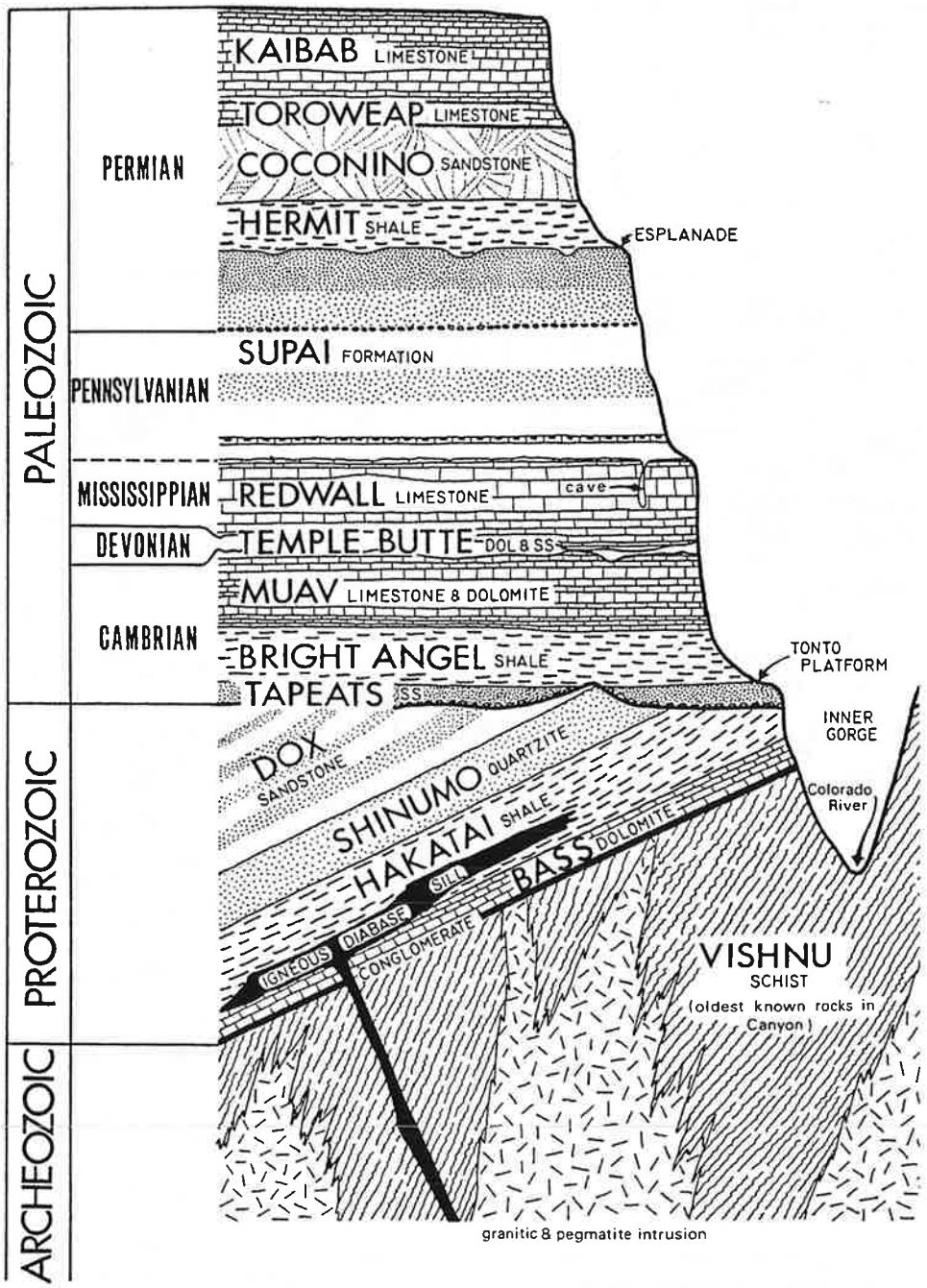

Figure 13. Cross section of crystalline and sedimentary rocks of Proterozoic age and the Paleozoic succession in eastern Grand Canyon. A pronounced unconformity separates younger Precambrian strata of the Unkar Group from the overlying Cambrian (from Breed and Roat, 1974).

EARLY AND MIDDLE JURASSIC PALEOGEOGRAPHY AND VOLCANOLOGY OF ARIZONA AND ADJACENT AREAS

Nancy R. Riggs and Ronald C. Blakey
Department of Geology
Northern Arizona University
Flagstaff, AZ 86011

ABSTRACT

Early to Middle Jurassic sedimentary rocks and their bounding unconformities on the Colorado Plateau in northern Arizona and southern Utah can be divided into six major sequences. These sequences, when coupled with coeval volcanic successions in the magmatic arc of southern and western Arizona and eastern California, provide a basis for tectonic interpretation of arc and back-arc regions.

Sequence 1 (Lower Jurassic Wingate Sandstone and Dinosaur Canyon member of the Moenave Formation) overlies the J-0 unconformity. Eolian and fluvial strata were deposited on a broad plain inclined gently from uplifted areas in the early magmatic arc.

The lower part of Sequence 2 (lower Kayenta Formation and Springdale Sandstone member of the Moenave Formation) overlies the sub-Kayenta unconformity. The Mogollon slope may have been close to the Colorado Plateau during deposition of Sequence 2, and the sources of streams draining into the Colorado Plateau were within a monsoonal belt as the Colorado Plateau drifted in an arid climate.

The upper part of Sequence 2 (upper Kayenta Formation and Navajo Sandstone) is overlain by the J-1 unconformity. Pronounced subsidence in the western Utah-Idaho trough contributed to preservation of tremendous thicknesses of eolian sandstone, and sand was driven as far south as the magmatic arc in southern Arizona. Widespread volcanic deposits of a similar age in southern Arizona reflect deposition in an extensional or transtensional environment. Numerous red bed deposits in these ranges may reflect periods of relative quiescence in arc activity, although the correlation of several units in southern Arizona is not confirmed.

Sequence 3 (Middle Jurassic Temple Cap Sandstone) lies between the J-1 and J-2 unconformities. The presence of numerous bentonite horizons within this eolian-sabkha unit indicates active volcanism, although fewer isotopic dates on volcanic rocks correspond to this time than to other sequences.

Sequence 4 (Lower Page Sandstone and Carmel Formation) was deposited in a time when volcanic activity may have reached a maximum. Bentonite horizons probably derived from explosive eruptions throughout the Mojave and Sonoran deserts are common in the Page Sandstone and Carmel Formation, and some uplift of the area south of the Colorado Plateau is indicated.

Sequence 5 (Upper Page Sandstone and Carmel and Entrada Formations) reflects a complex series of uplift and subsidence events across the Colorado Plateau and Utah-Idaho trough. Volcanism in the magmatic arc persisted well into this period.

Sequence 6 (Curtis Formation and Summerville and Romana Sandstones) reflects drying upward sequences that represent transgression and regression. Sequence 6 is truncated by the J-5 unconformity, which separates Middle from Upper Jurassic strata.

INTRODUCTION

The Mesozoic Cordilleran magmatic arc was originally referred to as an "Andean" arc (Burchfiel and Davis, 1972), evoking images of high-standing volcanic edifices, a well-developed fold-and-thrust belt, convergent tectonics, and a topographic barrier between arc and back-arc. Increasing evidence suggests that from Late Triassic or Early Jurassic time through at least early Middle Jurassic time, the northeastern portions of the arc were low-standing and occupied an extensional or transtensional regime.

We summarize here data from Arizona and southern Utah that form the basis of a paleogeographic reconstruction of the arc and back-arc during Late Triassic to Middle Jurassic time (Fig. 1). We have confined our synthesis of the magmatic arc to exposures west of approximately 110°30'. Controversies and debate are active in the following topics concerning paleogeography and tectonic reconstruction: 1) the height and continuity of the magmatic arc: low lying and discontinuous vs. high-standing and continuous topographic barrier; 2) the nature of the landscape between the arc and the present Jurassic outcrops on the Colorado Plateau: low featureless plains or gentle slopes vs. rugged highlands that strongly influenced streams in the back-arc area; 3) the distance between the magmatic arc and the back-arc area now represented by exposures on the Colorado Plateau: modern-day configuration vs. significant translation owing to late Mesozoic and Cenozoic tectonism; 4) the cor-

In Dunn, G., and McDougall, K., eds., 1993,
Mesozoic Paleogeography of the Western United States-II
Pacific Section SEPM, Book 71, p. 347-375

Figure 1. Map of the southern Colorado Plateau and adjacent Basin and Range showing locations referred to in text, line of sections in Figure 4, and restorations (after Marzolf, 1990; 1991) of selected ranges in southern Nevada and eastern California to pre-Cenozoic positions. Shaded line shows present approximate southern margin of Jurassic outcrops on the Colorado Plateau.

relation of rock units between the relatively stable back-arc and the active magmatic arc: correlation of discrete formations and unconformities vs. tenuous correlations hampered by controversial lithostratigraphic and geochronologic dating.

We propose that the sequences we describe in general reflect drying-upward cycles. Drying and wetting refer here to sedimentological, not climatological, trends (e.g. Clemmensen and others, 1989). A sequence that dries upward contains, for example, sabkha deposits overlain by dune deposits, or perennial stream deposits overlain by ephemeral stream deposits or dunes.

Paleogeographic reconstruction of this part of the Mesozoic orogen contributes to an understanding of the tectonic forces active in the arc and backarc regions, and how patterns of sedimentation across the region were affected by these forces.

Early and Middle Jurassic Time Scales

Controversy surrounding correlation of stratigraphic units, especially eolianites, between the magmatic arc province and Colorado Plateau may stem in part from uncertainties in the various chronostratigraphic time scales. The time scales of Haq and others (1988) and Harland and others (1990) are very similar for Lower and Middle Jurassic time (Fig. 2), but deviate considerably for Upper Jurassic time. We have therefore adopted the Harland and others (1990) scale throughout this paper. Biostratigraphic zones of Imlay (1980) are shown and correlated with the chronostratigraphic scale of Harland and others (1990; Fig. 1).

Additional precision is added to the Middle Jurassic portion of the time scale by $^{40}Ar/^{39}Ar$ dates by Everett and others (1989) on bentonite ash from the Judd Hollow Member of the Carmel Formation (Co-op Creek Member of Doelling and others, 1989). Limestone beds containing several ash beds in the Judd Hollow Member contain Bajocian/Bathonian marine fauna (Imlay, 1980).

REGIONAL STRATIGRAPHY

Mesozoic volcanic and sedimentary rocks were deposited on a basement of Proterozoic metamorphic and plutonic rocks overlain by Paleozoic stable-margin platform/shelf sedimentary rocks. The northeast-trending passive margin was truncated in late Paleozoic time (Walker, 1988; Stone and Stevens, 1988), and a superposed northwest trend dominated the configuration of the continental margin during Jurassic time and has been maintained to present time. This northwest trend strongly affected tectonic elements (Fig. 3) that in turn controlled certain aspects of sedimentation, including loci of deposition and source areas.

Lower and Middle Jurassic Strata, Colorado Plateau and Vicinity

Introduction

The correlation and depositional history of the Lower Jurassic Glen Canyon Group and the Middle Jurassic San Rafael Group has received thorough recent examination (Peterson and Pipiringos, 1979; Pipiringos and O'Sullivan, 1979; Blakey, 1988, 1989; Blakey and others, 1988; Peterson, 1988a). We briefly review these studies and focus on the interpretation of the several depositional sequences and the unconformities. The sequences, their internal lithostratigraphic composition, and bounding unconformities are shown on Figure 4.

Lower Glen Canyon Group [J-0 to J-sub-Kayenta (J-sub-Kay) unconformities].

J-0 Unconformity

The J-0 unconformity (Pipiringos and O'Sullivan, 1979) marks the base of the Glen Canyon Group (as restricted by Dubiel, 1989) across the southern Colorado Plateau

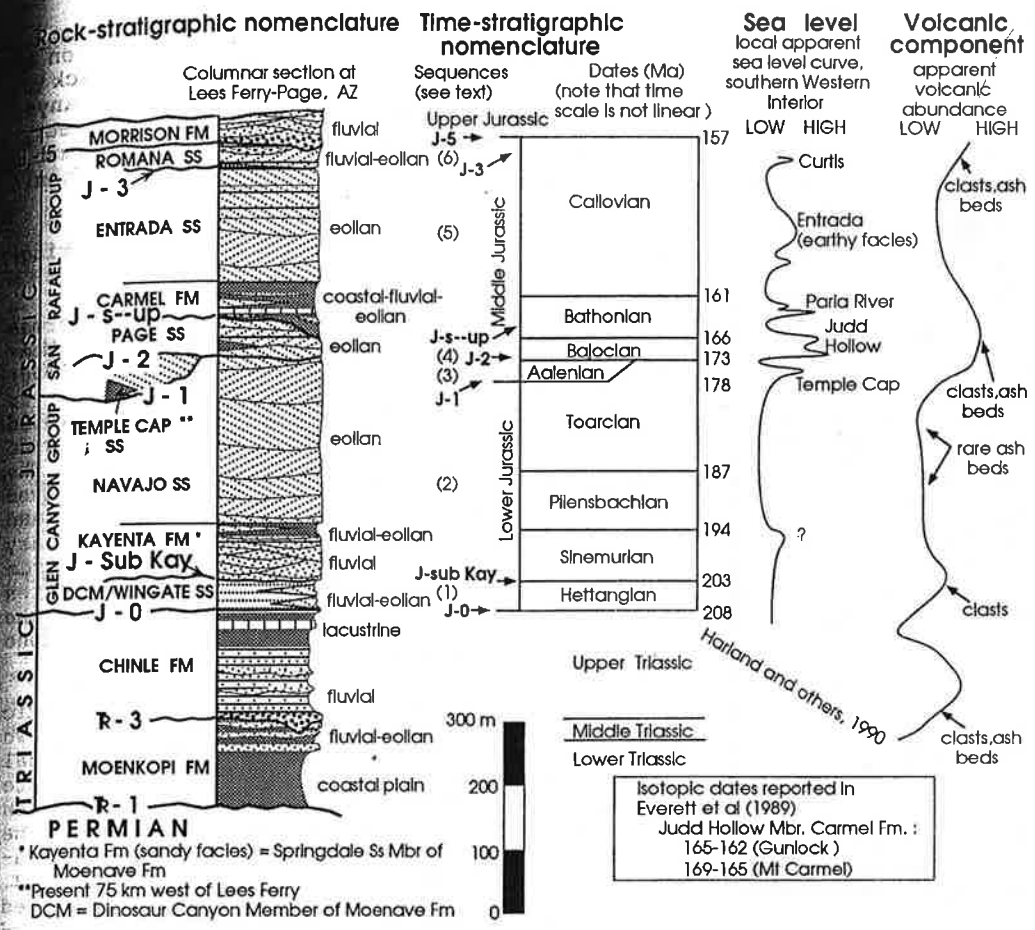

Figure 2. Rock- and time-stratigraphic nomenclature, apparent sea-level curve, and known volcanic components of Triassic and Jurassic rocks, southern Colorado Plateau.

Because strata in the overlying Moenave Formation contain Early Jurassic palynomorphs and the underlying Chinle Formation is considered entirely Late Triassic in age, the J-0 is believed to mark the Triassic-Jurassic boundary in this region (Peterson and Pipiringos, 1979).

The J-0 is regionally a low-angle unconformity (Blakey, 1990; Marzolf, 1991; Fig. 5). As much as 24 m of basal conglomerate in the Moenave-Kayenta formation (undivided) overlies the J-0 unconformity west of the present Colorado Plateau near Las Vegas, and Marzolf (1991) has traced it into the arc terrane of southeastern California where it overlies Paleozoic rocks in the Cowhole Mountains (Fig. 1). Reynolds and others (1989) reported that Jurassic rocks in the Buckskin-Harquahala area of western Arizona rest unconformably on rocks ranging from Proterozoic to Middle(?) Triassic in age. In general, the low-angle discordance of the J-0 across the Colorado Plateau suggests gentle epeirogenic up-to-the-southwest tilting of the region (Blakey, 1990). A few tens of kilometers off the west and southwest edges of the present Colorado Plateau, however, the J-0 represents sharp orogenic uplift (Marzolf, 1991; Reynolds and others, 1989). This tectonic activity may represent upwarping associated with the early stages of construction of the Mesozoic Cordilleran arc.

Wingate Sandstone and Dinosaur Canyon Member

The lower Glen Canyon Group comprises the eolian Wingate Sandstone (Blakey and others, 1988; Nation, 1990) and coeval ephemeral stream deposits of the Dinosaur Canyon Member of the Moenave Formation (Clemmensen and others, 1989). The two units are coeval facies that intertongue along a northwest-trending alignment roughly coincident with the Zuni lineament (Blakey, 1988). Northwest-flowing streams followed broad open terrain defined by remnants of the pre-J-0 uplift to the southwest and Wingate ergs to the northeast. The streams were deflected northward into the southern Utah-Idaho trough in southwestern Utah. Northerly to westerly winds deflated the stream courses and transported fine sand into the western and southern portions of the Wingate erg. The nearly opposite paleocurrent flow of the fluvial-eolian transportation systems probably trapped much of the sediment on the south-central Colorado Plateau (Blakey and others, 1992). Northwest-moving fluvial sediment was blown back to the southeast and sand that escaped the Wingate erg was recycled northward by Moenave streams (Fig. 6).

North of Flagstaff, Arizona, volcanic granules occur in the Dinosaur Canyon Member. Although these grains have been neither dated isotopically nor studied petrographically, paleocurrent data in fluvial deposits suggest that they were derived from volcanic rocks to the south.

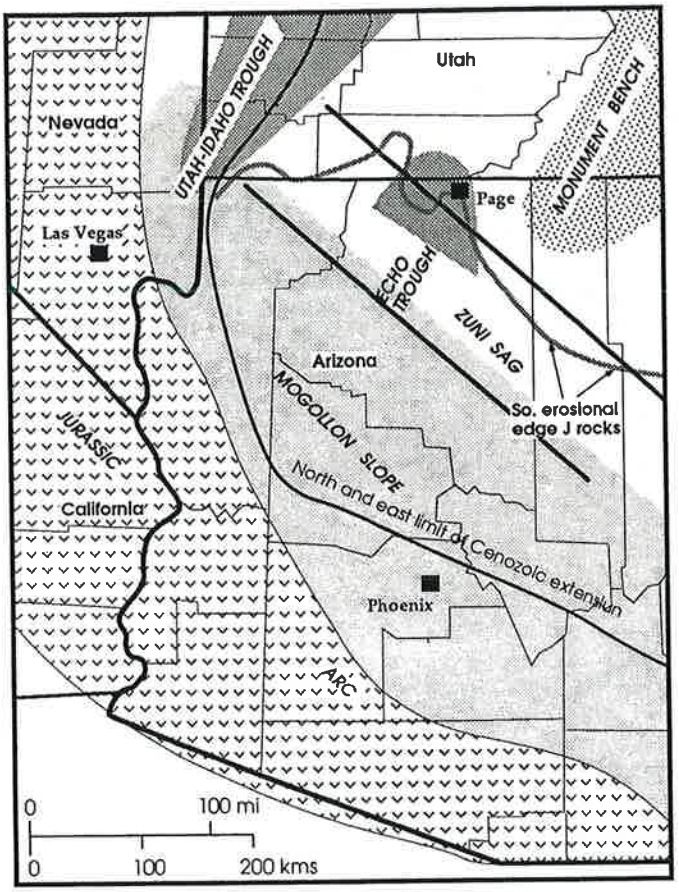

Figure 3. Generalized Early and Middle Jurassic tectonic elements. Northeastern extent of arc reconstruction after Marzolf (1990, 1991). The north and east limit of Cenozoic extension theoretically marks the maximum possible northeastward extent of the arc as no known Jurassic intrusions occur in non-extended rocks.

Upper Glen Canyon Group (J-sub-Kayenta to J-1 unconformities)

Sub-Kayenta Unconformity

Nation (1990) and Clemmensen and others (1989) document that appreciable erosion affected the top of the Wingate Sandstone - Moenave Formation sequence. This contact has local relief of up to 15 m but lacks any angular discordance (Fig. 4). Evidence supporting an unconformity includes the presence of silcrete with extensive burrows, roots, tree trunks, and soil horizons northeast of Flagstaff (Edwards, 1985). The unconformity is present across most of the Colorado Plateau; its extent to the west is unknown, and eastward it is truncated by younger unconformities. According to F. Peterson (pers. communication, 1993), there is no evidence indicating an unconformity at this stratigraphic position in the Uinta Mountains of northern Utah.

The sub-Kayenta unconformity represents a period of downcutting of unknown, but probably short, duration following deposition of the lower Glen Canyon Group. The lack of angularity (the Wingate-Dinosaur Canyon isopach has a irregular, sheet-like geometry) suggests a fall in base level or climatic changes rather than significant tectonic uplift.

Kayenta Formation (sandy facies) and Springdale Sandstone

The sandy facies of the Kayenta Formation and equivalent Springdale Sandstone Member of the Moenave Formation (Blakey, 1990) define a widespread sandy perennial to locally ephemeral stream system that flowed west to northwest across much of the Colorado Plateau (Luttrell, 1985; Bromley, 1991). The large, mature, perennial streams were derived well east of the Colorado Plateau, and entrained sediment from older sedimentary rocks as well as Precambrian clasts from small remnants of the Ancestral Rockies (Luttrell, 1985). The upper contact of the Kayenta Formation with the Navajo Sandstone is gradational and intertonguing.

It is paradoxical that a mature dynamic fluvial system would be encased between two major eolian deposits. Scoured erosional features at the top of the underlying Wingate Sandstone, together with sandstone clasts in the Kayenta Formation likely derived from the Wingate Sandstone, strongly suggest cementation of the older eolian deposits (M.J. Nation, personal commun., 1992). Coupled with recognition of the sub-Kayenta unconformity, this suggests that Kayenta streams flowed across bedrock and did not erode through loose sand.

As Kayenta streams flowed westward across the porous Wingate Sandstone and across a semi-arid to arid region, water loss downstream contributed to more ephemeral structural characteristics such as smaller and fewer cross beds and an increase in planar (upper flow regime) stratification. The last remnants of the Springdale Sandstone occur near the edge of the Colorado Plateau at St. George, Utah (Fig. 7). Only the southern margin of the Kayenta/Springdale system is clearly defined. South of the pinchout near Tuba City, Arizona, the sub-Kayenta unconformity is marked by extensive silcrete deposits.

The cause of the great influx of perennial fluvial systems onto the Colorado Plateau during the arid Jurassic Period is unknown but we speculate a climatic cause. During the break-up of Pangea, the Colorado Plateau "drifted" northward through the monsoonal belt several degrees north of the equator (Late Triassic Megamonsoon of Dubiel and others, 1991). The Plateau was under the arid influence of the subtropical high during most of Jurassic time (Parrish, 1992). Areas to the south and east, however, may still have been under the monsoonal belt. Perhaps the western tilt of the Colorado Plateau (as documented by paleostream flow) during this time coupled with undocumented tectonic tilting southeast of the study area (rejuvenation

mediately south of the restored transect in Buckskin Mountains (Reynolds and others,).

SYNTHESIS

Introduction and Terminology

The six Lower and Middle Jurassic sedimentary sequences and their bounding unconformities provide the foundation for a tectonic synthesis. For each of these sequences, we have established: 1) a regional belt, 2) distribution of volcanic ash and clasts, 3) general paleoenvironmental setting, and 4) relation between preserved sedimentary and volcanic rocks and tectonic elements. These factors, isotopic dates from arc rocks, distribution (and reconstruction) of arc rocks, and petrographic and structural data from the arc, can be synthesized into a comprehensive analysis of the western Colorado Plateau and adjacent arc terrane (Figs. 21, 22). The details gleaned from the tectonic interpretation of rocks on the Colorado Plateau provide a basis for the extrapolation of tectonic events into the structurally complex and less well understood arc terrane. We have attempted to keep tectonic terminology to a minimum. Although a number of tectonic elements have been named and recognized as being active during Jurassic time (Peterson, 1988a, 1988b; Blakey, 1988), the following were most influential and are used in the ensuing synthesis, and are shown on Figure 3.

1) The Utah-Idaho trough was a strongly topographically negative area in which subsidence rates either matched or exceeded sedimentation rates. The trough provided the pathway for several marine transgressions into dominantly continental sequences, and during continental episodes of sedimentation it was a locus of north-directed stream deposition.

2) The Mogollon slope (Bilodeau, 1986) was apparently a gently inclined buttress along the southern margin of the Colorado Plateau. At times a gentle slope confined northwesterly flowing streams that entered the Colorado Plateau from the south. More rarely, the slope was steeper, and vigorous streams that drained mountainous terrain to the south or southeast flowed across it. During times in which an extensional arc terrain is envisioned, we speculate that Mogollon slope was a topographic rift shoulder or a low arch between the arc graben-depression and the back arc or Colorado Plateau region. Before establishment of the extensional/transtensional regime, the southward termination of the Mogollon slope may have been primary volcanic highlands. The slope was not a hindrance to ergs that periodically migrated southward into the arc (Bilodeau, 1986).

3) The Monument bench subsided at a slower rate than areas to the south and west. Throughout lower Middle Jurassic time, younger deposits onlapped the gentle west-dipping plain (manifested as the J-2 erosion surface) and eventually buried it in early Callovian time (Fig. 20).

4) The Echo trough (King and Blakey, 1991) was a rapidly subsiding feature in Middle Jurassic time. Present-day erosion truncates the Page Sandstone and upper member of the Carmel Formation, but isopach studies show a continuing thickening of these forma-

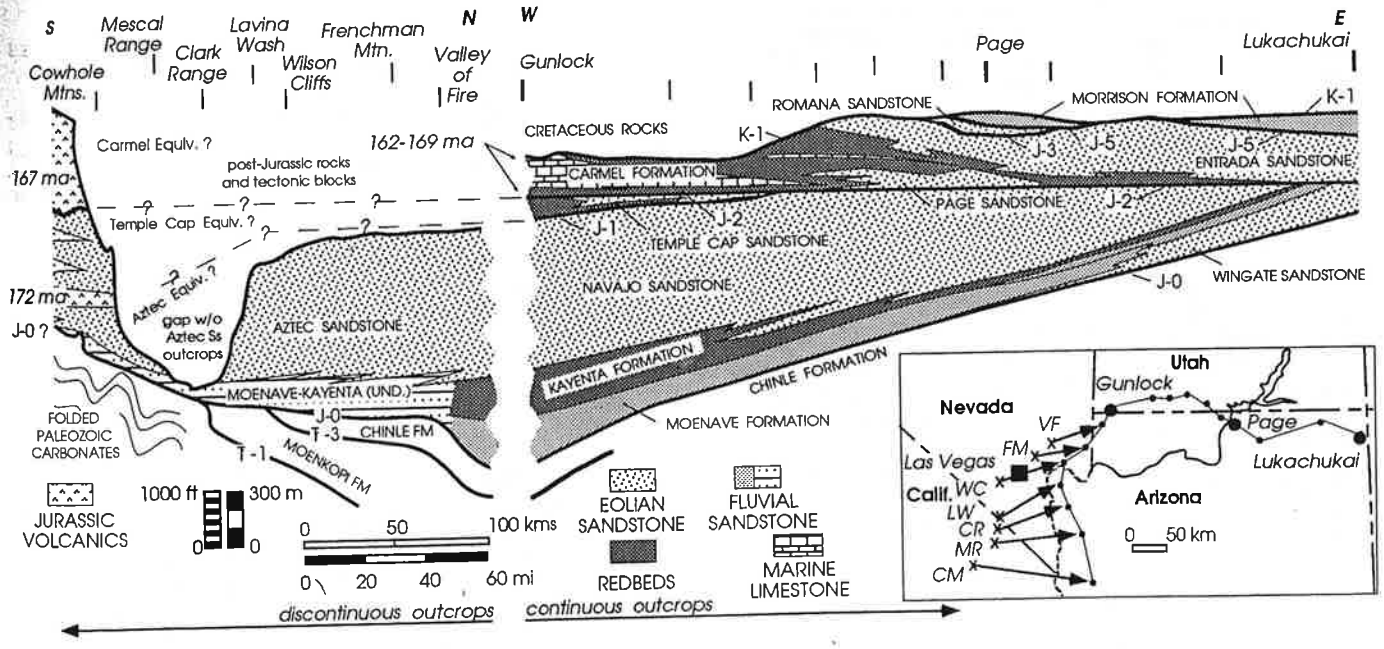

Figure 20. Restored and partly idealized cross section of Jurassic rocks from the Cowhole Mountains to Fort Defiance, Arizona. Correlation in the discontinuous outcrops south and west of the Colorado Plateau partly after Marzolf (1990, 1991); however, correlation of post-172 ma rocks in Cowhole Mountains to rocks on Colorado Plateau follows our suggestions discussed in text.

LATE CRETACOUS PALEOGEOGRAPHY OF THE SOUTHERN SEVIER FORELAND, SOUTHWEST UTAH, SOUTHERN NEVADA, AND NORTHWEST ARIZONA

Robert P. Fillmore
Department of Geology
University of Kansas
Lawrence, Kansas

ABSTRACT

Late Cretaceous sedimentary rocks in southwest Utah, southern Nevada, and northwest Arizona were deposited in a continental setting, in the proximal reaches of the southern sector of the Sevier foreland basin. These strata record deformation in the Sevier fold and thrust belt to the west, and provide insight into the evolution of this part of the foreland basin.

Sedimentologic and compositional data indicate that basal conglomerate throughout the study area was deposited on a regional pediment surface of Jurassic rock by east-flowing, bedload-dominated, braided fluvial systems. Abundant quartzite clasts suggest a provenance in the Wheeler-Gass Peak thrust system in the south, and the Wah Wah thrust in the north. In the northern part of the study area, at Three Peaks, Utah, north-flowing, mudflow-dominated fan deposits that interfinger with east-directed, quartzose fluvial deposits are interpreted to reflect incipient movement on the Iron Springs thrust.

Claystone, bentonitic tuff, fine-grained sandstone, and carbonate that overlie the basal conglomerate indicate a change to low-energy fluvial and paludal environments. The preservation of these deposits in a proximal foreland setting suggests continued subsidence and sediment starvation.

The last phase of Cretaceous basin evolution is marked by the eastward advancement of the thrust belt, and a change in regional drainage patterns. The change in drainage from an earlier east-flowing, transverse system to a north-northeast flowing system, parallel to the orogenic front, is attributed to increased subsidence caused by thrust loading. Compositional data from sandstone and conglomerate indicate erosion of Paleozoic carbonate rocks suggesting that eastward thrust migration was manifested by development of the Summit-Willow Tank and Muddy Mountain thrusts in the south, and the Blue Mountain and Escalante thrusts in the north.

INTRODUCTION

Late Cretaceous strata in southwest Utah, southern Nevada, and northwest Arizona were deposited in the proximal reaches of an extensive foreland basin that reached from northern Canada to southern Nevada (Fig. 1). These continental strata were deposited in the southernmost sector of the foreland, adjacent to the east-vergent Sevier fold and thrust belt that lay to the west and were a source for clastic material (Armstrong, 1968). Thus, these sediments provide a record of Late Cretaceous contractional deformation and associated basin evolution.

Previous studies of proximal Sevier foreland deposits have concentrated on strata to the north (e.g. Wiltschko and Dorr, 1983; Lawton, 1983, 1985, 1986; Dickinson and others, 1986; DeCelles, 1988). The southern sector, however, remained largely unstudied except for regional stratigraphic and structural studies (e.g. Bissell, 1952; Bohannon, 1983).

Strata in the study area include the Dakota and Iron Springs Formations, southwest Utah (Mackin, 1947; Fillmore and Middleton, 1989; Fillmore, 1991), the Willow Tank Formation and Baseline Sandstone in the Muddy Mountains of southern Nevada (Longwell, 1949; Fleck, 1970; Bohannon, 1983), and the Jacobs Ranch and Cottonwood Wash Formations of northwest Arizona (Moore, 1972) (Fig. 2). Correlations between these formations are dominantly based on stratigraphic position and lithologic character, in addition to radiometric and biostratigraphic data.

In this paper stratigraphic and sedimentologic data, including sediment dispersal patterns, and provenance of clastic facies, are used to reconstruct the regional paleogeography of the southern sector of the foreland. This paper builds on previous work on the Dakota and Iron Springs Formations (Fillmore and Middleton, 1989; Fillmore, 1991) with new data on Cretaceous strata in Nevada and Arizona to provide an expanded view of the regional paleogeography.

STRATIGRAPHY

Southwest Utah - Dakota Conglomerate and Iron Springs Formation

The study area in southwest Utah includes the Beaver Dam Mountains to the south, near the town of Gunlock, and the Three Peaks area (Fig. 2). Throughout this area upper Cretaceous strata rest unconformably on various members of the Jurassic Carmel Formation with up to 60 m of erosional relief (Hintze, 1986; Fig. 3). At Gunlock, conglomerate of the basal Dakota Formation ranges from 0 to 15 m in thickness and is separated from the overlying Iron Springs Formation by a 7-m-thick bentonitic

In Dunn, G., and McDougall, K., eds.,1993,
Mesozoic Paleogeography of the Western United States-II
Pacific Section SEPM, Book 71, p. 417-432.

28

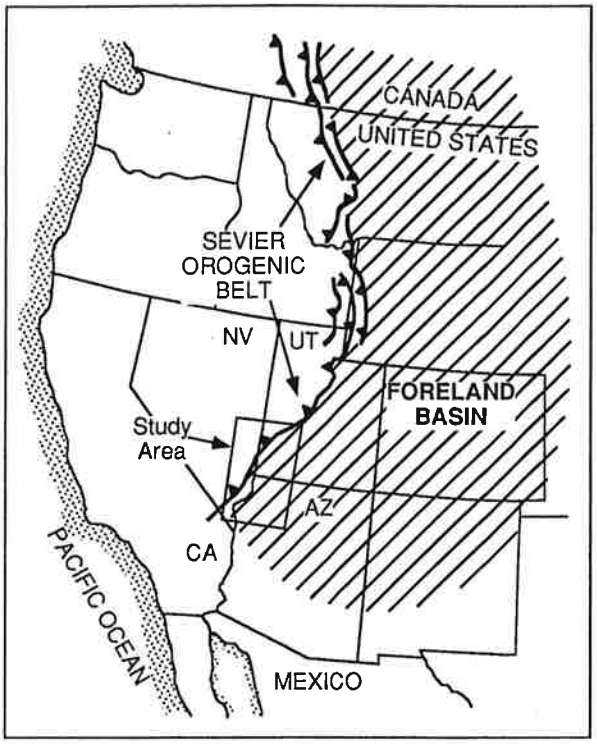

Figure 1. Map of western North America showing the study area and the extent of the Cretaceous Sevier orogenic belt and associated foreland basin.

tuff bed (Hintze, 1986). The sandstone-dominated Iron Springs Formation ranges to ~1000 m in thickness and grades upwards into, and intertongues with, the upper Cretaceous(?)-Paleocene(?) Grapevine Wash Formation (Wiley, 1963; Goldstrand, 1992), which is overlain by the Lower Tertiary Claron Formation.

At Three Peaks no Dakota Formation is recognized; the Iron Springs Formation is up to 830 m thick and consists of sandstone, siltstone, and conglomerate (Fillmore, 1991). Basal conglomeratic strata at Three Peaks, however, are interpreted to be correlative to the Dakota at Gunlock (Fillmore, 1991). The Iron Springs Formation is unconformably overlain by the Claron Formation (Mackin, 1947; Mackin and Rowley, 1976; Goldstrand, 1992).

Although the previously assigned Late Cretaceous age for these strata, based on stratigraphic correlation, was correct (Bissell, 1952; Van de Graff, 1963), recent data have provided significantly tighter constraints. A Cenomanian age for the fluviatile Dakota Formation in southwest Utah is based on correlation with fossiliferous fluvial and marine Dakota strata to the east, in south-central Utah (am Emde, 1991; Eaton, 1991). At Gunlock, Hintze (1986) reported an 80+/-10 Ma zircon fission track age from the bentonitic tuff that lies between the Dakota and Iron Springs Formations. Only the upper range of error for this fission track age fits the Cenomanian to Turonian age that is indicated by palynomorphs from lower Iron Springs strata at Gunlock (Hintze, 1986). Vertebrate fossils from the upper part of the formation, in the Pine Valley Mountains immediately east of Gunlock (Fig. 2), indicate a Santonian age (Eaton, 1992). No age data from the Three Peaks area have been obtained.

Southern Nevada - Willow Tank Formation and Baseline Sandstone.

In the Muddy Mountains, southern Nevada, the Willow Tank Formation lies unconformably on an erosional surface cut into the Jurassic Carmel Formation and Aztec Sandstone (Longwell, 1949; Bohannon, 1983). The Willow Tank Formation is ~80 m thick and consists of a basal conglomerate and a relatively thick sequence of claystone, siltstone, and carbonaceous shale. In the conformably overlying Baseline Sandstone three members are recognized (Fig. 3). The sandstone-dominated basal white member is conformably overlain by the red member, which is defined by its red color. To the north, in the North Muddy Mountains, the red member interfingers with the Overton Conglomerate Member. The Overton Conglomerate, over most of its extent, is conformable with the underlying white member, but locally is unconformable and angular (Bohannon, 1983). The Baseline Sandstone is overlain by the Miocene Horse Spring Formation (Bohannon, 1983).

The age of Cretaceous strata in southern Nevada is well-constrained, although a minimum age has not been established. Fleck (1970) reported K-Ar ages from tuffs in the Willow Tank Formation of 98.4 and 96.4 Ma, on the Albian-Cenomanian boundary (97.5 Ma, from the DNAG time scale of Palmer, 1983). Similarly, the occurrence of the fern *Tempskya* suggests an Albian age (Ash and Read, 1976). Tuffs in the lower white member of the Baseline Sandstone have yielded K-Ar ages of 95.8+/-3.5 and 96.9+/-3.6 Ma, and an age of 93.1+/-3.4 Ma has been obtained from the overlying red member (biotite concentrates; Carpenter and Carpenter, 1987). All age data from the Baseline Sandstone indicate a Cenomanian age.

Northwest Arizona - Jacobs Ranch and Cottonwood Wash Formations.

Cretaceous(?) strata in the Virgin Mountains, northwest Arizona, include the Jacobs Ranch Formation and the Cretaceous(?) or Eocene(?) Cottonwood Wash Formation (Moore, 1972). The Jacobs Ranch Formation unconformably overlies the Navajo (Aztec) Sandstone and is up to 90 m thick. The formation comprises a 2- to 6-m-thick basal conglomerate overlain by interbedded sandstone, siltstone, and conglomerate. The Cottonwood Wash Formation lies unconformably on the Jacobs Ranch Formation and comprises up to 425 m of conglomerate, tuff, and carbonate (Moore, 1972). Locally the contact exhibits an angular discordance of up to 15°, and where the Cottonwood Wash Formation truncates the Jacobs Ranch Formation, it rests on Navajo Sandstone (Moore, 1972).

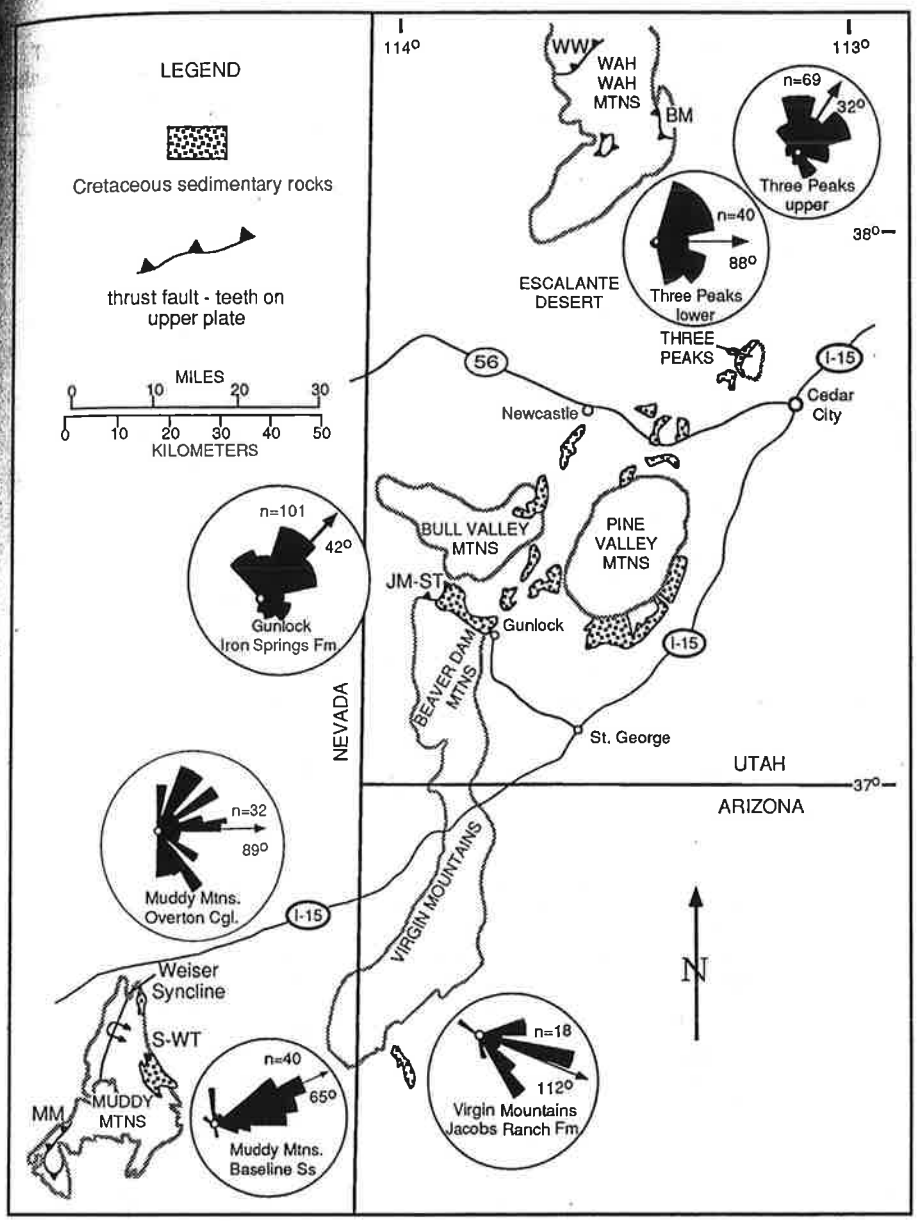

Figure 2. Map of the study area showing distribution of Cretaceous sedimentary rocks and thrust faults discussed in text. Rose diagrams show paleocurrent data with mean vector for each locality. WW: Wah Wah thrust; BM: Blue Mountain thrust; JM-ST: Jackson Mountain-Square Top thrust; S-WT: Summit-Willow Tank thrust; MM: Muddy Mountain thrust.

No age data are available for these strata, but based on stratigraphic location and lithologic character, Moore (1972) correlated the Jacobs Ranch Formation with the Willow Tank Formation and Baseline Sandstone in Nevada and the Iron Springs Formation in Utah. Moore (1972) correlated the Cottonwood Wash Formation with the Overton Conglomerate and the Horse Springs Formation in Nevada, and the Claron Formation in Utah. These correlations were made prior to the assignment of the Overton Conglomerate to the Baseline Sandstone and the establishment of a Miocene age for the Horse Spring Formation. Basal conglomerate of the Cottonwood Wash Formation is herein correlated with the Overton Conglomerate Member of the Baseline Sandstone based on stratigraphic, lithologic, and compositional similarities (Fig. 3). It is possible that the overlying tuff and carbonate is much younger than the basal conglomerate, and unrelated to foreland basin development.

METHODS

Interpretations of Late Cretaceous paleogeography reported in this paper are based on data obtained from detailed measured stratigraphic sections. Lithofacies analysis using facies associations and vertical successions are used to interpret depositional environments. Directional data from cross-stratification and clast imbrication are used to establish sediment dispersal patterns. These are used in conjunction with compositional data from modal analysis of thin-sectioned sandstone samples, and clast counts from conglomeratic units to determine the provenance of clastic facies.

Sandstone compositional data were obtained from point counts of 49 thin-sectioned Iron Springs Formation samples from the Three Peaks and Gunlock areas (Fillmore,

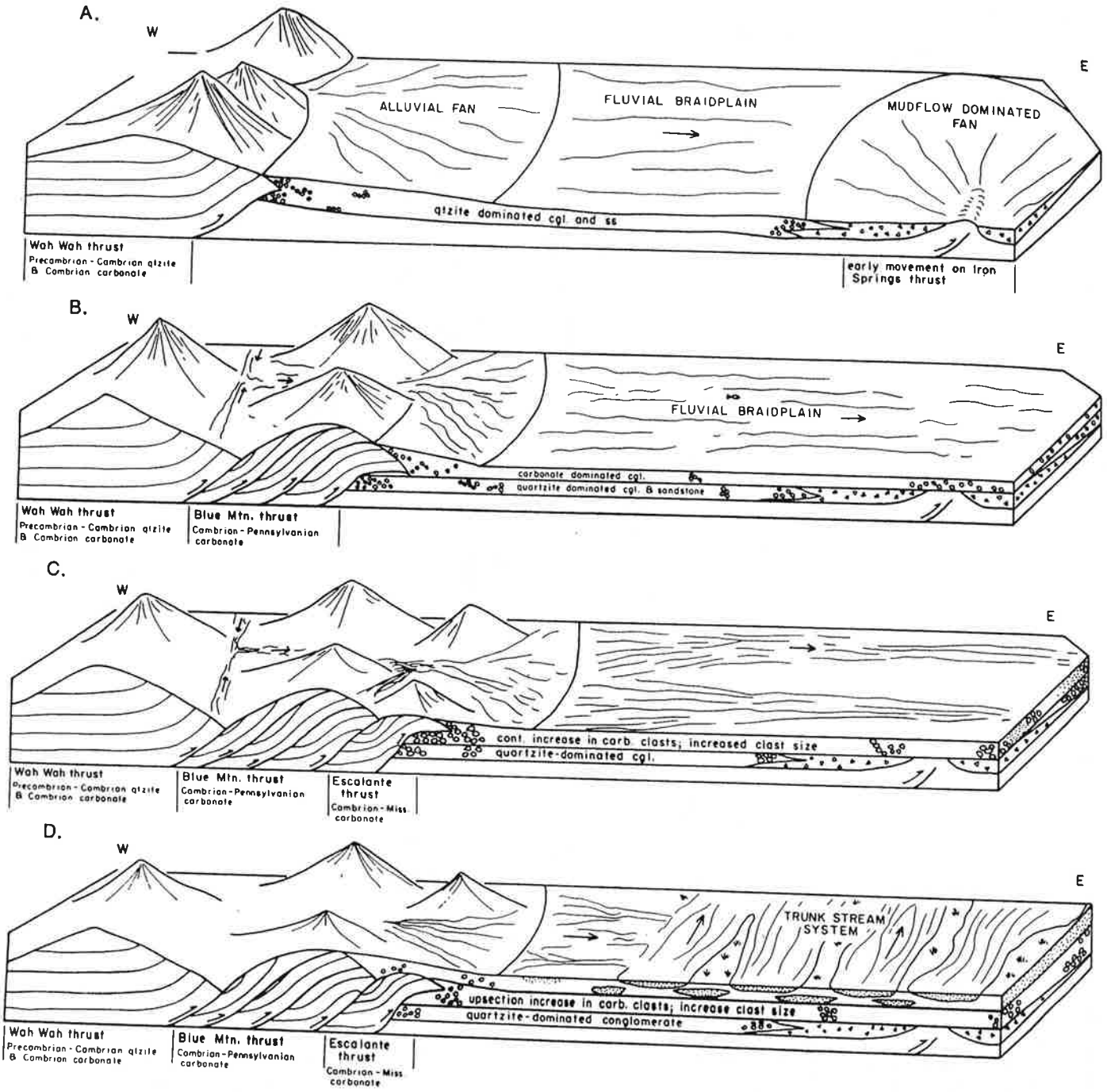

Figure 7. Tectonic evolution of thrust belt and depositional basin at Three Peaks. (A) Time 1: Uplift of the Wah Wah thrust producing quartzite conglomerate and subsurface movement on the incipient Iron Springs thrust, resulting in intrabasinal alluvial fan development. (B) Time 2: Ramping and erosion of the Blue Mountain thrust and influx of carbonate detritus into the basin. (C) Time 3: Escalante thrust as frontal expression of the thrust belt and coarsening of conglomerate due to eastward migration of tectonism. (D) Time 4: Development of trunk system in which flow parallels the strike of the Sevier mountain front (from Fillmore, 1991).

North America. We are incredibly fortunate that the rocks exposed in the Grand Canyon record this time period like no other place on the continent. This great chasm is truly a unique "window into the past."

The Grand Canyon (Fig. 1) lies entirely in the northwestern part of Arizona. It extends nearly 278 miles (448 kilometers) between Lake Powell on its eastern end and Lake Mead to the west. In 1919, the region became a national park, which today encompasses approximately 1900 square miles (4921 square kilometers) of land. This most famous of all canyons was formed by swiftly flowing waters of the Colorado River cutting into rock layers of the southwestern Colorado Plateau, a vast uplifted tableland that includes a large portion of the Four Corners states: Arizona, Colorado, New Mexico, and Utah. The land surrounding the Grand Canyon includes six local plateaus and one low lying platform, all of which are bounded by faults or monoclines (Fig. 2). In a west-east cross section to the north of the canyon

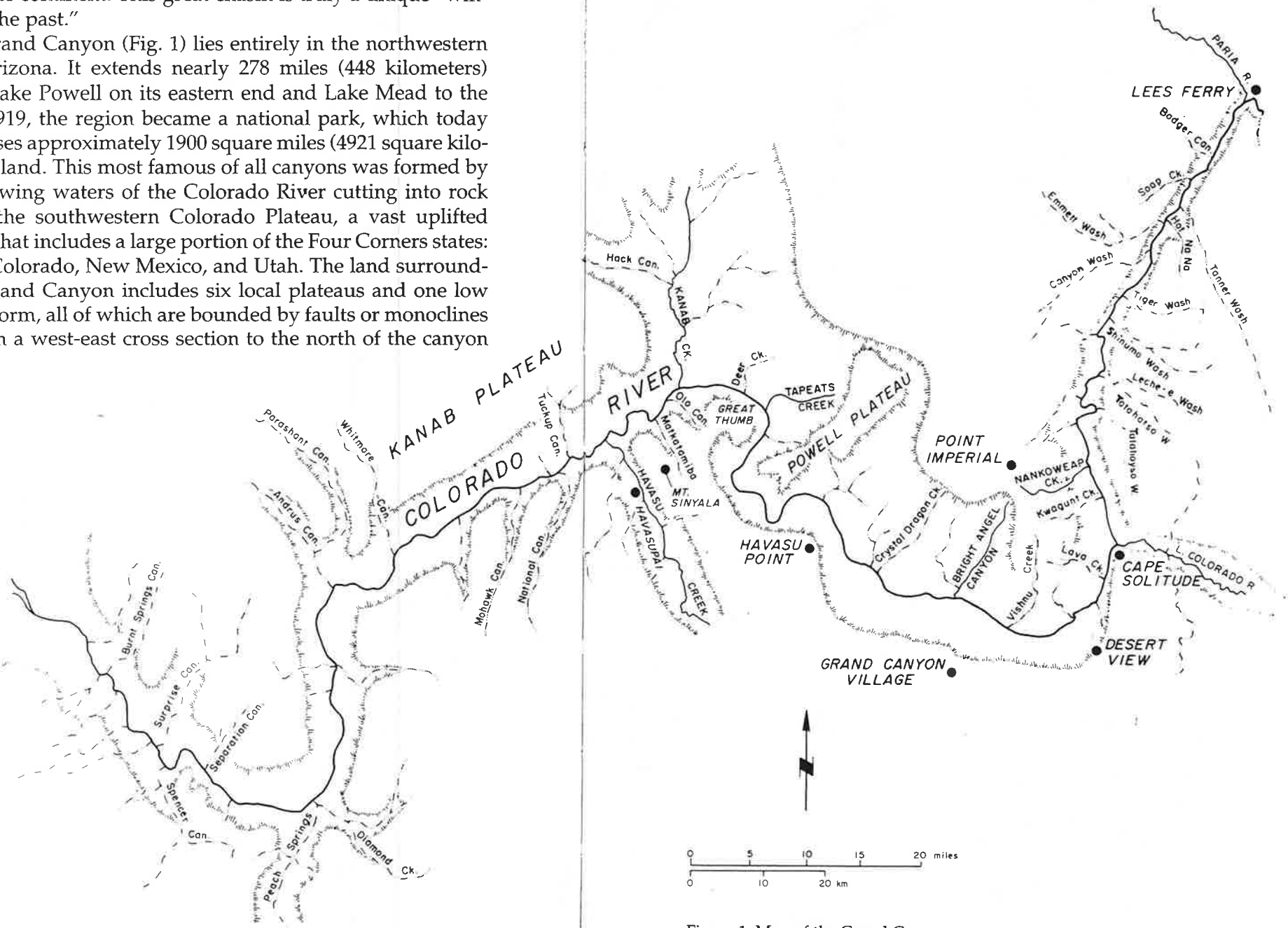

Figure 1. Map of the Grand Canyon

(Fig. 3), you can see how each of these blocks of land has been uplifted, downdropped, or tilted relative to its neighbor.

At its narrowest, the Grand Canyon is a little less than a mile (1.6 kilometers) across. Along the canyon's north and south rims, the relief is relatively gentle, except for incisions made by runoff waters flowing into the gorge. Within the canyon itself, however, the topography is quite varied and spectacular. The maximum depth of the canyon at any single place is about 6000 feet (1829 meters) from the rim to the floor. The maximum drop in elevation of the canyon as a whole, however, is approximately 6600 feet

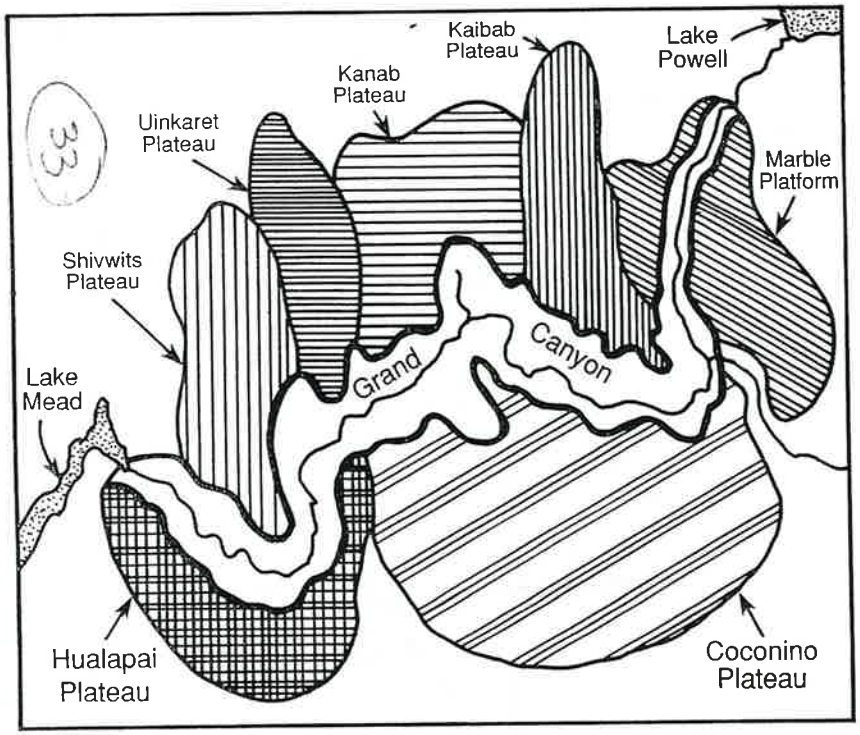

Figure 2. Generalized map of the area surrounding the Grand Canyon

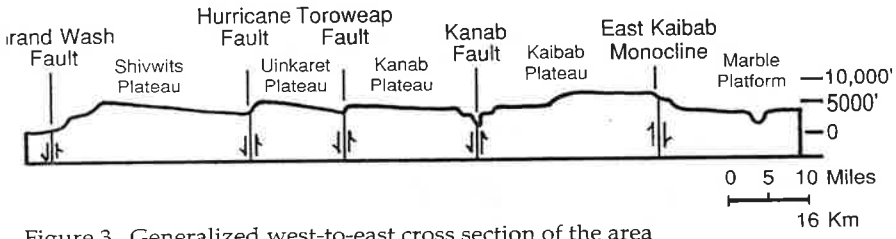

Figure 3. Generalized west-to-east cross section of the area just north of the Grand Canyon

(2012 meters) between Point Imperial on the north rim (8803 feet [2683 meters]) and the floor of the canyon near Lake Mead (1200 feet [366 meters]).

Many people are surprised to learn that there is a difference in elevation between the north and south rims. On the canyon's southern edge, the altitude ranges from 6000 to 7500 feet (1829 to 2286 meters) above sea level. The northern edge, however, is 1000 to 1200 feet (305 to 366 meters) higher even though both rims are capped by the same rock unit, the Kaibab Formation. The difference in height occurs because the various rock layers into which the canyon has been cut do not lie completely flat in this region. Instead, they arch or dome upward. The Colorado River carved the canyon through the southern flank of the dome, where the rock layers are tilted gently down to the south. Layers on the north rim, therefore, have been uplifted higher than the same layers on the south rim (Fig. 4).

Water that flows into and through the Grand Canyon comes primarily from four merging rivers—the Green, San Juan, Little Colorado, and Colorado—that drain hundreds of square miles of the Four Corners states (Fig. 5). As it courses through the canyon, the Colorado River drops about 2000 feet (610 meters) in elevation (Fig. 6). This steep gradient allows the river to continue its erosion of the chasm's floor.

Humans have been in the Grand Canyon for at least four thousand years, but the early records are sparse. Rare artifacts, remains of prehistoric dwellings, and the numerous mescal pits all attest to the early exploration and habitation by American Indians such as the Anasazi and the Cohonina. The first Euro-

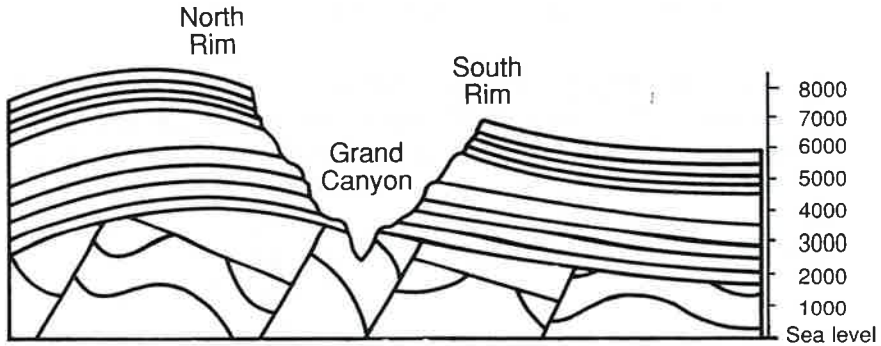

Figure 4. Generalized cross section through the Grand Canyon from the north rim to the south rim

Figure 5. Drainage area for runoff water that flows into and through the Grand Canyon

peans to see the canyon were a Spanish party of thirteen in search of the fabled lost cities of gold, under the command of Captain Don García López de Cárdenas. In 1540, Hopi Indian guides led hem to the south rim in the eastern part of the Grand Canyon, but hey were unable to reach the river below. In the next three

centuries, only two visits to the region have been reliably recorded. In 1776, Father Francisco Tomás Garcés, a Spanish missionary, explored Havasu Canyon in the south-central part of the Grand Canyon. In the same year, two Spanish priests, Father Silvestre Vélez de Escalante and Father Francisco Domíngues, led an expedition to the region and discovered a ford across the Colorado River (Crossing of the Fathers).

Among the earliest geological reports of the Grand Canyon country are those of Jules Marcou (1856) and John Strong Newberry (1861), who described the region's Paleozoic stratigraphy from their explorations of the canyon and the land to the south. Newberry was a geologist in the War Department-sponsored Ives expedition of 1857-58. Ives' rather discouraging and, as it turned out, unprophetic statement about the Grand Canyon was:

> Ours has been the first, and will doubtless be the last party of whites to visit this profitless locality. It seems intended by nature that the Colorado River, along the greater portion of its lonely and majestic way, shall be forever unvisited and undisturbed.

In 1869, John Wesley Powell led a party of ten men (reduced later to nine and finally only six) on an epic journey by boat down a thousand miles of the Colorado River from Green River, Wyoming, across Utah, and finally through the Grand Canyon to the mouth of the Virgin River at what is today the north end of Lake Mead. Powell's work was followed up by a small group of outstanding scientists through the turn of the nineteenth century. These included G.K. Gilbert, who was the first to apply formal rock unit names to Grand Canyon rocks; C.E. Dutton, who wrote

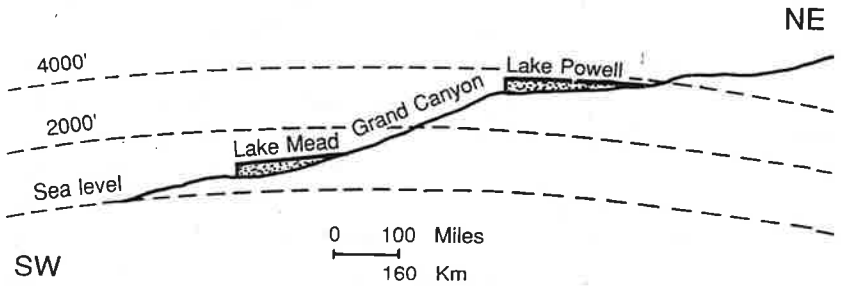

Figure 6. Diagrammatic profile of the Colorado River through the Grand Canyon, from Lake Powell to Lake Mead

The first monograph on the geology and geologic history of the Grand Canyon; A.R. Marvine, who participated in the U.S. Geographical Survey West of the 100th Meridian; and C.D. Walcott, who described both Paleozoic and Precambrian rocks in the canyon's central and eastern parts. These pioneer studies laid the groundwork for all subsequent research in the Grand Canyon.

Edwin D. McKee, to whom this book is dedicated, stands out as the premier research scientist of Grand Canyon geology in the twentieth century. Between 1933 and 1982, McKee either authored or coauthored five monographic publications on various Paleozoic rock units of the canyon—including the Redwall Limestone, Supai Group, Coconino Sandstone, the Toroweap and Kaibab formations, and Cambrian units. McKee also organized a special symposium in 1964 at the Museum of Northern Arizona to summarize the data and interpretations on the origin and evolution of the canyon. Much of our present understanding of the stratigraphy and age of Grand Canyon rocks (Fig. 7) is based on McKee's seminal work.

For more than a century, then, the Grand Canyon has attracted the extraordinary interest and effort of geologists to map its course, examine its rocks and fossils, and understand its record of earth history. In 1870, Powell wrote of the canyon country of the Colorado River:

> ... the thought grew in to my mind that the canyons of this region would be a Book of Revelations in the rock-leaved Bible of geology. The thought fructified and I determined to read the book.

Since then, several generations of earth scientists have searched the river and its canyon for answers to questions of when and how this part of our planet's crust developed. Although some questions have been answered, new ones are raised, and so the search goes on. This book is written for those who inquire about the revelations of the Grand Canyon. It is a compilation of the best efforts of a number of authors, all experts in their field, to summarize what is now known about the geology of the canyon. Much of the information presented here is an update and refinement of earlier works by pioneer scientists of the past. All of us who have written for this volume owe a great debt to those who preceded us in the search for the geologic secrets of the Grand Canyon.

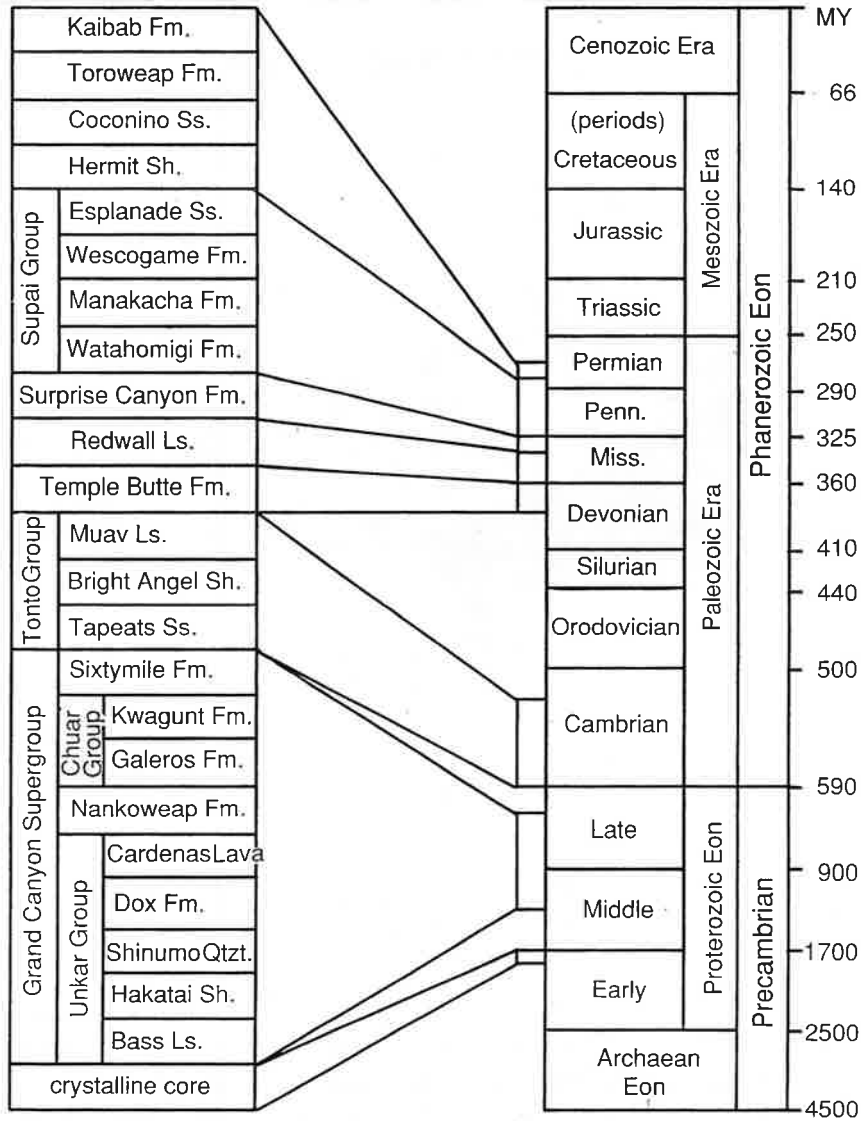

Figure 7. Comparison of the geologic column of the Grand Canyon with the Geologic Time Scale (After Haq and Van Eysinga, 1987)

Shinumo Quartzite

In contrast to the slope-forming argillaceous beds of the Hakatai Shale below and the Dox Formation above, the Shinumo Quartzite is a series of massive, cliff-forming sandstones and quartzites. The color of the Shinumo ranges from muted red, brown, and purple to white.

Four or possibly five poorly defined members have been recognized within the Shinumo Quartzite (Elston 1987, Daneker 1974). The lower units, in ascending order, consist of conglomeratic subarkose and submature quartz sandstone; to mature quartz sandstone; to brown quartz sandstone with abundant cross beds, clay galls, and mudcracks.

Near Shinumo Creek, the uppermost unit is the thickest member. It consists of fine-grained, well-sorted, and rounded quartz grains in a siliceous cement. Beds in the upper part of the upper member are contorted by fluid evulsion, which suggests that there might have been tectonic activity during this period.

The thickness of the Shimumo Quartzite shows a general increase to the west and ranges from 1132 feet (345 m) at Papago Creek in the east to 1328 feet (405 m) (Daneker 1974) or 1542 feet (470 m) (Noble 1914) in Shinumo Creek. Because the Shinumo is such a resistant unit, it formed hills where exposed during the pre-Tapeats erosional event.

This feature, the pinching out of the Tapeats Sandstone against Shinumo Quartzite highs, can be seen today in exposures near the bottom of the Grand Canyon. Analysis of the lithology and the sedimentary structures of the Shinumo suggests that the environment of deposition was near-shore, very shallow, marginal marine and part fluvial, part deltaic (Daneker 1974). The contact between the Shinumo and the overlying Dox Formation appears to be conformable in most locations and is marked by the lowermost shaley interval of Dox lithology.

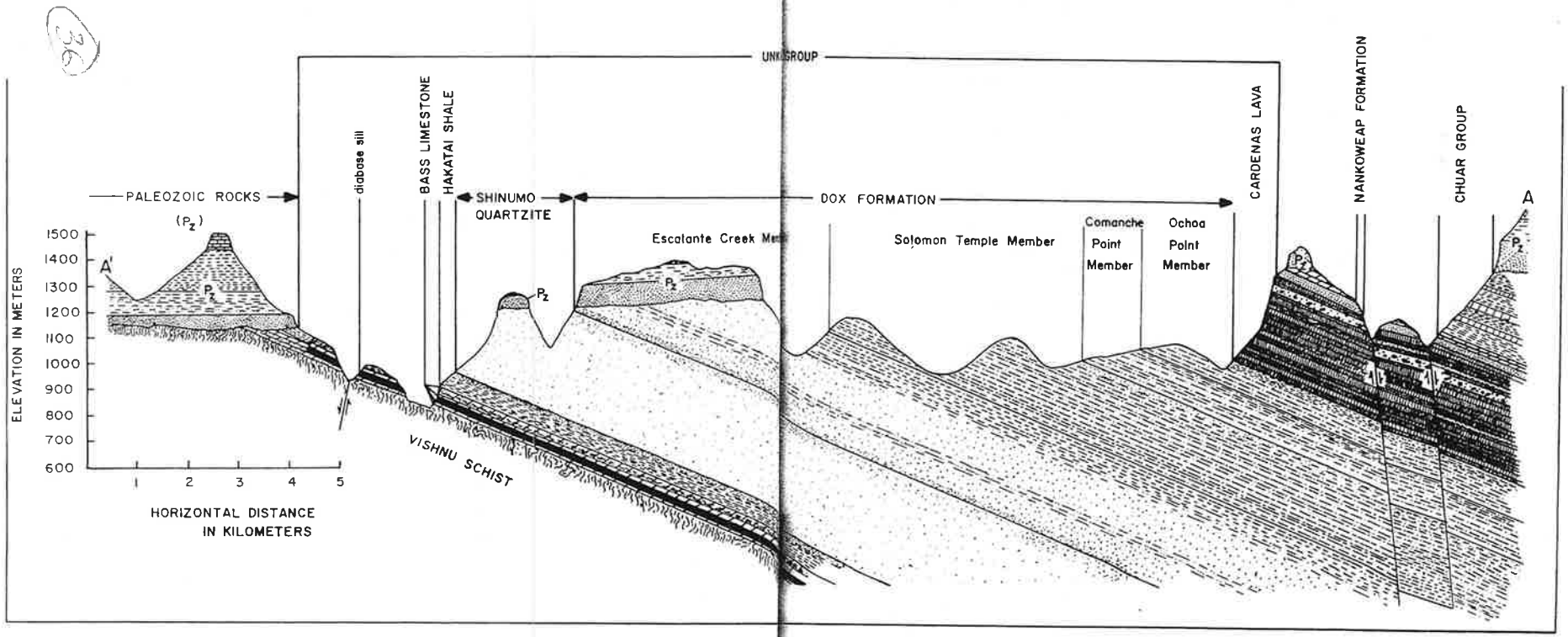

Figure 3. Cross section A - A' (eastern Grand Canyon). See Figure 1 for location of section.

Canyon Supergroup during Middle and Late Proterozoic time upon the deeply eroded Lower Proterozoic Vishnu crystalline complex. It was folded, faulted, and beveled by erosion before deposition of the Middle Cambrian Tapeats Sandstone.

Geologists now divide the Grand Canyon Supergroup, from the base to the top, into the Unkar Group, Nankoweap Formation, and Chuar Group. The groups are subdivided further into formations and, in some cases, members. Chapters three and four detail the stratigraphy and depositional history of the Grand Canyon Supergroup. This chapter summarizes its geologic structure and tectonic history.

Figure 1 identifies Precambrian rock exposures in the eastern Grand Canyon. The exposures are limited to the area below the

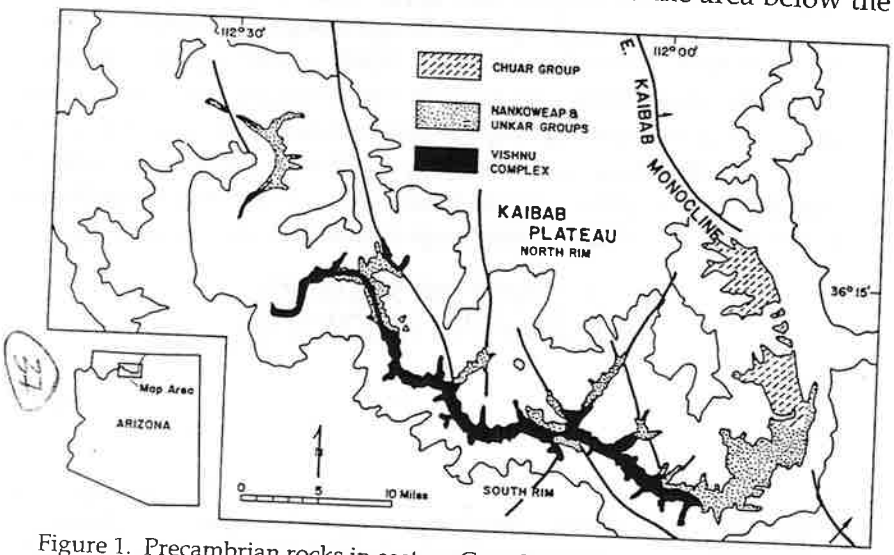

Figure 1. Precambrian rocks in eastern Grand Canyon. Major structures with Precambrian ancestry also are shown.

Kaibab Plateau, Powell's "Kaibab division" of the Grand Canyon, where the canyon is deepest and the Paleozoic section rises to its greatest elevation. Precambrian rocks emerge from beneath the Paleozoic cover in deep canyons along the East Kaibab monocline, the great, steplike fold on the east edge of the Kaibab Plateau, where Paleozoic rocks rise almost 3000 feet (900 m) from east to west. Exposures of Precambrian rocks end fifty miles (80 km) to the west, where regional tilt carries the Paleozoic rocks below the level of the Colorado River. Farther west, Precambrian metamorphic rocks emerge again in the lower Granite Gorge, but the Grand Canyon Supergroup is absent.

The Grand Canyon Supergroup occurs in isolated, wedge-shaped remnants as shown in the cross section of Figure 2. The underlying Vishnu metamorphic rocks rise to the southwest to intersect the base of the Paleozoic section at the left edge of the section. The unconformity at the base of the Paleozoic cuts out the Precambrian section from northeast to southwest. The Grand Canyon Supergroup, therefore, is found only in fragments where down-dropped geologic structures protected it from pre-Paleozoic erosion. We can piece these fragments together to decipher the late Precambrian tectonic history of the Grand Canyon region.

Figure 3 provides a hypothetical view of the geology of the Grand Canyon region as it might have looked at the close of Precambrian time—before Paleozoic sediments buried the region. This figure covers the same area as Figure 1 and was constructed by matching Precambrian structural trends from one exposure to the next. The Precambrian rocks occupy several great fault blocks, each tilted down to the northeast. The Vishnu Metamorphic Complex emerges on the southwestern edges of the blocks, and Unkar, Nankoweap, and Chuar beds appear successively toward the northeast. The youngest part of the Grand Canyon Supergroup forms a synclinal downwarp against the Butte fault, where it accumulated during a period of faulting (Elston 1979).

Three main types of structures disrupted the Grand Canyon Supergroup during late Precambrian time. These occurred as successive episodes of igneous intrusion, crustal contraction, and crustal extension affected the Grand Canyon region.

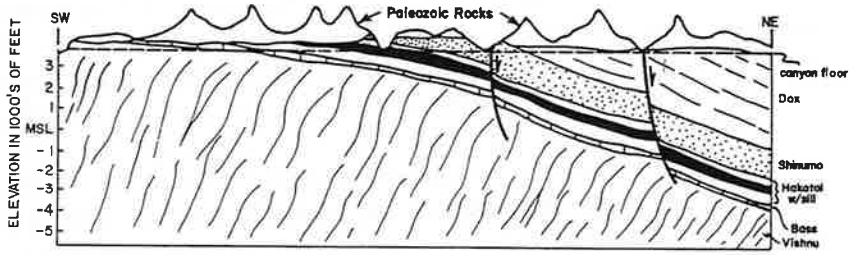

Figure 2. Cross section along the course of Bright Angel Creek, illustrating the wedgelike character of remnants of the Grand Canyon Supergroup. Great thicknesses of the tilted strata are exposed between the canyon floor, shown by the dashed line, and the base of the Paleozoic section.

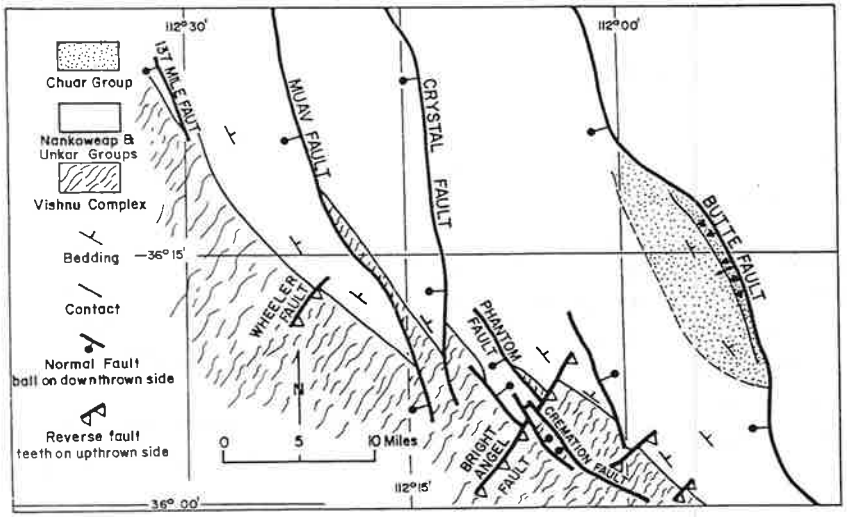

Figure 3. Schematic map of the Precambrian structure as it might have looked before burial by Paleozoic sediments. Triangles near Butte fault represent deposits shed from fault scarp as the blocks shifted. This figure shows the same area as Figure 1.

STRUCTURES RELATED TO IGNEOUS INTRUSION

The Unkar Group contains abundant diabase—a dark, intrusive igneous rock much like basalt in composition. The diabase magma spread out along the beds to form thick sills. In some places, it followed fractures across beds to form dikes. The sills are most common in the lower two units of the Unkar Group: the Bass Formation and Hakatai Shale. Diabase is most abundant in the western exposures, where sills are nearly 1000 feet (300 m) thick. In Galloway Canyon, two thick sills inflate the lower Unkar Group. In eastern exposures, however, sills are thin or absent. None exist in the Unkar beds near Phantom Ranch. Near Hance Rapids, a single 80-foot (24-m)-thick sill lies within the Bass Formation.

When the hot magma invaded the cooler sedimentary rocks, it produced zones of contact metamorphism—baking the ordinarily soft, red Hakati shales into hard, bluish hornfels and generating asbestos seams in the Bass dolomites.

The invasion of the diabase caused structural adjustments within the Unkar strata (Fig. 4). At some localities (Fig. 4a), sills end abruptly against steep contacts. The strata above the sills moved upwards relative to neighboring beds, forming faults in the overlying rocks. Without exposures of the underlying sills, such faults could be mistaken for tectonic features. In some cases, as Figure 4b shows, sills invading favorable bedding planes encountered older faults that prevented further lateral spreading. The faults moved again as the sills inflated. The fault shown in Figure 4b illustrates opposite senses of displacement above and below the sill; the rock on the right originally was downthrown. Figure 4c is an example of an expansion fault that served as a conduit for magma rising through the section. In Figure 4d, a sill steps from one bedding plane to another. A fault crosses the step, but beds above and below it are unbroken.

The diabase sills and dikes were the "plumbing system" for the Cardenas Lava, which erupted into the Unkar basin about the same time the diabase was crystallizing underground. McKee and Noble (1974) dated the diabase at 1150 million years. Radiometric dates reported by Ford, Breed, and Mitchell in 1972 and

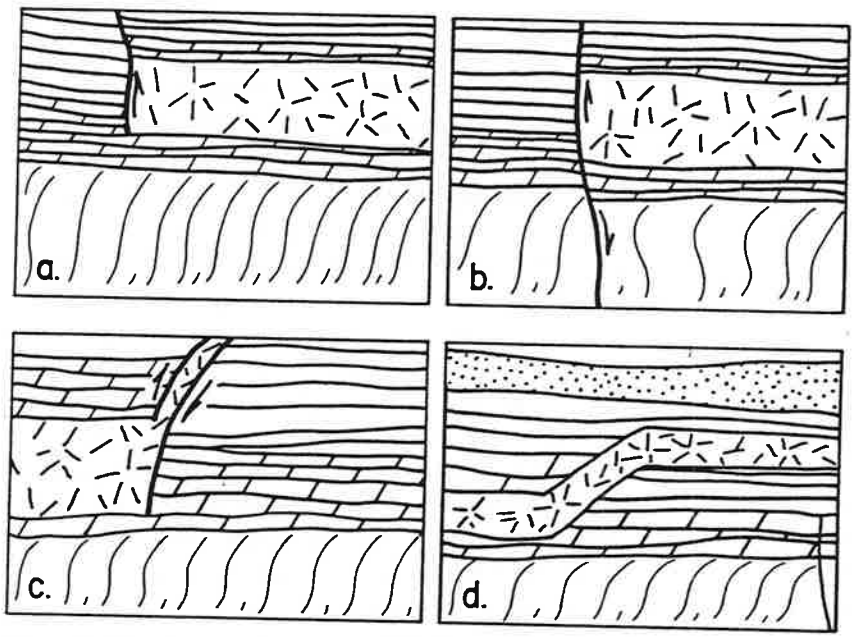

Figure 4. Types of structures formed by igneous intrusion

The erosion surface that developed on the Redwall Limestone during the Late Mississippian period, and on which the Surprise Canyon was deposited, must have been a relatively flat, resistant, limestone platform but with considerable local relief. Most of the Surprise Canyon outcrops occupy gently U-shaped or V-shaped notches cut into the top of the Redwall. By their nature and distribution, these notches appear to have been part of a major dendritic drainage system that flowed generally from east to west. They also appear to have been incised up to 400 feet deep (122 m) into the top of the Redwall Limestone near the western end. A preliminary reconstruction of the drainage pattern (Grover 1987) illustrates several major valleys that merge westward (Fig. 9). In addition, solution depressions and caves in the upper Redwall Limestone are filled locally with red mudstone of the Surprise Canyon Formation, indicating the development of a karst topography prior to Surprise Canyon deposition (Fig. 10). The time available for the development of this eroded and karsted topography on top of the Redwall is just a few million years—the interval between youngest Redwall (of middle Meramecian age) and oldest Surprise Canyon (of approximately middle or late Chesterian age). The depth of the stream valleys eroded into the top of the Redwall indicates an uplift or a several hundred foot (120 m) drop in sea level.

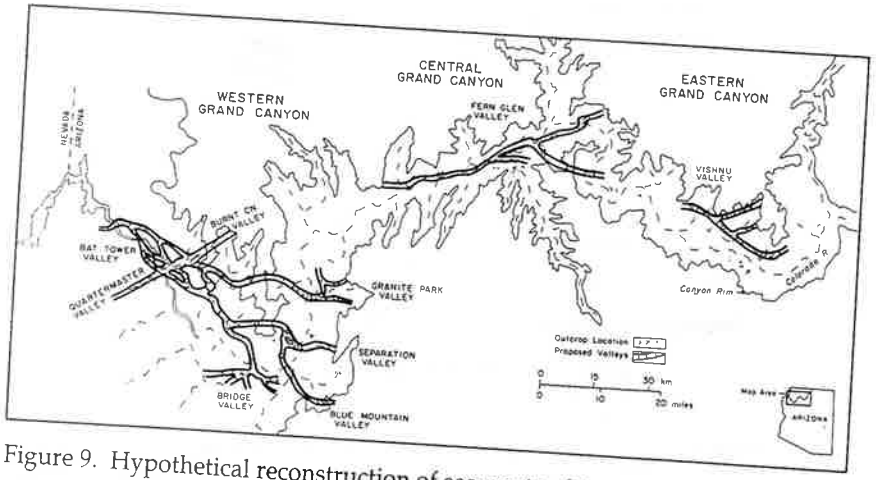

Figure 9. Hypothetical reconstruction of segments of the ancient valley system eroded into the Redwall Limestone in Late Mississippian time and into which the Surprise Canyon Formation was deposited

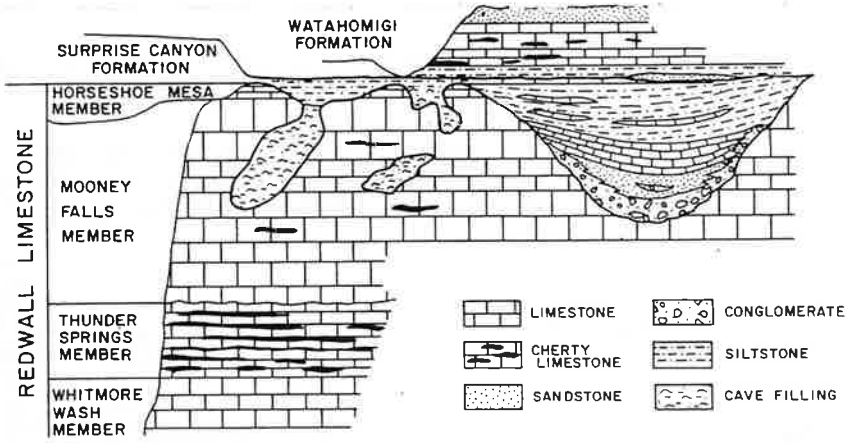

Figure 10. Cross section showing the stratigraphic relationship of the Surprise Canyon Formation to the underlying Redwall Limestone and overlying Watahomigi Formation of the Supai Group. Modified from Billingsley and Beus (1985, Fig. 3)

Stratigraphy and Lithology

The thicker sections of the Surprise Canyon Formation can be divided into three major rock units: 1) a lower conglomerate and sandstone, mainly of terrestrial origin; 2) a middle unit of skeletal limestone of marine origin; and 3) an upper, mainly marine unit of siltstone and silty, sandy, or algal limestone (Fig. 6). Since several lithofacies are included in each of the three units, the Surprise Canyon Formation exhibits a greater variety of sedimentary rock types than almost any other Paleozoic unit in the Grand Canyon.

The basal part of unit 1 in most sections consists of a ferruginous, pebble-to-cobble and local boulder conglomerate. Clasts are predominantly chert with minor limestone derived from the underlying Redwall Limestone. Some cobbles and boulders contain typical Redwall fossils. The clasts commonly are grain-supported and enclosed in a sandy matrix of nearly pure quartz grains and some hematite. Locally, the cobbles are sufficiently imbricated to indicate water current directions at the time of deposition (Fig. 11). In most sections, the conglomerate grades upward into a yellow or dark reddish brown or purple quartz sandstone or siltstone or, in some sections, a dark gray, carbonaceous shale. The sandstone beds commonly are flat bedded, but some

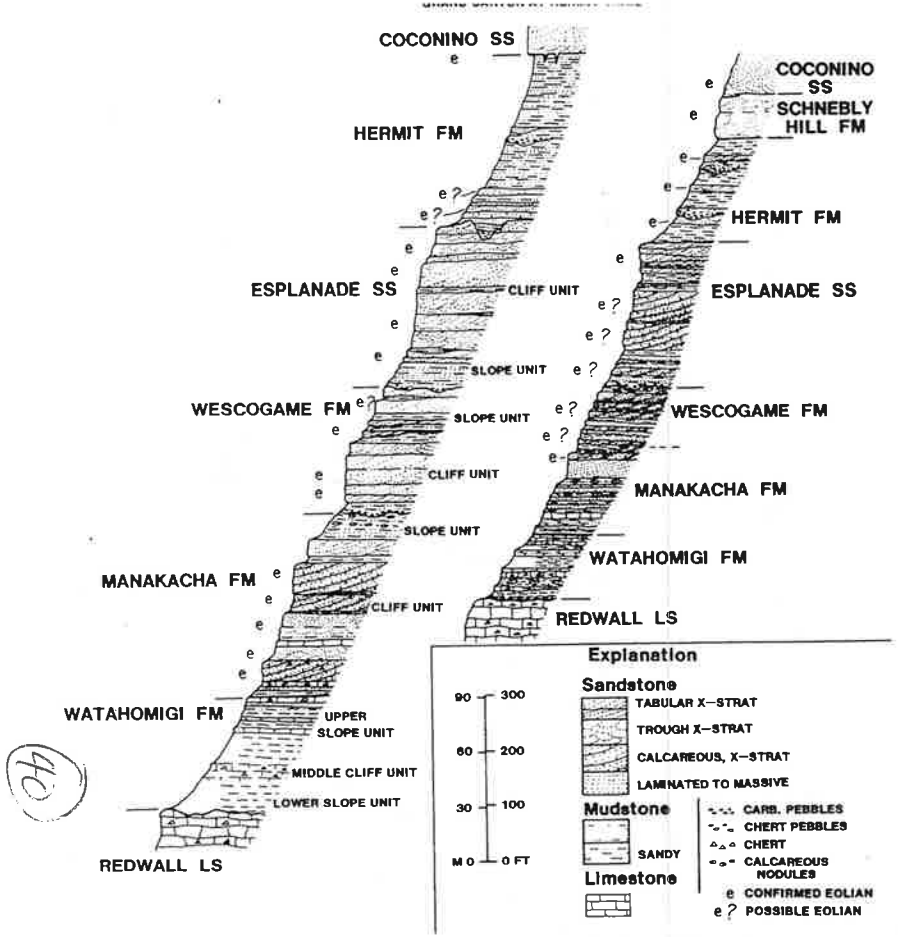

Figure 4. Columns of Supai Group and Hermit Formation and related strata showing distribution of known and suspected eolian strata

mudstone. The contact apparently occurs at the change from primarily slope below to steep slope or cliff above and, therefore, may not be a consistent stratigraphic level across the region.

The sharp increase in limestone west of a line paralleling the Hurricane Cliffs can be used to divide the Watahomigi Formation into an eastern redbed facies and a western carbonate facies (see McKee 1982, Fig. 6). The westward increase in thickness, carbonate content, and marine fossils is typical of many Paleozoic rock units in the Grand Canyon region.

Manakacha Formation

The Manakacha Formation marks an important change in the trend of Paleozoic depositional patterns in the Grand Canyon region. Following initial Cambrian sand deposition, the area was dominated by carbonates and minor mudstones from Middle Cambrian to Early Pennsylvanian time. The influx of quartz sand during the deposition of the Manakacha reflects a significant change across the western interior of the United States.

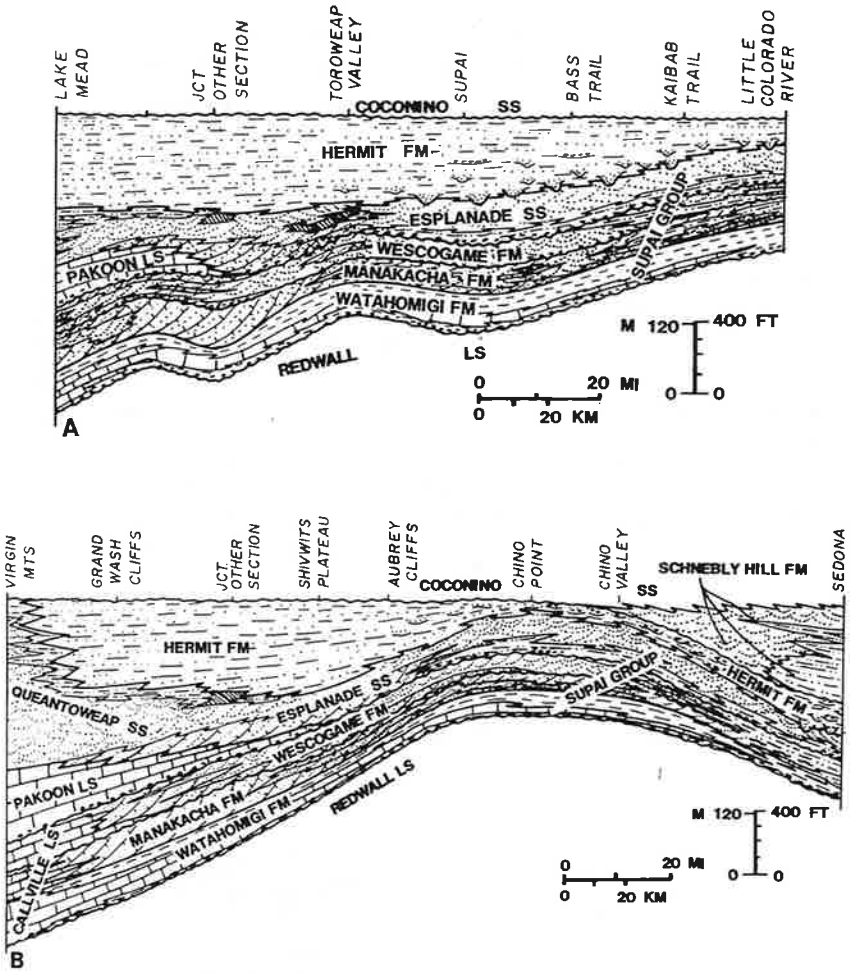

Figure 5. Restored stratigraphic cross section of Supai Group, Hermit Formation, and related strata. (a) West to east through Grand Canyon; (b) northwest to southeast from Virgin Mountains to Sedona

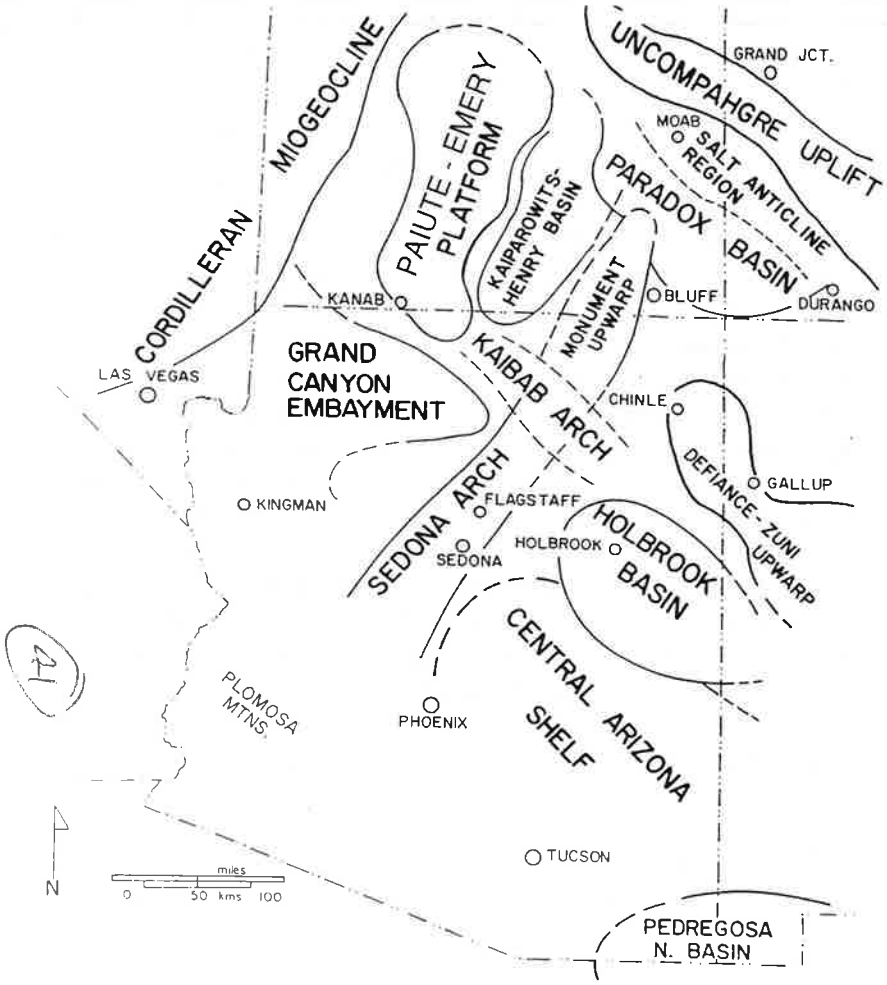

Figure 10. Map showing late Paleozoic tectonic elements of northern Arizona and vicinity. Note that Grand Canyon lies between more negative regions to the west and more positive areas to the east.

The influx of quartz sand into the Colorado Plateau region from the north also complicates the setting. The sand tended to accumulate between the arches and adjacent shelves or basins as extensive eolian deposits (Blakey 1988). When sea level was relatively low, eolian deposits became widespread, often expanding into basins and across shelves; when the sea level was high,

eolian deposits, at present, were confined to narrow belts along the flanks of arches (Chan and Kocurek 1988).

The Grand Canyon and the western Mogollon Rim region lay in a somewhat intermediate position between more negative areas to the northwest and higher ones to the southeast. Not unexpectedly, the resulting sedimentation is intermediate in character; cyclic sedimentation with more continental aspects is present in the east while cyclic sedimentation with more marine aspects is present in the west.

The general structural grain of northwestern Arizona tended southwest-northeast during Supai and Hermit time. Shorelines and marine trends should have paralleled this pattern, and fluvial deposits should have flowed northwesterly, perpendicular to this grain. Indeed, marine and shoreline patterns do parallel the trend, but the sandstone bodies that McKee (1982) suggested might be of fluvial origin show a paleocurrent reading to the south and southeast; this is as much as 180° from the expected trend. We have not documented the trends of Hermit Formation sandstone bodies.

Any one of the above controls on deposition was sufficient to produce a complicated depositional pattern. Together, they combined to produce a heterolithic record that varies abruptly, both vertically and laterally. The summary presented below must be considered preliminary. We have much to learn about the depositional history of the Supai Group and the Hermit Formation.

Depositional Environments

Recent studies tend to confirm the long-standing belief that the Supai Group was deposited on a broad coastal plain. Individual depositional settings ranged from shallow marine to continental. However, the recent identification of eolian-deposited sandstone units throughout the section necessitates a reinterpretation of Supai depositional history. Most of our knowledge of the Supai is based on the work of McKee, who provided a general description of sandstone bodies in the Supai Group (1982, pp. 260, 261). He interpreted the large foresets planes in the Manakacha Formation as the fronts of large, subaqueous sand sheets or small Gilbert deltas in areas strongly affected by tides. Traditionally, geologists have interpreted sandstone bodies of the Wescogame Formation as having formed in a high-energy, fluvial environment. Marine bioclastic debris was thought to have been trapped in an estuarine setting.

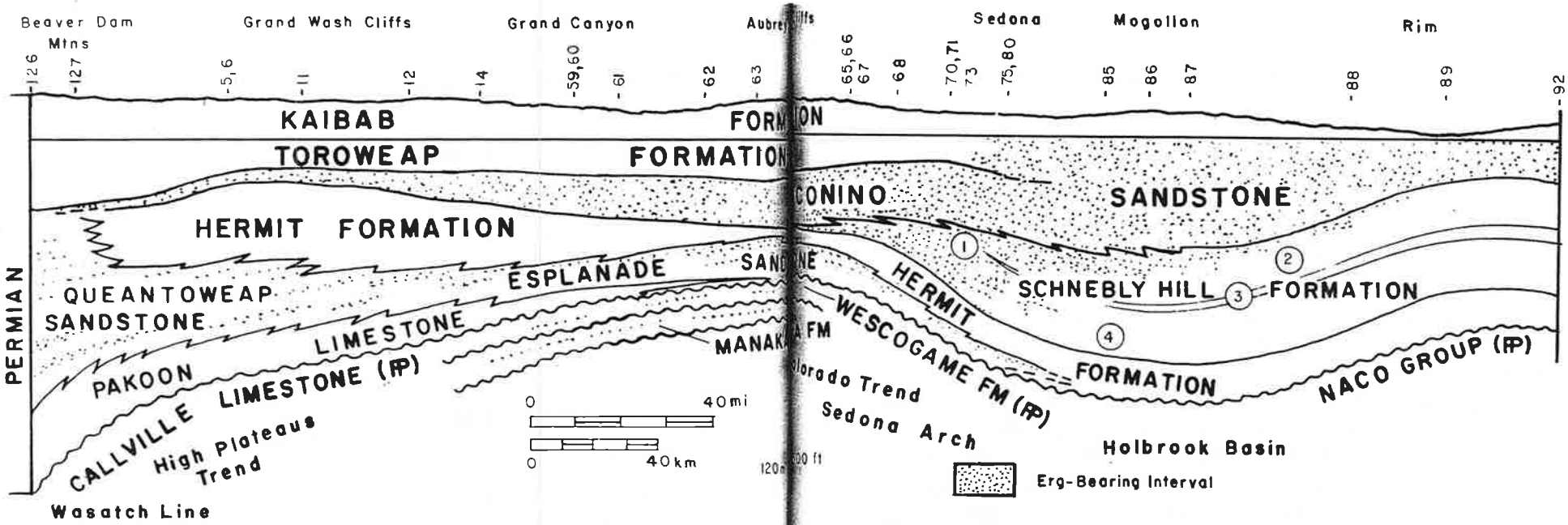

Figure 1. Regional stratigraphic relationships of Permian strata along the southern margin of the Colorado Plateau (after Blakey and Knepp)

In the 1940s, McKee conducted a series of experiments designed to duplicate the Coconino tracks. He filled a long trough with sand that formed a hill in the center. A variety of small vertebrates and invertebrates then were induced to walk along the sand and over the hill. By varying the slope of the hill and the moisture content of the sand, McKee was able to test the trace-forming capabilities of a variety of animals in a number of different environments. He tested the animals on a variety of surfaces—including dry sand, damp sand, saturated sand, and even sand that had been soaked and then allowed to dry. He found that only the largest animals tested (chuckwalla lizards) were able to make tracks in wet sand or crusted sand, and even then, the tracks were not as clear as those formed in dry sand. Smaller animals, such as millipedes and scorpions, were unable to make tracks in wet sediment and left clear traces only in dry, loose sand. He also found that at slopes below 27°, both uphill and downhill tracks were likely to be preserved. Avalanching, however, tended to destroy tracks on steep slopes.

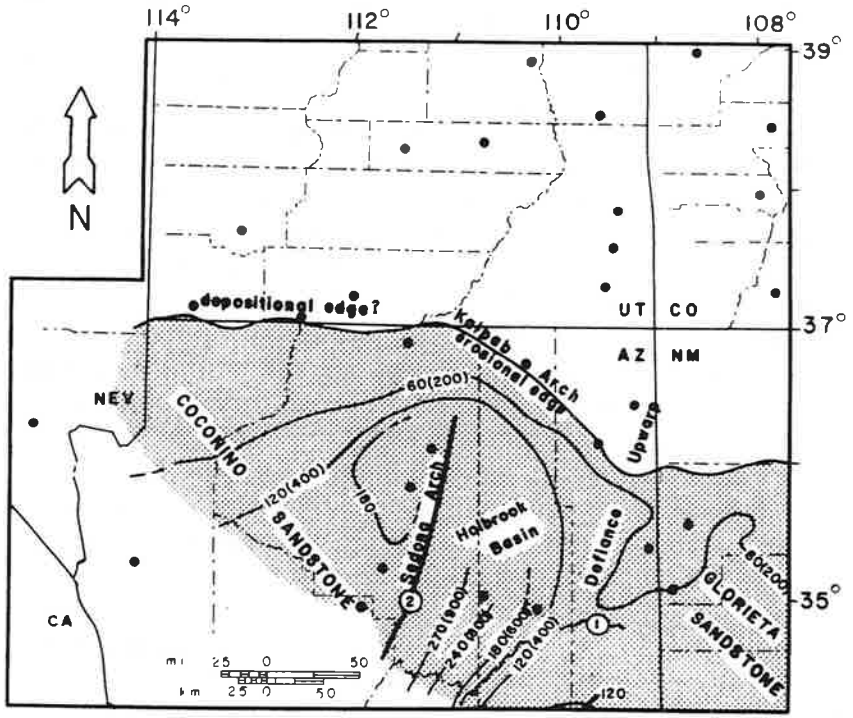

Figure 2. Isopach map of the Coconino Sandstone illustrating thinning away from the Sedona arch (after Blakey and Knepp)

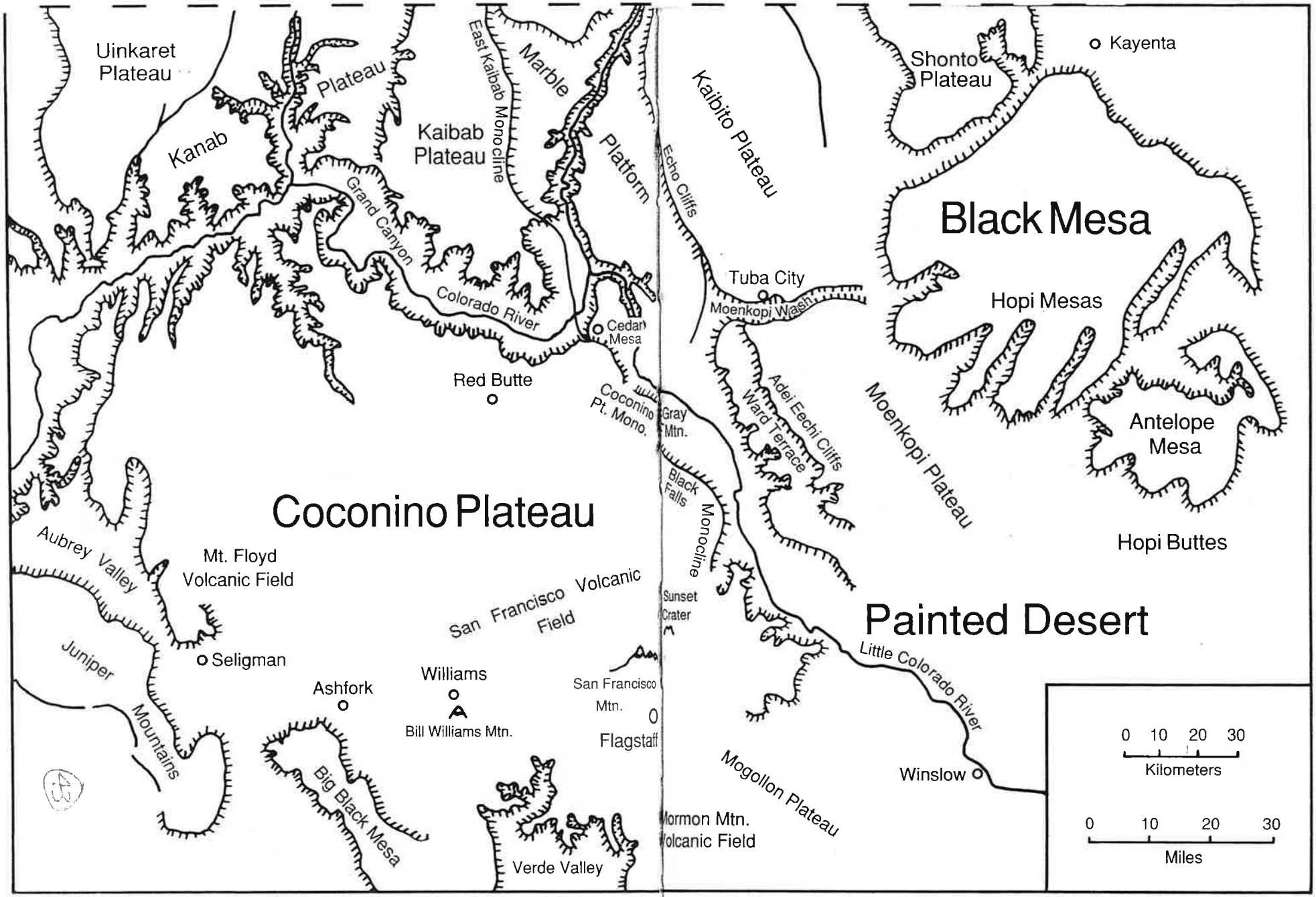

Figure 2. Physiographic map of the central and eastern Grand Canyon and surrounding areas (after Gregory 1950, Cooley and others 1969, King 1977, Billingsley and Hendricks 1989)

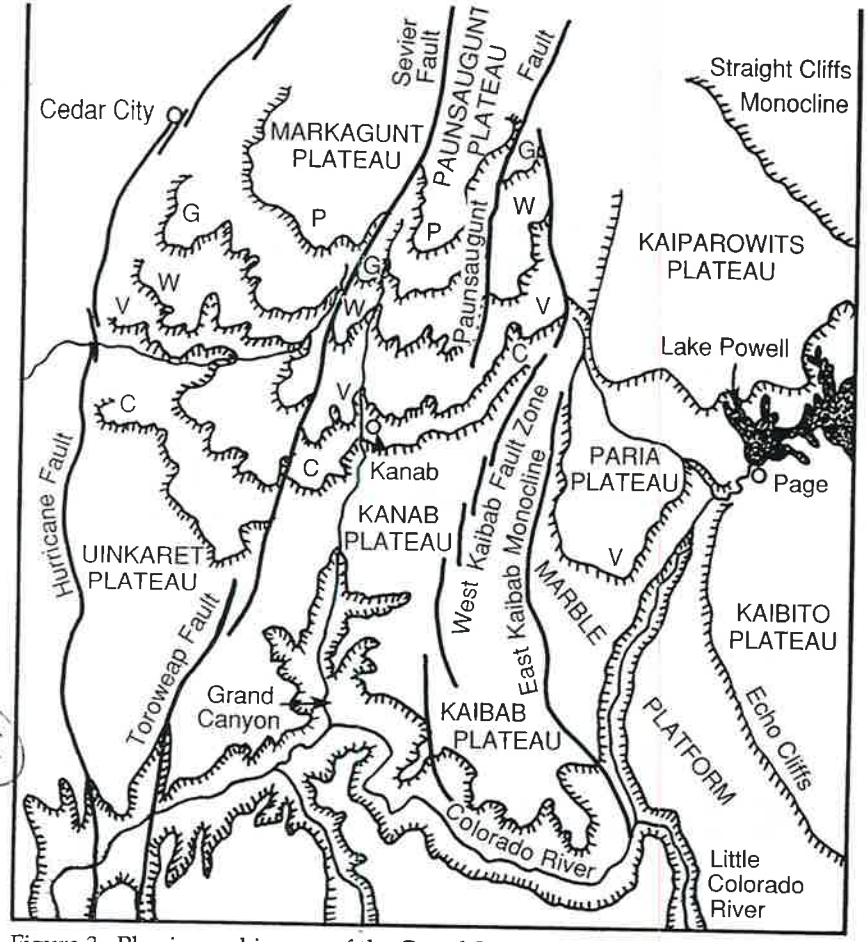

Figure 3. Physiographic map of the Grand Staircase section of the Colorado Plateau (after King 1977, Stokes 1986, Billingsley and Hendericks 1989)
C - Chocolate Cliffs; V - Vermilion Cliffs; W - White Cliffs; G - Gray Cliffs; P - Pink Cliffs; T - Terrace; Cyn - Canyon.

The first line of cliffs north of the Grand Canyon is the Chocolate Cliffs. The name is derived from the red-brown mudstone of the Lower and Middle Triassic Moenkopi Formation that forms the majority of the cliff profile. This escarpment sometimes is called the Shinarump Cliffs after sandstones and conglomerates of the Shinarump Member of the Upper Triassic Chinle Formation that cap the cliffs. Although the Chocolate Cliffs officially terminate at the northern end of Kaibab Plateau, the same rock units form a cliff and slope line along the southern

margin of Paria Plateau. There, however, the Moenkopi-Shinarump cliffs are not as well developed as the true Chocolate Cliffs. Erosional unconformities, which represent gaps in the rock/time record, separate the Moenkopi from the underlying Kaibab and overlying Chinle formations. The Moenkopi contains both marine and nonmarine sediments, whereas the Shinarump member of the Chinle is composed primarily of fluvial channel deposits. The flatlands and slopes above the Chocolate Cliffs, including Little Creek Terrace, Telegraph Flat, and related areas to the east, are formed by different fluvial and lacustrine members of the Chinle Formation.

The next step up the Grand Staircase is the very prominent Vermilion Cliffs. Starting at the base, red and purple deposits of the Chinle Formation, Wingate Sandstone, and the Moenave and Kayenta formations make up these cliffs, with the lower part of the Navajo Sandstone forming the caprock. The latter four formations comprise the Lower Jurassic Glen Canyon Group and are of

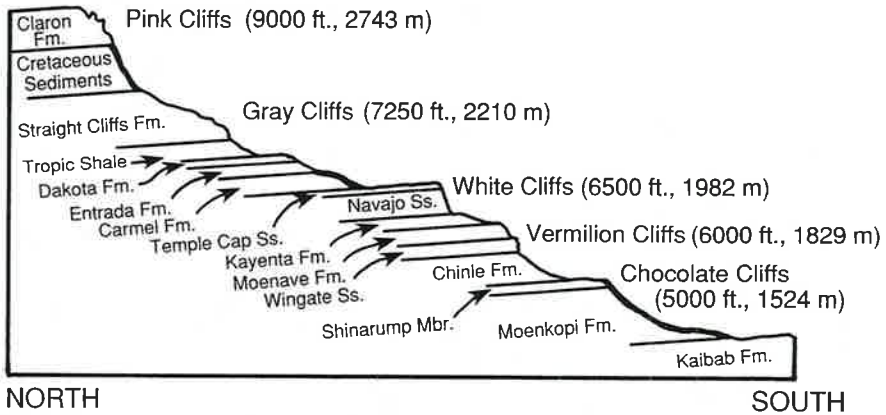

Figure 4. Diagrammatic cross section of the Grand Staircase—vertical scale greatly exaggerated (after King 1977, Stokes 1986, Hintze 1988, and Clemmeson and others 1989)

primarily eolian and fluvial origin. An unconformity separates the Wingate Sandstone from the underlying Chinle Formation; however, contacts between the other units are gradational to intertonguing. Above the Vermilion Cliffs, the Navajo Sandstone forms the bench that includes Moccasin Terrace, Wygaret Terrace, and their equivalents to the east.

The foregoing synopsis of Laramide events underscores the vast progress that has been made during the past century in deciphering the tectonic record preserved in the rocks of the Grand Canyon. Not only have we been able to map and date structures and deduce causative stresses, but we are beginning to weave these elements into the larger contexts of cordilleran tectonics, regional paleogeography, and sedimentation.

A number of important themes will be developed in this chapter. These include relating variations in the styles of deformation to different causative stress fields and documenting the overwhelming evidence for periodic reactivation of inherited fault zones by successive stress regimes. Another important theme is correlating uplift and subsidence to paleogeography, regional drainage patterns, and the movement of sediments into and out of the region.

Recent data indicate that most of the structures observed in the walls of the Grand Canyon vastly predate the Colorado River and its canyon. In fact, early Tertiary deformations are dated by sediments found in the remnants of Laramide, northward-draining canyons. Both these canyons and the sediments in them are ten times older than the Grand Canyon.

Even though late Cenozoic extensional faulting is spectacularly exposed, and exhibits an unprecedented record of recurrent activity here, the Grand Canyon still is best known in tectonic forums for its exceptional three-dimensional exposures of Laramide monoclines. The primary value of the Grand Canyon exposures is that the roots of the monoclines are unambiguously open to examination on the floor of the canyon.

The terms "Colorado Plateau region" and "Grand Canyon region" are used in this text for orientation purposes. However, recognize that the Colorado Plateau did not become fully defined until Miocene time, and erosion did not produce the Grand Canyon until Pliocene time. "Mogollon Highlands" refers to the general series of Mesozoic and Cenozoic uplifts occurring in the geographic regions south of the Colorado Plateau.

This chapter summarizes the work of many dozens of researchers spanning over a hundred years of effort. Detailed citations for each borrowed concept or fact lie beyond the scope of a work of this type. Consequently, the literature that is cited is designed to lead the interested reader to the most germane contributions or to sources that carefully develop important lines

of inquiry. A reading of this text will be facilitated greatly by having the following set of geologic maps close at hand: Huntoon and others (1981, 1982, 1986) and Billingsley and Huntoon (1983).

THE COLORADO PLATEAU

As Figure 1 shows, the Grand Canyon occupies a position on the southwest corner of the Colorado Plateau, a geologic province that is underlain by a thick continental crust that became slightly separated on the east from the continental craton during the Cenozoic Era. The plateau is ringed by zones of intense deforma-

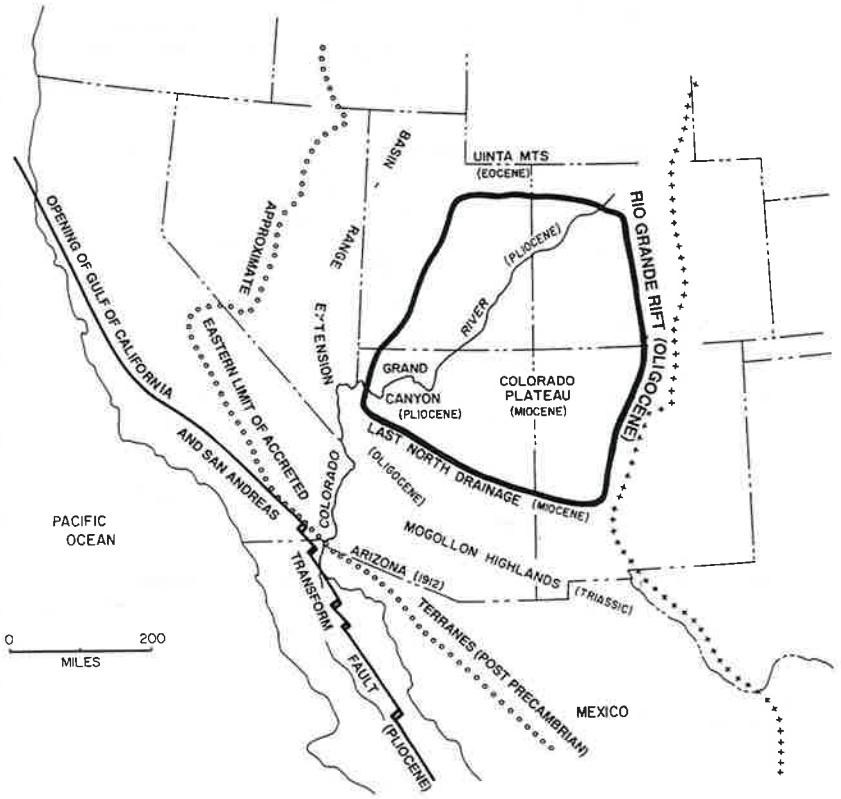

Figure 1. Selected tectonic elements in the western North American cordillera and the timing of their inception

miles (100 km) of north-northeastward translation of the Colorado Plateau along right-lateral, strike-slip faults. The movement partially decoupled the Colorado Plateau from the North American continent along the future Rio Grande rift. The early Eocene reorganization of stresses within the plateau region appears to have resulted in minor development, or reactivation, of northwest-trending monoclines in the Grand Canyon region.

Chapin (1983) proposed that the northward crowding of the Colorado Plateau into the Wyoming province was accommodated by crustal shortening manifested as thrust faulting and regional folding. The result was the production of east-and southeast-trending basins and ranges in Wyoming. The southernmost of these was the east-trending Uinta uplift bounded both to the north and south by thrust faults dipping under the range. Bernaski (1985) summarizes data that reveals that the Uinta uplift began to rise in Early Eocene time. Thus, Laramide structures outlined the eastern and northern boundaries of the Colorado Plateau as we know it today. The eastern boundary, now the Rio Grande rift, became better defined and more strikingly decoupled from the North American craton as a result of extension beginning in Late Oligocene time.

Grand Canyon Monoclines

As Figure 4 shows, Laramide monoclines formed in the Paleozoic and Mesozoic sedimentary cover throughout the Grand Canyon region in response to reverse movement along favorably oriented, preexisting faults in the Precambrian basement. The reactivated basement faults most commonly were steeply west-dipping Precambrian normal faults that served as preexisting structural discontinuities within the Precambrian basement complex. Typical east-west spacings between the monoclines in the Grand Canyon region are fifteen to twenty miles (24-32 km). These spacings gradually increase toward the east across the Colorado Plateau. The total crustal shortening that resulted from deformation within the monoclines on the western Colorado Plateau was less than one percent. The reason for this low percentage is that spacings between the monoclines are large in comparison to local shortening across them.

Figures 5 and 6 demonstrate that the Grand Canyon provides the finest cross sections through monoclines found on the Colorado Plateau. The exposures into the Precambrian basement are

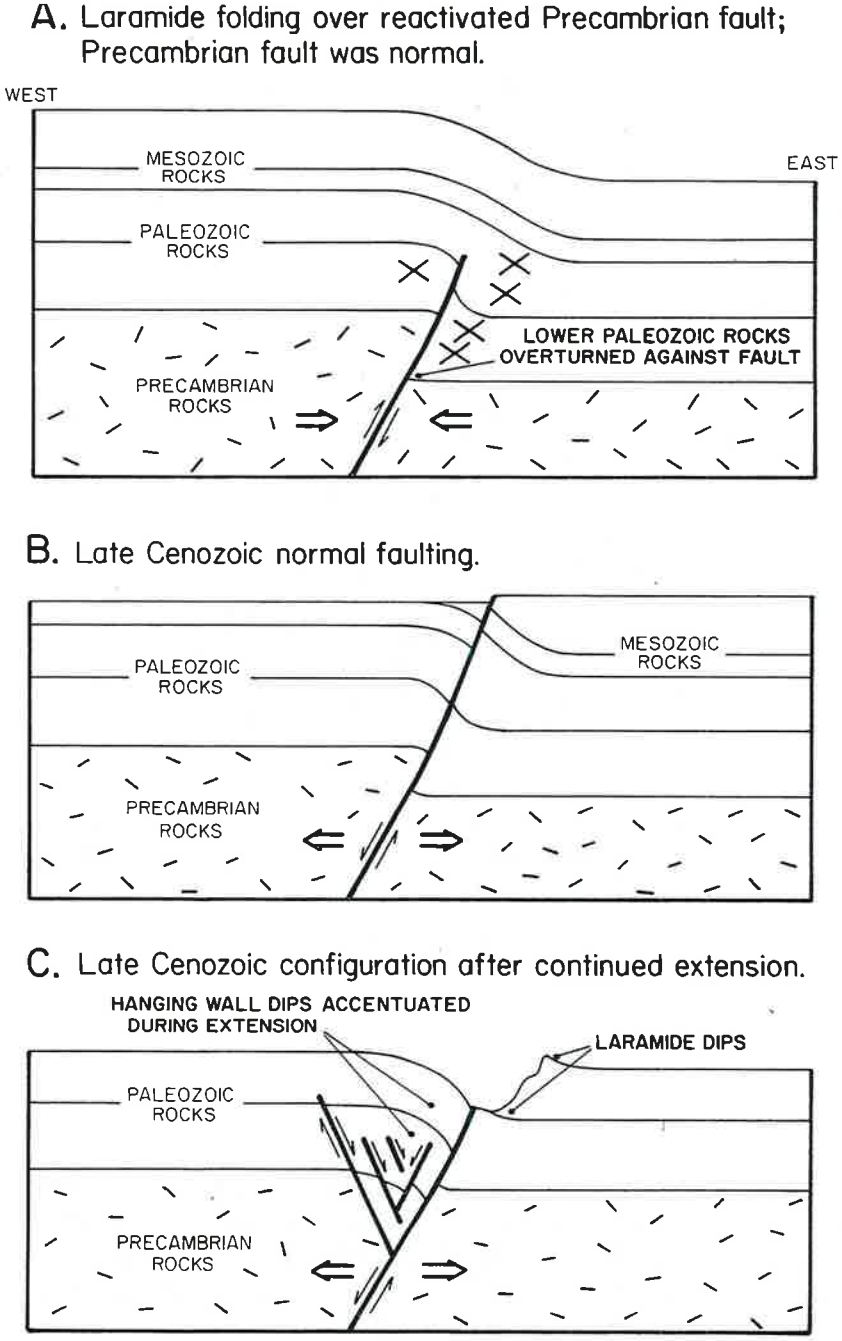

Figure 4. Stages in the development of a typical north-trending monocline-fault zone, Grand Canyon region, Arizona

tem . . . ne result was wholesale extension within the Basin-Range to the west and south of the Grand Canyon region during Late Oligocene through Middle Miocene time and east-west opening of the Rio Grande rift beginning in Late Oligocene time. The opening of the Rio Grande rift caused between two and four degrees of clockwise rotation of the Colorado Plateau. The plateau was fully defined as a structural entity by Middle Miocene time, and its modern style of tectonic deformation commenced. In addition, more than 3000 feet (900 m) of uplift occurred along the Grand Wash Cliffs at the mouth of the Grand Canyon in Pliocene time, indicating that rates of uplift in the region have accelerated during Late Cenozoic time.

The major phase of Basin-Range extension in the vicinity of the Whipple Mountains along the lower Colorado River southwest of the Colorado Plateau commenced in Late Oligocene time, considerably earlier than the first surface manifestations of normal faulting on the Colorado Plateau. Detachment faulting in the Whipple Mountains is characterized by east-northeast dipping, low-angle normal faults in which the upper plate glided downslope to the northeast on an unextended lower plate (Davis and others 1980). Although presently unproven, similar extension also may have been occurring during this period at middle and lower crustal levels under the southwestern part of the Colorado Plateau.

A speculative tectonic model accommodating Late Oligocene-Late Miocene extension at deep crustal levels under the Colorado Plateau and at shallower levels in the Basin-Range involves either a gently northeasterly dipping, crustal-penetrating normal fault or lateral extension within shear–bounded lenses, respectively illustrated in Figures 13D and 13C.

Figure 14 illustrates that northwest-striking blocks calving off the thin, trailing edge of the Colorado Plateau could account for tectonic erosion of the southwestern edge of the Colorado Plateau. These upper plate blocks now comprise the ranges in the area south and west of the plateau—including the Hualapai, Cerbat, Juniper, Aquarius, and Peacock ranges. In either scenario, the northeasterly tilted mountain blocks rest in tectonic contact on lower plate rocks, such as observed in similar environments in the Whipple Mountains. The detachment surface defining the base of the plateau appears to be spoon shaped and concaved upward, thus accounting for the southwestern bulge of the Colorado

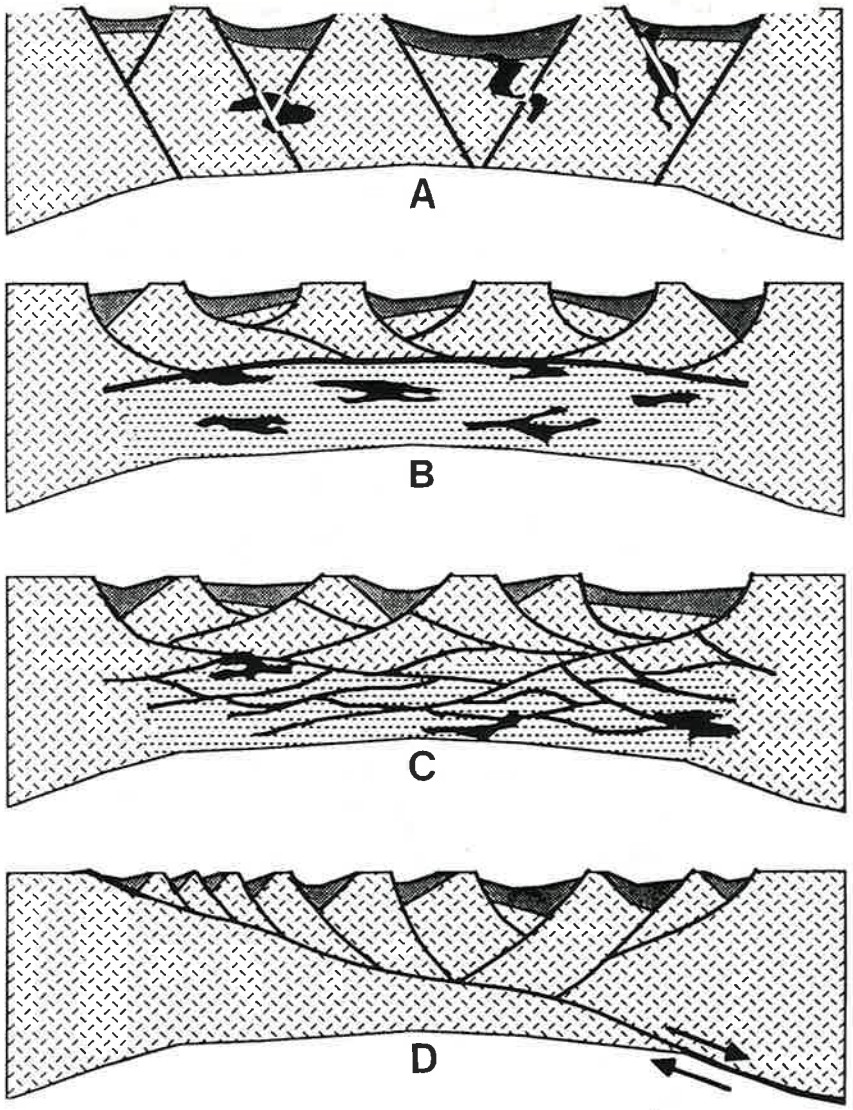

Figure 13. Summary of models used to explain extension in the Basin and Range Province southwest of the Colorado Plateau, Arizona (from Allmendinger and others 1987, Fig. 7). (A) Classic horst-graben model, (B) subhorizontal decoupling zone model, (C) shear zone bounded lense model, (D) crustal penetrating shear zone model. Either models C or D could have produced crustal thinning and subsidence along the southwestern Colorado Plateau in Late Oligocene-Early Miocene time.

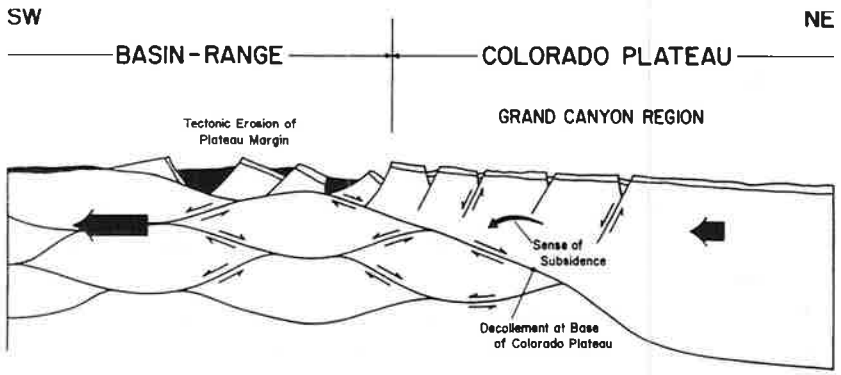

Figure 14. Cartoon illustrating tectonic erosion and subsidence along the southwestern edge of the Colorado Plateau over extending shear-bounded lenses in Late Oligocene-Early Miocene time. Lense concept from Hamilton (1982). Heavy arrows show absolute motions within the Basin-Range and Colorado Plateau provinces. Fine arrows show relative motions between shear surfaces. Notice that the relative motion between the lenses causes the crust to both thin and lengthen. Vertical scale greatly exaggerated, particularly at top

Plateau along the Hualapai Plateau over the thickened, northeasterly plunging axis of the upper plate.

Deep crustal extension probably was underway in Late Oligocene time. This allowed for (1) progressive tectonic erosion of the Colorado Plateau toward the northeast, (2) structural differentiation of the plateau from the Basin-Range in Miocene time, (3) thinning of the crust under the western part of the Colorado Plateau from about twenty-five to nineteen miles (40-30 km), and (4) nearly one degree of down to the southwest tilting of the southwestern edge of the Colorado Plateau. The latter easily accommodates sufficient subsidence of the Laramide erosion surface on the Colorado Plateau to force the abandonment of Laramide paleocanyons and to force the establishment of the west-flowing Colorado River in Late Miocene(?)-Pliocene time. Such subsidence also readily explains why early Tertiary rocks in the southern high plateaus of Utah now lie 2000 feet (600 m) or more above some of their source areas in the Grand Canyon region.

The relative motion of the Colorado Plateau above the decollement was down toward the northeast. Because such motion also corresponded to the opening of the Rio Grande rift, absolute regional motions had to include a slight clockwise rotation of the

plateau (Fig. 15) and southwestward extrusion of lower plate rocks from under the plateau. This model implies that the Colorado Plateau was rotating into extensional space created within the Basin-Range Province, wherein the lower plate was moving into, and westward in concert with, the Basin-Range at a rate slightly greater than the upper plate carrying the Colorado Plateau. Thus, the entire Basin-Range Province was moving away from the Colorado Plateau to the southwest at all crustal levels.

By Miocene time, the western part of the Colorado Plateau was undergoing the first significant east-west crustal extension to affect the region since late Precambrian time. The Grand Canyon

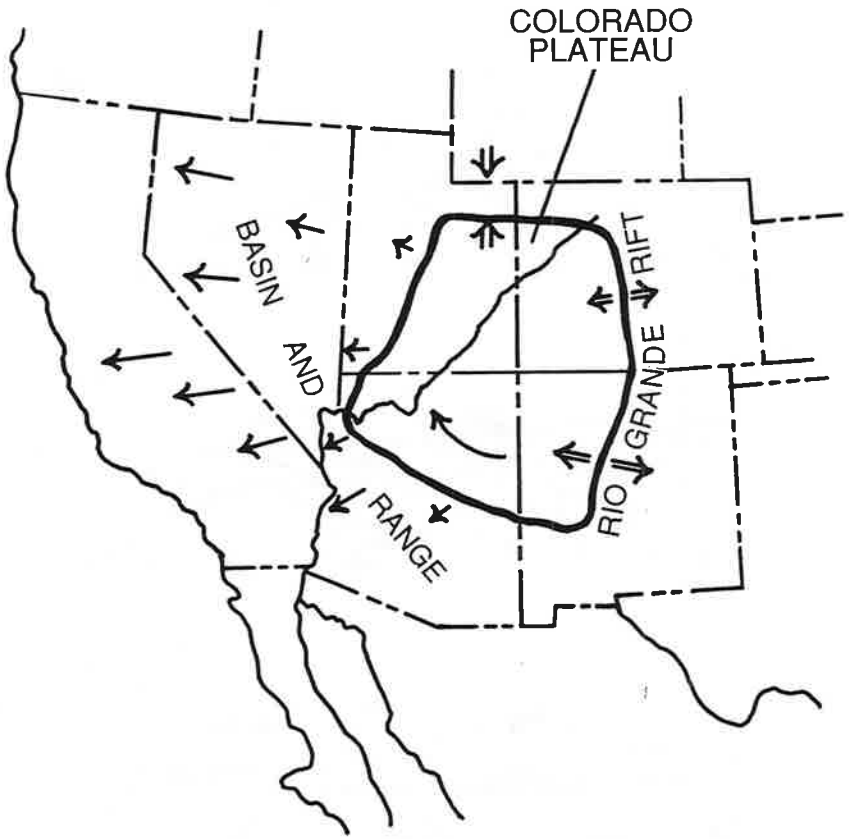

Figure 15. Postulated clockwise rotation of the Colorado Plateau into extensional space created in the Basin-Range during Late Oligocene-Early Miocene time. Arrows in the Basin-Range schematically illustrate that all rocks within the province moved away from the Colorado Plateau at rates which increased to the west as the crust within the Basin-Range simultaneously extended.

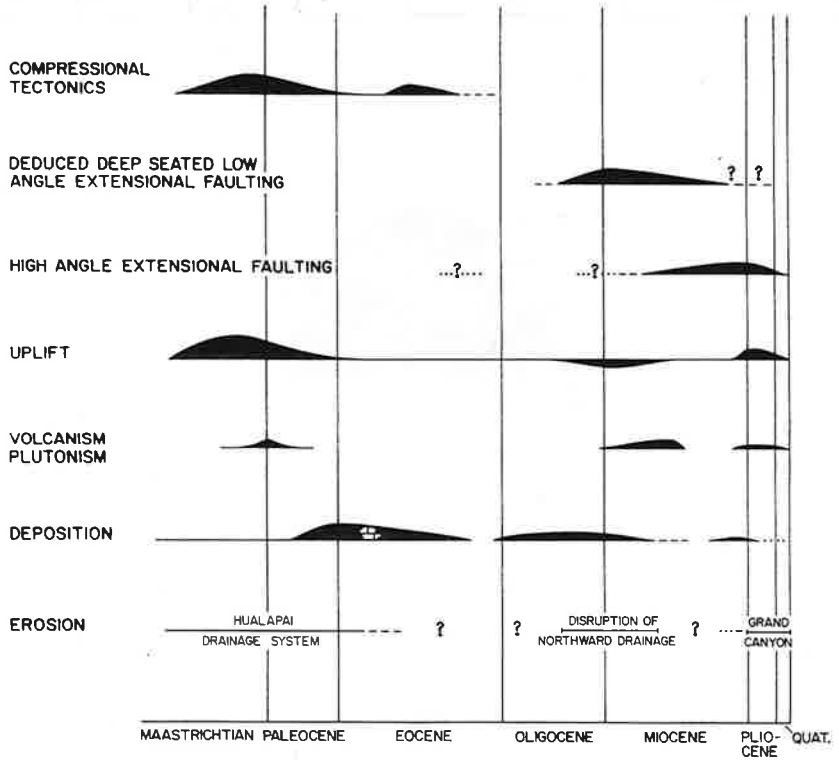

Figure 20. Temporal relationships between tectonics, sedimentation, and erosion in the Grand Canyon region, Arizona, during Laramide and post-Laramide time

velopment along the fault and the fact that the tuff is tilted on ranges that subsequently were partially buried by the Muddy Creek Formation. Therefore, major movement occurred along the Grand Wash fault after deposition of the Peach Springs Tuff, but prior to deposition of the upper part of the Muddy Creek Formation. These relationships bracket the major offsets across the fault between earliest Middle Miocene and latest Late Miocene time.

Some of the offsets along the Grand Wash fault probably were synchronous with deposition of the lower Muddy Creek Formation in the deepening Grand Wash trough, but relationships proving this remain buried. Minor post-Muddy Creek displacements along the Grand Wash fault appear to account for the folding of the Muddy Creek Formation in the vicinity of Lake Mead and for the faulting, by a few feet, of a gravel deposit located three and one-half miles (5.6 km) south of the Diamond Bar Ranch

(Lucchitta 1967). Clearly, however, most of the activity along the Grand Wash fault in Arizona was finished by the beginning of Pliocene time.

The Hurricane fault is the southern, waning extension of the Wasatch fault zone that, in Utah, comprises the physiographic boundary between the Colorado Plateau and the Basin-Range Province. The province boundary steps westward to the Grand Wash fault in Arizona. Maximum late Tertiary offset across the Hurricane fault zone in the Grand Canyon is in excess of 3000 feet (900 m) at Granite Park.

The timing of the onset of late Cenozoic normal faulting along the Hurricane fault is difficult to determine. Young and Brennan (1974) point out that Truxton Valley and upper Peach Springs Canyon, which are aligned along the Hurricane fault, are unusually wide and filled with sediments that predate the Peach Springs Tuff. They conclude that the fault existed prior to eruption of the tuff, so erosion progressed more rapidly along the trend. Thus, they push the inception of faulting back in time. An alternative explanation is that erosion followed the coeval trend of a southern, now eroded, segment of the Laramide Hurricane monocline. This interpretation does not require such early faulting.

The Peach Springs Tuff and underlying Tertiary rocks are offset by the Hurricane fault near the head of Peach Springs Canyon. Unfortunately, the closest exposed offset Paleozoic rocks lie three miles (5 km) to the north, precluding accurate differentiation of pre- and post-Peach Springs Tuff faulting. The offset across the tuff is between 200 and 300 feet (60 and 90 m) as is the offset associated with the Paleozoic rocks to the north. Consequently, it is doubtful if there was pre-Peach Springs Tuff displacement in the area. However, the uncertainties in correlating the similar offsets between the two sites does not justify discounting the possibility of small pre-Peach Springs Tuff displacement.

If we assume that there was no faulting along the Hurricane fault prior to the eruption of the tuff, the inception of late Tertiary faulting is post ~17 m.y., which is post-earliest Middle Miocene in age. Gardner (1941) concluded from outcrops in southern Utah that 75 percent or more of the total offset across the fault occurred in Late-Miocene(?) and Pliocene time, an observation that commonly is cited to support a peaking in the rate of normal faulting in the region during Pliocene time.

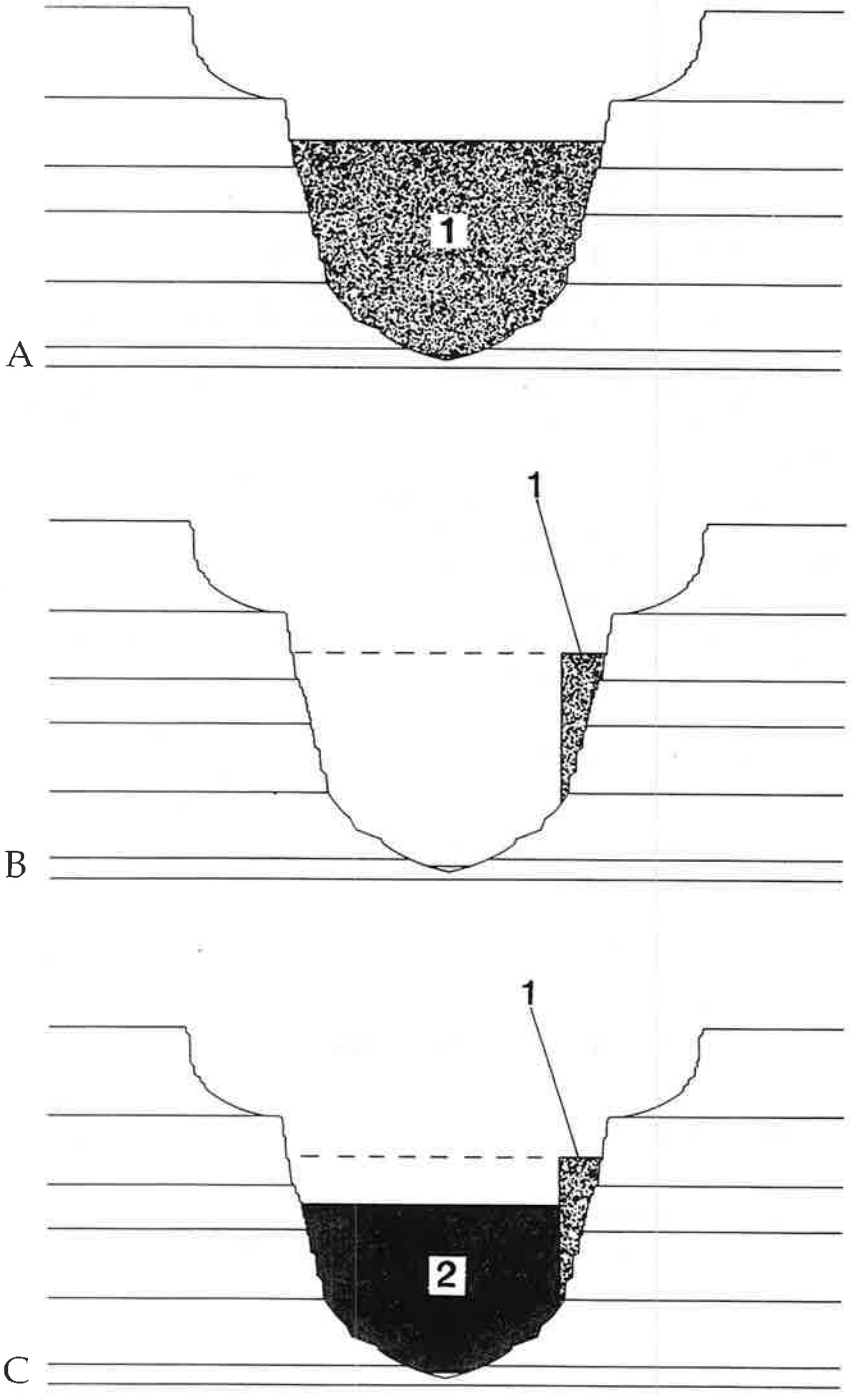

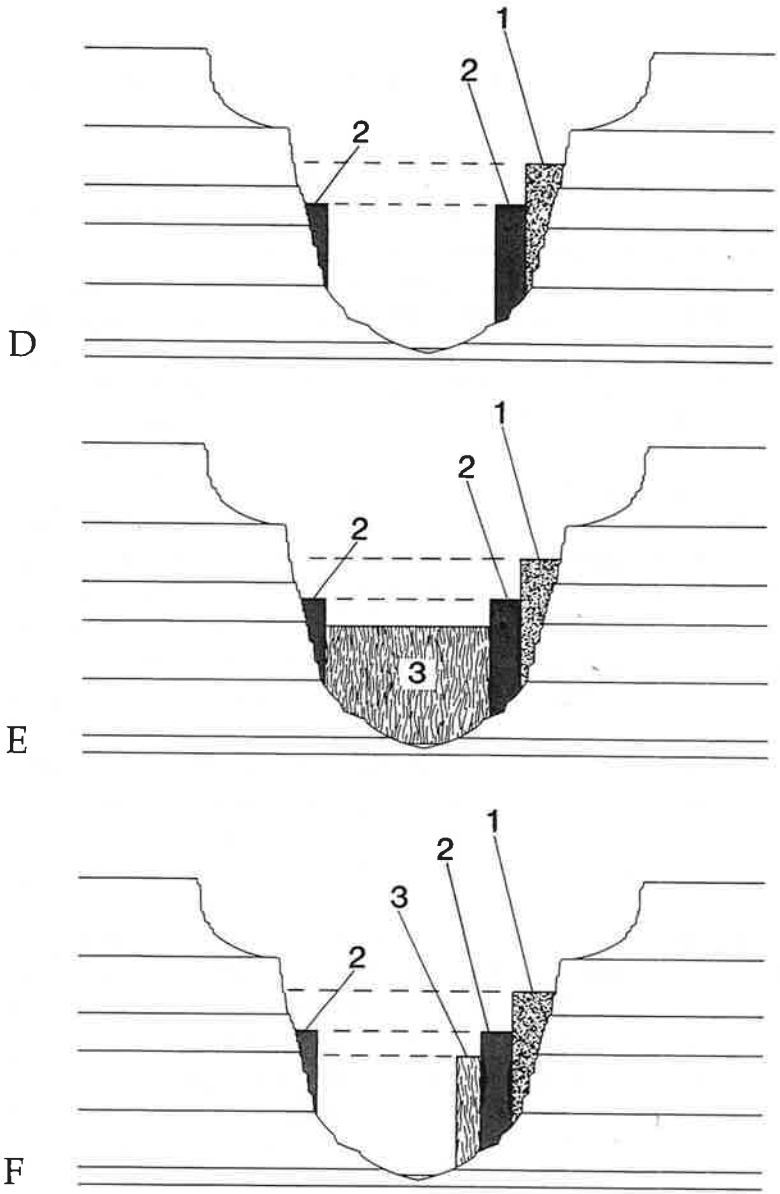

Figure 2. Diagrams showing the development of juxtaposed flows in the Grand Canyon. (A) Flow partly fills the canyon. (B) Erosion leaves small remnants of flow 1 adhering to the canyon wall. (C) Flow 2 refills the canyon. (D) Erosion removes most of flow 2, leaving remnants juxtaposed against flow 1 and against the canyon wall. (E) Flow 3 fills the canyon. (F) Erosion of flow 3 leaves remants of flows 1, 2, and 3 stacked side-by-side according to relative age.

...ble 1.

	DAM	ELEVATION	HEIGHT ABOVE RIVER	RADIOMETRIC DATE	VOLUME OF LAVA (mi 3)	LAKE LENGTH	WATER FILL TIME	SEDIMENT FILL TIME
1	Prospect	4000	2330		4.0		23 yrs.	3018 yrs.
2	Ponderosa	2800	1130		2.5		1.5 yrs.	163 yrs.
3	Toroweap	3093	1443	1.2 Ma	3.7		2.62 yrs.	345 yrs.
4	Esplanade	2600	960		1.8		287 days	92 yrs.
5	Buried Canyon	2480	850	0.89 Ma	1.7		231 days	87 yrs.
6	Whitmore	2500	900		3.0	100	240 days	88 yrs.
7	"D" Flows	2295	635	0.57 Ma	1.1	74	87 days	31 yrs.
8	Lava Falls	2260	600		1.2		86 days	30 yrs.
9	Black Ledge	2033	373		2.1	53	17 days	7 yrs.
10	Gray Ledge	1813	203		0.3	37	2 days	10.3 mos.
11	Layered Dbs.	1938	298	0.64 Ma	0.3	42	8 days	3 yrs.
12	Massive Dbs.	1826	226	0.14 Ma	0.2		5 days	1.4 yrs.

DEVELOPMENT AND DESTRUCTION OF LAVA DAMS

The hydrologic data from the Bureau of Land Management's Lake Mead Survey (1963 and 1964) provide the basic information from which we are able to calculate the rates at which the lakes behind the various lava dams were filled with water and, subsequently, sediment. These data also provide some indication of the time necessary for a lava dam to be eroded away completely (Table 1).

Rates of Formation of Dams

Although the formation of a lava dam in the Grand Canyon was a significant event that dramatically changed canyon morphology, the time needed to create a lava dam was remarkably short by any standard and certainly would be considered instantaneous in a geologic time frame. Observations of basaltic eruptions in historic times indicate that most basaltic extrusions occur in a matter of days or weeks. The major flows in the Grand Canyon, most of which were 100 to 200 feet (30 to 60 m) thick, probably moved tens of miles down the Colorado River in a matter of days.

This conclusion is supported by the fact that the upper colonnade and/or a clinkery upper surface of the flow often is preserved, essentially unmodified by erosion. This indicates that the flow was extruded in a period of time less than that required for the lake impounded behind the dam to overflow. If extrusion occurred during a longer period of time, the lake behind the dam would overflow, and erosion would modify the upper surface features of the basalts quickly.

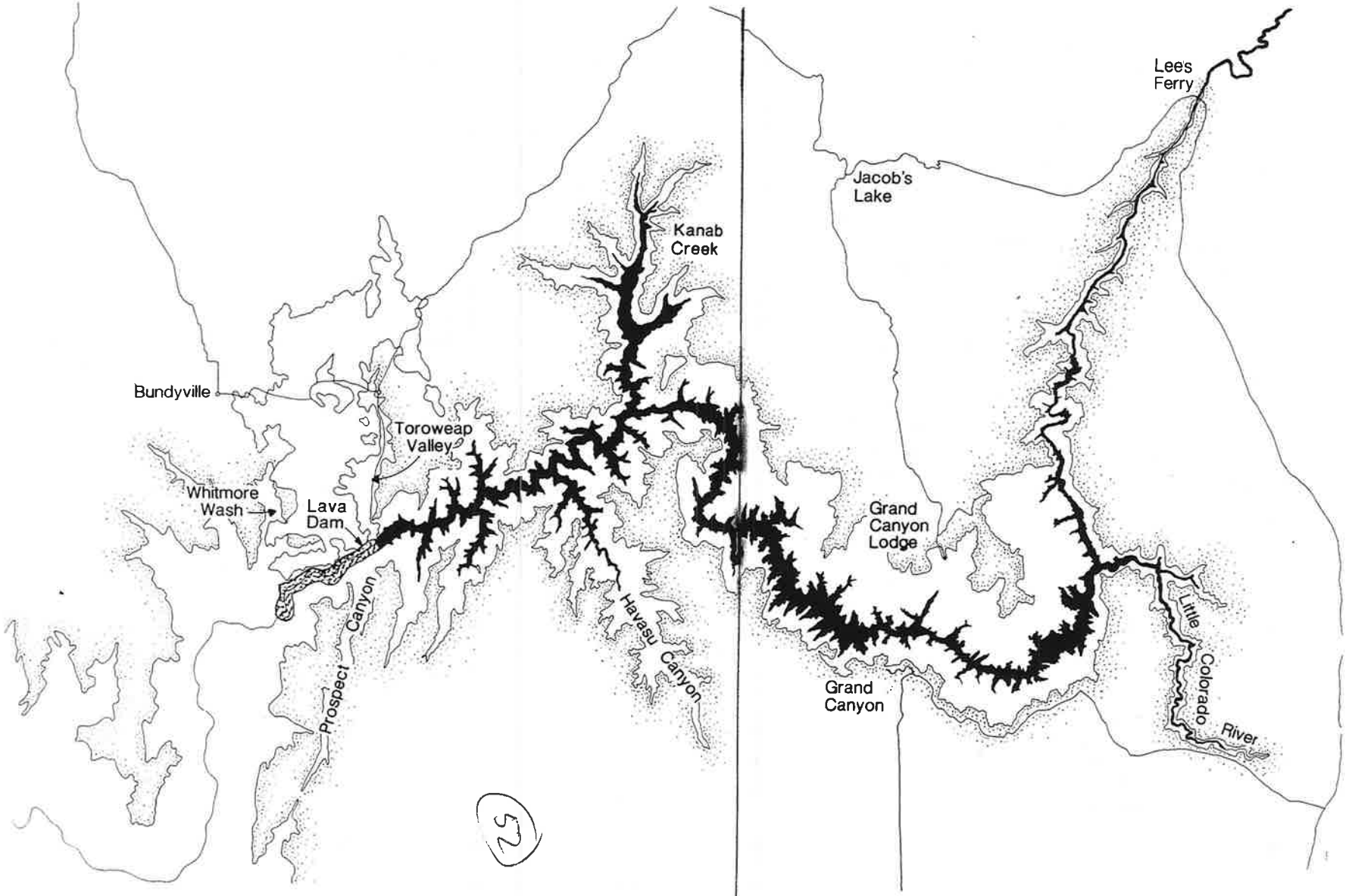

Figure 7. The Prospect Lake. The Prospect Dam was the highest lava dam formed across the Colorado River. The lake formed behind the dam that extended all the way through the Grand Canyon and up into Utah. It formed more than 1.2 million years ago.

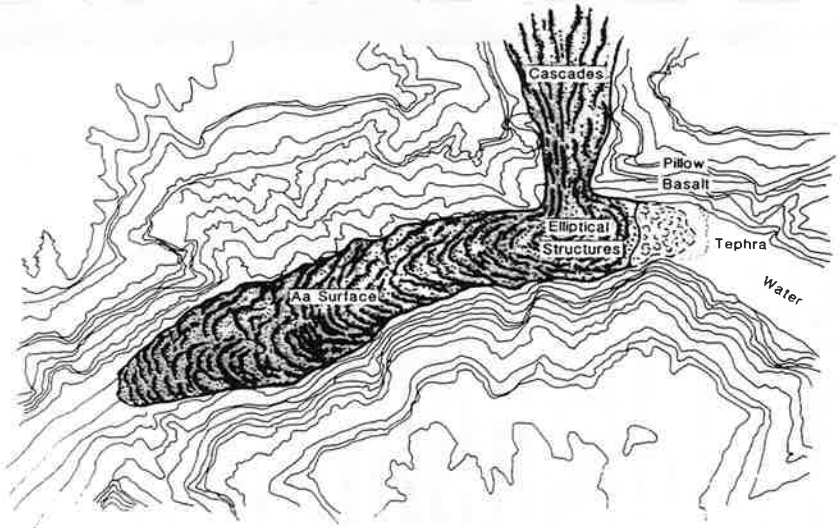

A

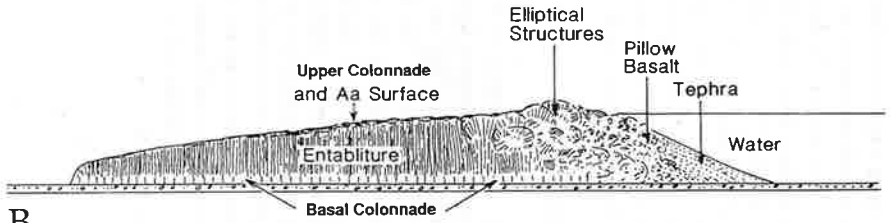

B

Figure 11. The structure of a hypothetical flow 200 feet thick in the Grand Canyon. Only the upstream margin of the flow would interact with water from the river. This would produce hydroexplosive tephra, which would be deposited at the upstream margin of the dam. Some pillow structures would be produced where lava came into direct contact with the river. Most of the flow would move downstream essentially dry until the backwater overflowed the barrier. The Colorado River would overflow the barrier of a simple flow within two days. It would flow over the top of the basalt and influence the cooling of the lava. The interaction of the river water with the lava would be most intense near the front of the dam and would form the elliptical structure. The overflow also may have had an effect on the development of the entablature in the downstream part of the flow.

Grand Canyon. It extended all the way through the present National Park Visitor's area and upstream into the vicinity of Lees Ferry (Fig. 12). Throughout much of the park region, the lake's

depth was approximately 750 feet (225 m). In the region of the visitor's center, the lake essentially flooded all of Granite Gorge—with the shoreline occurring very close to the vertical wall of the Tapeats Sandstone.

The gravel, sand, and silt that form the terrace deposits at Lees Ferry at an elevation of 3600 feet (1080 m) probably were deposited as a delta built by the Paria and Colorado rivers where they emptied into the Toroweap Lake. Likewise, the silt deposits that form the main floor of Havasu Canyon represent a major remnant of Toroweap Lake deposits.

If the Toroweap Dam formed instantaneously, the lake behind it would overflow in 2.6 years. It would be completely full of sediment in 345 years. Since the Toroweap Dam was constructed over a period of time, the lake undoubtedly was full of sediment by the time the dam was completed. After the extrusion that built the Toroweap Dam terminated, erosion by headwater migration of the waterfall and the downcutting of the stream channel probably destroyed the dam in less than 10,000 years.

The Esplanade Dam

On the north side of the river between Miles 181 and 182, a sequence of flows that formed a complex dam at an elevation of 2600 feet (780 m), or 960 feet (288 m) above river level, is preserved beneath the Esplanade Cascades (Fig. 13). These flows can be seen from viewpoints west of the present Toroweap Campground and resemble in some respects the Toroweap sequence. Both are preserved beneath major cascades.

The Esplanade sequence also is similar in some respects to that preserved in the Buried Canyon at Mile 184. These similarities have led some geologists to consider the Toroweap, Esplanade, and Buried Canyon lavas as part of a single complex lava dam. However, the stratigraphic sequence in each dam is distinctly different, and radiometric dates indicate three separate ages for the sequences.

Several small remnants of the Esplanade Dam are preserved in tributary canyons on the south wall of the inner gorge between Mile 183.5 and Mile 184. They provide important documentation concerning the height of the Esplanade Dam. All are preserved in "hanging valleys" at an elevation of 2600 feet (780 m).

The lake that formed behind the dam was similar to, but slightly smaller than, the Toroweap Lake and extended upstream

Migration of volcanism in the San Francisco volcanic field, Arizona

KENNETH L. TANAKA
EUGENE M. SHOEMAKER } *U.S. Geological Survey, 2255 North Gemini Drive, Flagstaff, Arizona 86001*
GEORGE E. ULRICH
EDWARD W. WOLFE } *U.S. Geological Survey, Hawaiian Volcano Observatory, Hawaii National Park, Hawaii 96718*

ABSTRACT

The remanent magnetization of volcanic rocks has been determined at 650 sites in the San Francisco volcanic field in the southern part of the Colorado Plateau. The polarity of remanent magnetization—combined with K-Ar age determinations, spatial and petrographic associations, stratigraphic relations, and state of preservation of the cinder cones—provides a basis for assignment to known magnetic polarity epochs of 610 mafic vents and >100 intermediate to silicic flows, flow sequences, and vents. The age assignments for basaltic rocks include 243 Brunhes (<0.73 Ma) vents, 220 Matuyama (0.73 to 2.48 Ma) vents, and 147 pre-Matuyama (2.48 to about 5.0 Ma) vents. Basaltic volcanism migrated northeastward before Matuyama time at a rate of ~1.2 cm/yr and eastward (S87° ± 5°E) over the past 2.5 m.y. at a rate of 2.9 ± 0.3 cm/yr. Concomitant acceleration in total magma production (from 75 to 1,400 × 10^{-6} km^3/yr) and frequency of basaltic eruptions (from 1 per 17,000 yr to 1 per 3,000 yr) occurred between 5 and 0.25 Ma. For the past 0.25 m.y., magma production (~180 × 10^{-6} km^3/yr) and perhaps eruption frequency have decreased. This evolutionary sequence, coupled with the lead and strontium-isotopic composition of the rocks, can be explained by magmatism caused by shear heating at the base of the lithosphere. We propose that this eastward drift of volcanic activity represents absolute westward motion of the North American plate. Our model is in agreement with a model in which the African plate is fixed to the deep mantle.

INTRODUCTION

Previous geologic investigations of the San Francisco volcanic field (Robinson, 1913; Colton, 1936; Cooley, 1962; Moore and others, 1976) established that its youngest rocks are located in its eastern part. Determination of K-Ar ages for silicic centers and some basalts (Damon and others, 1974; McKee and others, 1974) led to recognition of northeastward migration of volcanism along the Mesa Butte fault system (Ulrich and Nealey, 1976) and eastward migration in the eastern part of the field (Smith and Luedke, 1984).

In order to determine the stratigraphy of the volcanic rocks and to study the migration of volcanism in detail, we began a systematic paleomagnetic investigation in the summer of 1977. We determined directions of thermoremanent magnetization for >560 sites, adding to the ~90 sites already analyzed by other workers. The broad magnetostratigraphy of the volcanic field was worked out by combining paleomagnetic results, field relations determined from detailed geologic mapping, and K-Ar ages obtained by other workers. Assignment of virtually all of the rocks of the volcanic field to broad age classes enabled us to examine (1) the pattern of eruption loci and volume of volcanic material erupted as a function of time, (2) the migration of volcanism in this field compared with that of other volcanic fields in the western United States, (3) a possible model for deep-seated magma generation, and (4) implications for absolute motion of the North American plate.

GEOLOGIC SETTING

The San Francisco volcanic field in northern Arizona is one of several dominantly basaltic volcanic fields of late Cenozoic age on the southern Colorado Plateau (Fig. 1). The field extends somewhat more than 100 km east-west and ~70 km north-south (Fig. 2). It includes >600 basaltic volcanoes of Tertiary (Pliocene) and Quaternary age and associated lava flows and pyroclastic deposits that cover ~4,800 km^2. They rest on Miocene volcanic rocks and erosional surfaces of low relief cut on Permian and Triassic sedimentary rocks (Wolfe and others, 1983). Post-Miocene basaltic volcanism was broadly contemporaneous with the silicic and intermediate volcanism that formed Bill Williams Mountain, Sitgreaves Mountain, Kendrick Peak, San Francisco Mountain, O'Leary Peak, and isolated domes (Fig. 2).

An extensive Miocene–early Pliocene volcanic field, composed of rocks informally referred to as the "rim basalts," borders the San Francisco field on the south. This field makes up part of the Mogollon Rim that forms the southern margin of the Colorado Plateau. Its rocks were more extensively affected by Cenozoic normal faulting and are much more dissected than are the lavas of the San Francisco field. Most published K-Ar ages of the rim basalts lie in the range of 5 to 8 m.y. (Luedke and Smith, 1978). They are overlapped along their northern margin by rocks of the San Francisco volcanic field. The oldest volcanoes and lava flows of the San Francisco field also occur in this area, and it is not clear if there was a break in time between rim-basalt volcanism and volcanism of the San Francisco field. The southwest boundary of the field is hence ill defined and has been arbitrarily drawn.

Late Cenozoic activity along the regional fault systems (Fig. 2) caused normal offset of the rocks that underlie the San Francisco volcanic rocks and also locally of the volcanic rocks themselves. These fault systems are related to large, ancient systems of faults that cut the Proterozoic crystalline basement (Shoemaker and others, 1978). Several silicic volcanic centers, including Bill Williams, Sitgreaves, and Kendrick, are situated along or near the Mesa Butte system. The Oak Creek Canyon fault system trends north to underlie the San Francisco Mountain stratocone. Along its extent south of San Francisco Mountain, there are several 2- to 1-m.y.-old vents that produced benmoreite, dacite, and rhyolite. The Doney fault, which may be a northern extension of the Oak Creek Canyon fault system, underlies O'Leary Peak. Faults in the Mesa Butte and Oak Creek Canyon systems offset volcanic rocks that are 6 to 1 m.y.

Geological Society of America Bulletin, v. 97, p. 129–141, 8 figs., 3 tables, February 1986.

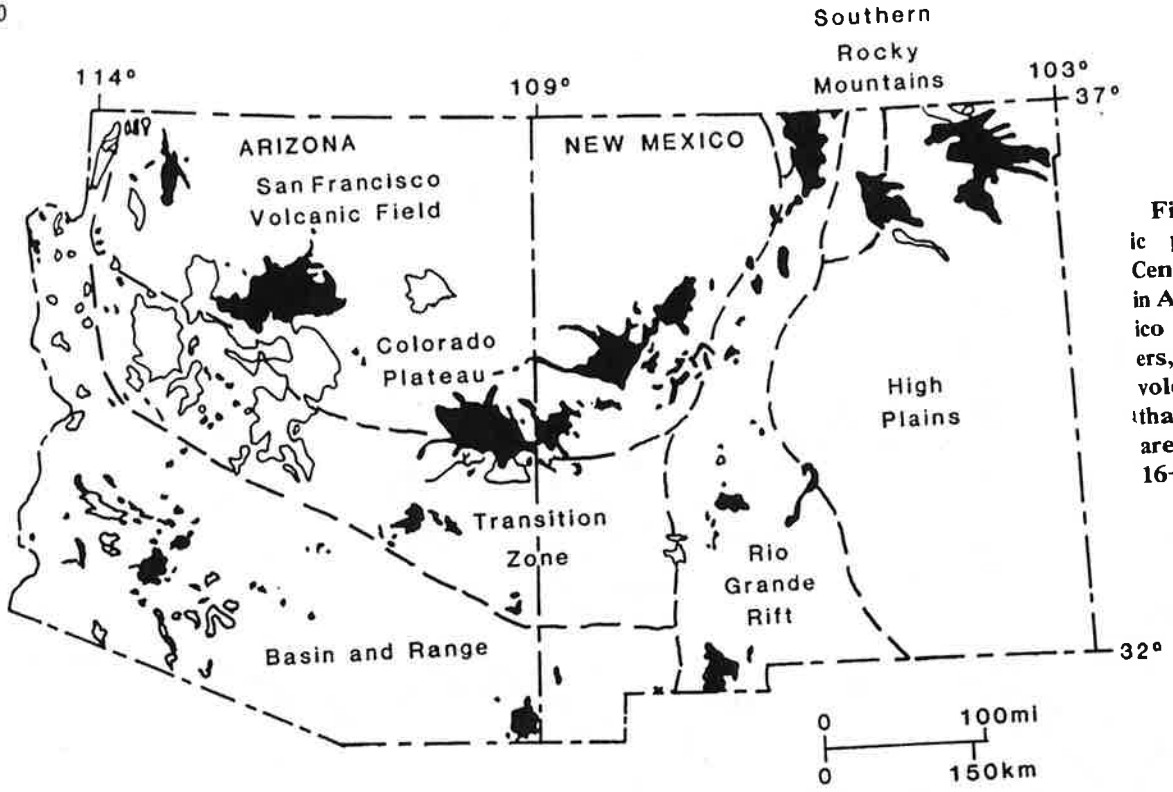

Figure 1. Physiographic provinces and late Cenozoic volcanic fields in Arizona and New Mexico (from Wolfe and others, 1983). Dark areas, volcanic rocks younger than 5 m.y.; outlined areas, volcanic rocks 5 to 16+ m.y.

old. Faults of the smaller Cataract Creek system (not shown in Fig. 2) trend northwest across the western part of the volcanic field. The Mesa Butte and other minor faults of various trends cut the rim basalts. Many basaltic cinder cones, as well as silicic volcanoes, are aligned along exposed faults or follow the trend of faults in each system.

PALEOMAGNETIC SAMPLING AND LABORATORY METHODS

At the 535 sample sites of mafic vents and lava flows analyzed in this study, 440 separate eruptions related to mapped cinder cones are represented. In some cases, deposits from a single eruption or eruptive episode were sampled at two or more sites. Vent locations of ~34 sampled lava flows and 1 basaltic tuff bed are unknown, because either the vents or the proximal parts of the flows are buried; other similar flows were not sampled. A few buried vents probably exist in the San Francisco field that are not represented in this study; however, their omission should not materially affect our conclusions. The sampled sites include nearly all of the vents or their associated flows, or both, west of the longitude of O'Leary Peak. A total of 115 sites was sampled at intermediate to silicic centers and isolated domes and flows, including a succession of andesite and dacite flows on San Francisco Mountain (T. C. Onstott, unpub. data). East and north of San Francisco Mountain, paleomagnetic studies were carried out by Babbitt (1963), Champion (1980 and 1983, written commun.), J. N. Kellogg (unpub. data), and T. C. Onstott (unpub. data). The total of 650 sample sites analyzed in this study includes 90 sites from these workers. In summary, the total paleomagnetic sampling survey is as follows: mafic sample sites, 535; mafic cinder cones sampled, 440; silicic and intermediate sites sampled, 115; silicic and intermediate eruptions sampled, >100.

We obtained oriented core samples with a portable rock drill similar to that described by Doell and Cox (1965). We usually took 6 to 8 samples per site, but for units in which we needed well-defined magnetic vectors, we took as many as 24 samples. We measured sample orientations by a sun compass when possible and oriented all samples by a Brunton compass. Lightning has extensively remagnetized the volcanic rocks, and so we preferred to sample oxidized vent rocks rather than lava flows, as discussed below. In some instances, minor rotations appear to have occurred in the tops and flanks of some block flows, many of which are andesitic to dacitic. We could sample some vents only from large bombs protruding through loose cinders. If samples from bombs yielded discordant data, the samples were presumed to represent slumped or rotated material; for this reason, several sites were not included in the data set.

Owing to the strong magnetization of most of the rocks sampled, measurements were made using either (1) a high-RPM, air-driven spinner magnetometer on 2.5-cm-diameter samples weighing generally 15 to 25 g or (2) a superconducting magnetometer on wafer-shaped samples 2.5 cm in diameter, 3 to 7 mm thick, largely weighing 3 to 8 g. Even so, some of the basalt samples have natural remanent magnetization (NRM) intensities beyond the range of the instrument, especially those with a strong lightning-induced, isothermal remanent magnetization (IRM) component. For cross-reference checking, we measured some samples with both instruments. Nearly all samples were subjected to alternating field (AF) demagnetization. Most samples were demagnetized stepwise at intervals of 250-Oe peak field to a maximum of 1,000 Oe. The number of steps used was based on the AF field required to remove most of the IRM component. Samples that probably retain a large component of IRM, as indicated by either high magnetic intensity or large deviation of direction from the majority of directions at a given sample site, were not included in calculations of the average direction of magnetization. This selection process did not alter any polarity determinations; however, data from ~15 sample sites

55

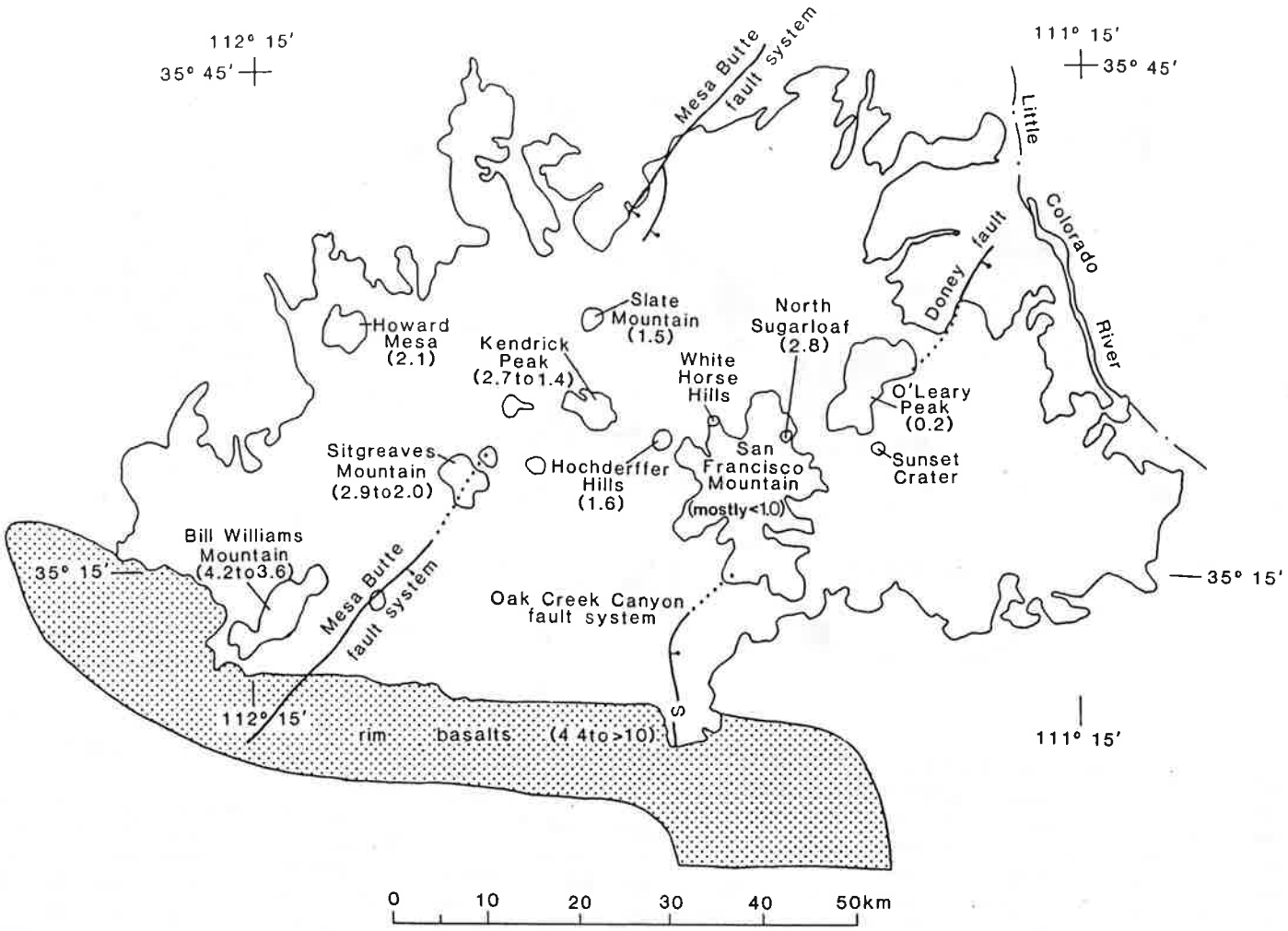

Figure 2. The San Francisco volcanic field and its silicic and intermediate centers (outlined within field), major structures, and northern extent of "rim basalts." Figures (in m.y.) indicate K-Ar ages of centers.

were insufficiently coherent to determine a polarity and were discarded. Average directions of magnetization for all inferred Matuyama and Brunhes mafic vents and flows at optimal demagnetization are shown in Figure 3.

MAGNETIC PROPERTIES OF THE VOLCANIC ROCKS

Magnetic studies of volcanic rocks in the San Francisco field (Babbitt, 1963; Coe, 1967; Strangway and others, 1968; Champion, 1980) showed that the major magnetic component in the basaltic lava flows is borne by titaniferous magnetite. This mineral has a Curie point generally between 400 and 550 °C, depending on the titanium content. All of the volcanic rocks studied, including dacitic blocks in pyroclastic flows, apparently came to rest at sufficiently high temperatures for their thermoremanent magnetization (TRM) to have been acquired in place. Emplacement temperature, then, was not a factor in sample-site selection.

The basalts sampled generally have NRM intensities of 10^{-3} to 1 G/cm^3, made up of TRM and IRM components. The components depend on a sample's dominant magnetic mineral phase and proximity to lightning strikes. Despite our efforts to avoid magnetic anomalies resulting from lightning strikes, the NRM's of most samples taken from lava flows are high in intensity and dominated by an IRM component. Samples taken from road-cuts, cinder pits, and oxidized vent material generally have low NRM intensities and only minor IRM overprints. Hematite is the primary magnetic mineral in the oxidized spatter, tuff, and cinder bombs sampled on the cinder cones. The coercivity of hematite

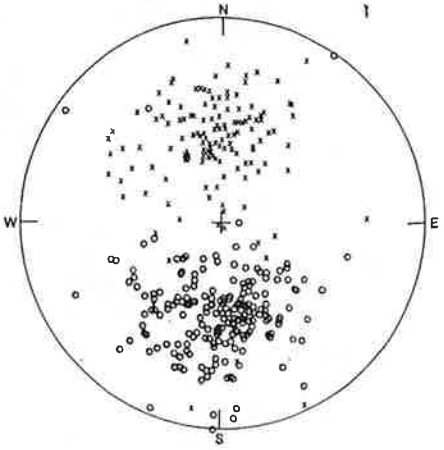

Figure 3. Equal-area plot of magnetic vectors of mafic sites inferred to be of either Brunhes or Matuyama chronozone. Crosses, positive inclination; circles, negative inclination. Vectors derived by averaging magnetic-field directions from optimally demagnetized samples from each site.

58

is sufficiently high that, despite the increased exposure to lightning on the rims of cinder cones, samples with magnetization dominated by hematite are relatively free of IRM.

POLARITY CHRONOSTRATIGRAPHY

Determination of Chronozones

The polarity time scale of Mankinen and Dalrymple (1979) for the past 5 m.y. provides the primary basis for polarity-chronostratigraphic correlation of Pliocene-Pleistocene rocks. The time scale is based on a statistical analysis of K-Ar ages and on magnetic polarity determinations that meet strict requirements of precision. The Brunhes, Matuyama, Gauss, and Gilbert chronozones defined originally by Cox and others (1964) are the principal units for which magnetostratigraphic correlations within the San Francisco volcanic field have been attempted by most workers. Although subchronozones such as the Jaramillo and Olduvai are represented in the field (T. C. Onstott, 1977, personal commun.), in most cases sufficient K-Ar and stratigraphic controls were not available for us to consistently identify the volcanic units belonging to these subchronozones. Age control, moreover, was insufficient for consistent distinction between Gauss and Gilbert (about 5.0 to 2.48 Ma) rocks. We therefore grouped rocks belonging to these chronozones with a few older rocks and considered their age to be pre-Matuyama.

Polarity determinations (Figs. 4 and 5), K-Ar ages, and stratigraphic relations provided the primary bases for our assignment of volcanic units to chronozones. Most of the K-Ar ages cited in Figure 5 are from the compilation of Luedke and Smith (1978) and are based on the work of Damon (1966), Damon and others (1974), and McKee and others (1974). These ages were slightly revised to reflect new decay constants (Dalrymple, 1979). Many additional K-Ar ages (P. E. Damon and M. Shaffiqullah, unpub. data; E. H. McKee, unpub. data) were critically important in establishing the volcanic stratigraphy and in making assignments to chronozones. Units dated by K-Ar were assigned to a single chronozone if the one standard-deviation interval included only that chronozone; otherwise, geomorphic or contact relations of the given unit with one or more dated units were used to ascertain the polarity zone.

Field evidence for local volcanic stratigraphy included superposition relations, lithologic correlations, geomorphic preservation, degree of weathering, and relative elevations of erosion surfaces that underlie the volcanic rocks. Fresh cinder cones and rough-surfaced lava flows in the eastern part of the field are clearly younger than the eroded vents with exposed feeder dikes and the smooth-topped flows in the western parts. Near the Little Colorado River (Fig. 2), late Quaternary rates of downcutting have been rapid enough to enable distinction of younger flows in stream bottoms and on successively higher terrace levels above the present drainage. These relations provided a basis for a relative-age classification by Colton (1936) and, more recently, for a stratigraphy for the eastern part of the volcanic field developed by Moore and others (1976). Radiometric ages indicate that lavas and tephra of the Tappan, Merriam, and Sunset stages of Moore and others (1976) fall in the Brunhes chronozone. Lavas dated as Woodhouse age by these workers can be shown on the basis of magnetic polarity and K-Ar ages to be-

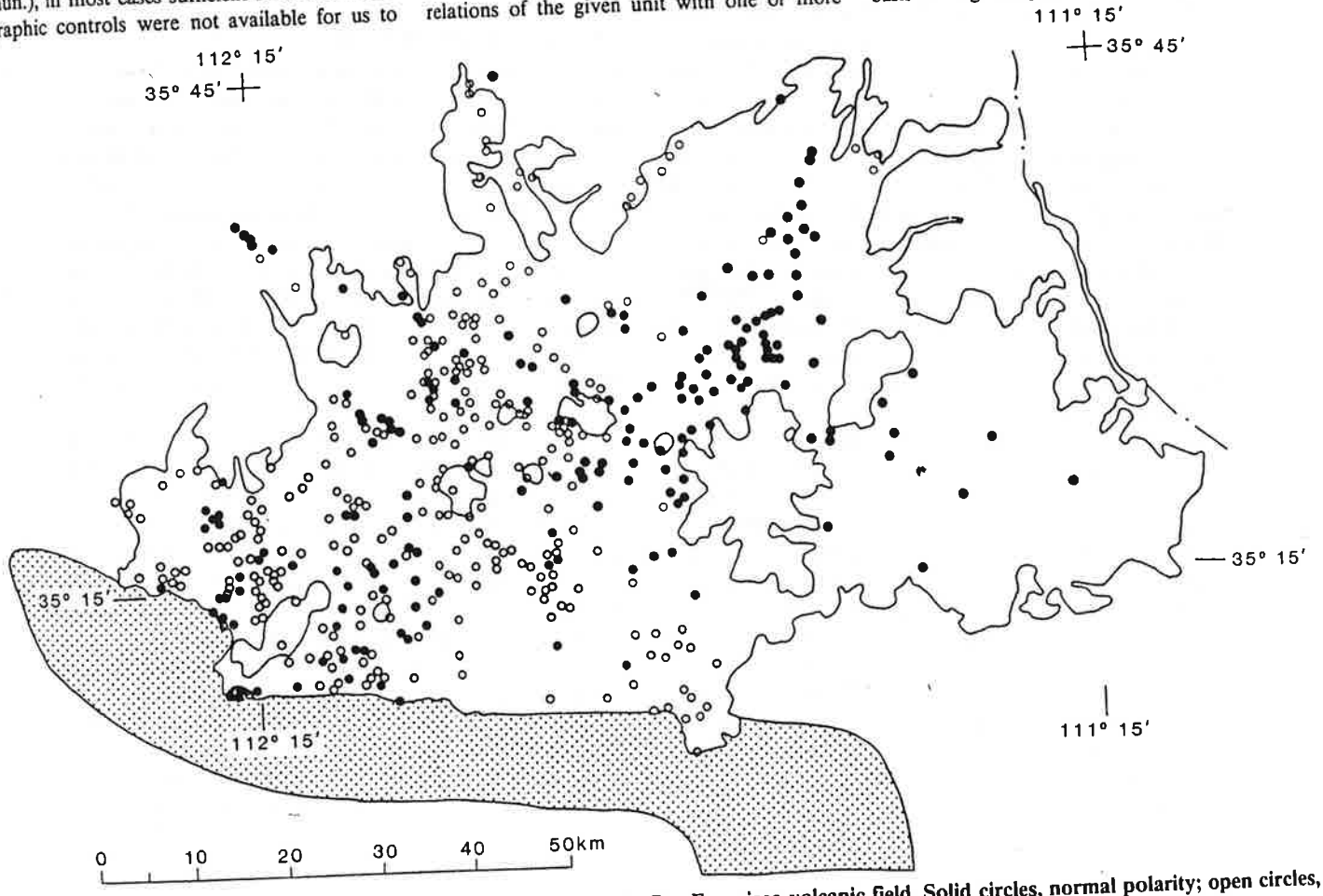

Figure 4. Paleomagnetic polarities measured in mafic vents in the San Francisco volcanic field. Solid circles, normal polarity; open circles, reverse polarity. Some vents occur within silicic centers (outlined).

57

RICHARD J. ARCULUS[1]* AND DAVID A. GUST[2]
[1]DEPARTMENT OF GEOLOGY, AUSTRALIAN NATIONAL UNIVERSITY, CANBERRA, A.C.T. 0200, AUSTRALIA
[2]SCHOOL OF GEOLOGY, QUEENSLAND UNIVERSITY OF TECHNOLOGY, GPO BOX 2434, BRISBANE, QUEENSLAND 4001, AUSTRALIA

Regional Petrology of the San Francisco Volcanic Field, Arizona, USA

A wide variety of rock types has been erupted during the past 5 Ma in the San Francisco Volcanic Field (SFVF) of north–central Arizona. Nepheline-normative to olivine hypersthene- and quartz-normative basalts form the mafic end of a spectrum that includes various lineages of relatively high-Na and high-K, intermediate and silicic volcanics. These evolved magmas have been erupted in individual centres that range in size from small craters to the San Francisco Peaks themselves, with a volume of ~50 km^3. Isotopic variability ($^{87}Sr/^{86}Sr$ ~0·7030–0·7046) and a spread of La/Yb in the basalts indicate a variety of upper-mantle sources. A number of petrographically distinct basalt types are related by varying degrees of olivine and/or clinopyroxene accumulation. The fractional crystallization of olivine, clinopyroxene, plagioclase and oxides (± amphibole), from alkali olivine basalt parents, to produce a relatively Na-rich lineage of hawaiite, benmoreite/high-Na andesite and trachyte is supported by least-squares fractionation and mixing calculations. Mixing with K-rich, crustally derived (radiogenic and unradiogenic $^{87}Sr/^{86}Sr$ and unradiogenic $^{206}Pb/^{204}Pb$) rhyolite has produced other trends towards alkali-rich andesite, dacite and rhyolite. Within some individual silicic centres, distinctive major and trace element geochemistry, petrographic features and isotopic data are interpreted to result from a combination of fractional crystallization of basalt in deep crustal magma chambers (cumulate blocks are widespread in basaltic rocks), crustal anatexis, and direct mixing of evolved basaltic and rhyolitic melts. In other centres, a combination of assimilation–fractional crystallization involving crustal components developed. Partially digested oligoclase–andesine and quartz xenocrysts, identical in composition to phases present in granulite xenolith assemblages, also occur widely in the basalt–rhyolite compositional spectrum. Reverse zoning of plagioclase and ferromagnesian phenocrysts and disequilibrium assemblages are common. The majority of the volcanic rocks are alkalic with respect to major element (IUGS) classifications, but mineralogical characteristics include the presence of phenocrystic and groundmass orthopyroxene in many of the intermediate rocks. Some meta- and peraluminous rhyolites have low La/Yb, massively negative Eu anomalies, <20 p.p.m. Ba and Sr, and extremely manganiferous fayalite (~10 wt % MnO). Rare peralkaline high-SiO_2 rhyolites contain ~900 p.p.m. Zr.

KEY WORDS: *San Francisco volcanic field; Arizona; petrology; geochemistry*

INTRODUCTION

The San Francisco Volcanic Field (SFVF) extends over an area of ~5000 km^2 on the southwestern margin of the Colorado Plateau in the transition zone between the Plateau and the Basin and Range Province. At least five major, differentiated silicic centres (Fig. 1) rise up to 2000 m above the surrounding basalt-capped Plateau surface. Approximately 600 individual vents, many with lava flows, cap the Plateau and conceal the Mesozoic–Precambrian sequences exposed in the canyon country to the southwest of the SFVF. The depth to the Moho in this region is on the order of 45 km (Warren, 1969).

The SFVF was formed within the last 5 Ma—the most recent activity taking place ~900–750 years ago, culminating in the twelfth century AD eruption of the Sunset Crater Ash and Bonito lava flow [see Holm & Moore (1987) for review]. There has been an overall migration of volcanism from the southwest to northeast (Tanaka *et al.*, 1986), and a complex history of volcanic development in any individual centre. Basaltic activity has been broadly contemporaneous with the development of the silicic centres. In the sense that lavas of intermediate SiO_2 content (52–63%) are significant volumetrically in these centres, the SFVF represents an atypical occurrence of a near-continuum of compositions

*Corresponding author.

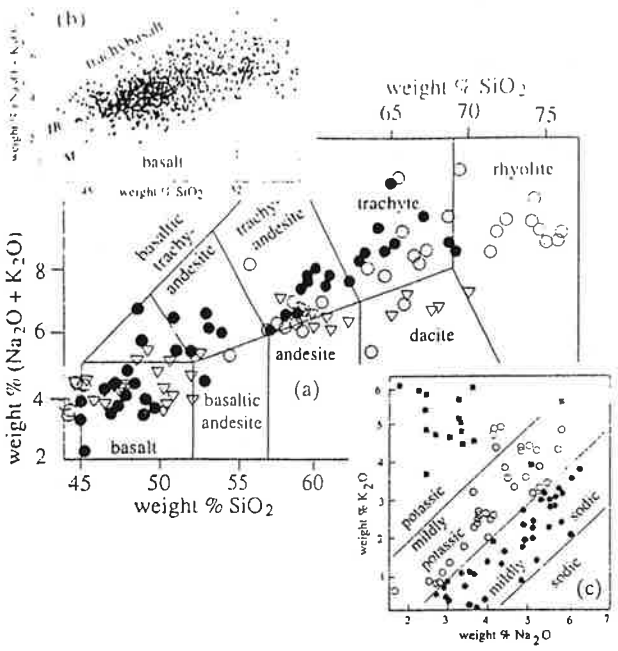

Fig. 2. (a) Combined alkalis vs SiO_2 plot for the SFVF 'Type Suite', analyses calculated to 100% volatile-free. Main boundaries in this diagram and in (b) and (c) are those of Le Bas *et al.* (1986). ●, High-Na or mildly sodic [see (c)] samples. ○, High-K or mildly potassic to potassic types. ▽, Samples from the MMVF. (b) Alkalis vs SiO_2 plot for all samples from the SFVF <54 wt % SiO_2. IB represents the Irvine & Baragar (1971) and M the Macdonald & Katsura (1964) discriminant boundaries between alkalic and tholeiitic fields. (c) Wt % K_2O vs Na_2O for the Type Suite with symbols shaded according to the classification boundaries of Le Bas *et al.* (1986); ●, mildly sodic; ○, mildly potassic to potassic. ■, Microprobe analyses of glasses in groundmass and inclusions.

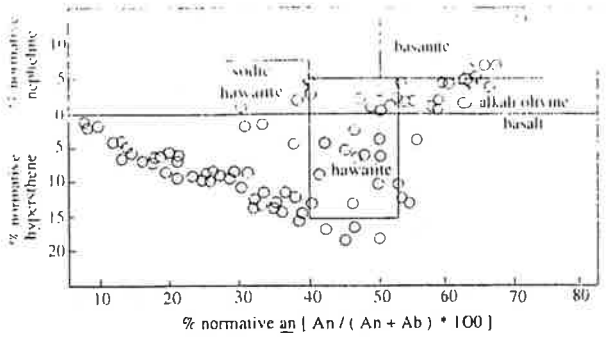

Fig. 3. Normative plagioclase composition vs degree of SiO_2 saturation for the Type Suite compared with the fields for basalts erupted in the transition zone with the Basin and Range of the northern Colorado Plateau (Best & Brimhall, 1974). There is no obvious separation on this projection of the high-K and high-Na types.

small negative (and in one case, positive) anomalies appear in the more evolved (hawaiitic) lavas.

High concentrations of compatible elements are present in some of the mafic basalts (~550 p.p.m. Cr; ~450 p.p.m. Ni; ~60 p.p.m. Cs; ~80 p.p.m. Co), and the abundances of these elements are also abnormally high in some more evolved types (Fig. 5).

Within the large group of intermediate rock types (broadly andesite, dacites and benmoreites), a number of features of the trace element abundances are similar to those of the basalts. For example, the LREE are enriched and La/Yb is strongly fractionated (Fig. 5). Values of Ba/La* (chrondrite-normalized ratio) >1 and Sr/La* <1 are characteristic of both intermediate and basaltic rocks. Small negative Eu anomalies are present in a limited number of samples. In general, a positive correlation of LILE and HFSE abundances with SiO_2 concentration characterizes the intermediate rocks, although a wide range is present at any specific SiO_2 content (Ba~600–1600 p.p.m.; Rb~20–60 p.p.m.) (Fig. 5). Likewise, a considerable range of compatible element concentrations exists at specific SiO_2 contents (e.g. ~100 p.p.m. Cr and Ni at ~60 wt % SiO_2; Fig. 5).

In contrast, the trace element abundances of some of the most silicic rock types (trachytes and rhyolites) are distinctively different in terms of the relative fractionations observed, compared with the mafic and intermediate rocks. For example, although La/Yb*~30 and LREE~300 times chondritic are characteristic of some trachytes, strongly negative Eu anomalies, low La/Yb* (~10 to 1) (Fig. 4), very low Ba and Sr (<10–15 p.p.m.), and divergent Zr and Hf (Fig. 5) are found in other silicic rocks.

PETROGRAPHY

The basalts of the SFVF vary widely in appearance from essentially aphyric to rather strongly porphyritic with phenocrysts up to 15–20 mm in maximum dimension. Groundmass textures range from intersertal and microcrystalline to intergranular and holocrystalline subophitic. The major phenocryst phases are clinopyroxene, olivine and plagioclase, and different basalt types are recognized partly on the mode and relative abundance of these phenocrysts. Microcrystalline inclusions of spinel are present in many olivine and clinopyroxene phenocrysts, and single- and two-phase fluid inclusions are ubiquitous in olivine grains. Crystalline groundmass assemblages are dominated by the same phases that appear as phenocrysts together with abundant, dusty-appearing titaniferous magnetite and, in some samples, ilmenite. Glass and minute needles of apatite are present in the groundmass of many basalts. Recognizable xenocrysts include quartz (both single grain and polycrystalline fragments), usually of ovoid appearance and rimmed by clinopyroxene,

Holocene scoria cone and lava flows at Sunset Crater, northern Arizona

Richard F. Holm, Department of Geology, Northern Arizona University, Flagstaff, Arizona 86011
Richard B. Moore, U.S. Geological Survey, Hawaiian Volcano Observatory, Hawaii 96718

LOCATION AND ACCESS

Sunset Crater, about 15 mi (25 km) north of Flagstaff, Arizona (Fig. 1), is in the eastern part of the San Francisco volcanic field, on the southern margin of the Colorado Plateau. Access to the Sunset Crater National Monument is by Forest Road 545, an all-weather road off of U.S. 89. Included within the boundaries of the monument are the scoria cone of Sunset Crater and most of one of its associated lava flows, the Bonito flow. Another lava flow associated with Sunset Crater, the Kana-a flow, occurs in the Coconino National Forest east of the monument. Hiking is prohibited on Sunset Crater scoria cone, and collection of specimens is not permitted within the boundaries of the national monument.

Topographic maps published by the U.S. Geological Survey that cover the monument and surrounding area are the Sunset Crater East, Sunset Crater West, O'Leary Peak, and Strawberry Crater quadrangles of the 7½-minute series. The geology of the area is shown by Moore and Wolfe (1976).

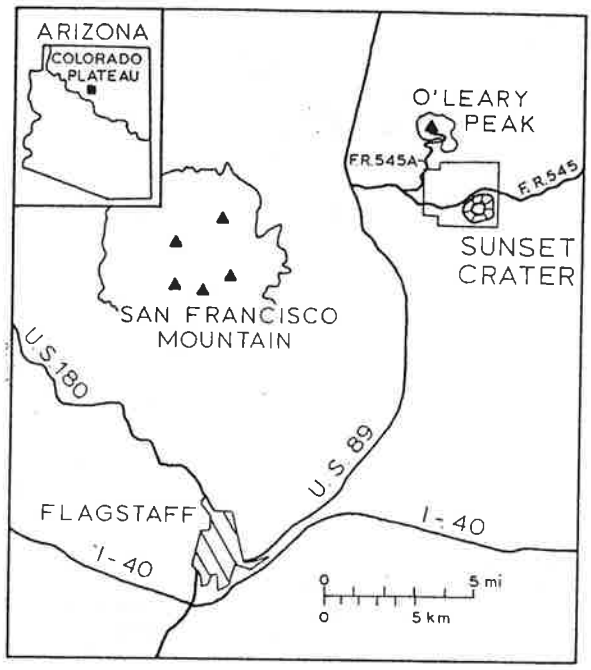

Figure 1. Index map showing location of Sunset Crater and access roads. *Triangles* are major peaks.

SIGNIFICANCE

Sunset Crater and its associated lava flows, together with nearby small scoria and agglutinate cones, are the youngest volcanic features in the San Francisco volcanic field, a late Miocene to Holocene volcanic province in northern Arizona. Although Sunset Crater is only one of more than 550 basaltic vents in the volcanic field, the colorful, nearly symmetrical cone and its basalt lava flows are distinctive because they are virtually untouched by weathering and erosion. Many primary flow structures are well preserved and displayed on the Bonito lava flow. Studies in volcanology, archeology, dendrochronology, and paleomagnetism provide an exceptionally detailed documentation of the history of the Sunset Crater eruption and its effects on the indigenous Indian population of northern Arizona (Pilles, 1979). The volcano was originally named Sunset Mountain by Major J. W. Powell when he was director of the U.S. Geological Survey, in reference to the colorful appearance of the top, as though it was bathed in the rays of the setting sun (Colton, 1945).

VOLCANIC GEOLOGY

Introduction

Volcanic deposits formed during the Sunset Crater eruption include the scoria cone of Sunset Crater, two basalt lava flows that extruded from its base, three rows of small scoria and agglutinate cones east-southeast of Sunset Crater, a basalt lava flow from vent 512 about 6.2 mi (10 km) east-southeast of Sunset Crater, and a tephra blanket that originally covered over 800 mi^2 (2,080 km^2) (Colton, 1932; Moore and Wolfe, 1976; Fig. 2). The vents lie in a zone that trends S 60° E from Sunset Crater and probably were controlled by a major fracture in the Paleozoic and Precambrian rocks beneath the volcanic field. The lava flows and essential pyroclasts are all similar in chemistry and petrography (Moore, 1974), having formed from alkali basalt magma (ne = 1.5%) that contained microphenocrysts of plagioclase (An_{70}), olivine, augite, and magnetite, and sparse phenocrysts of olivine (Fo_{83}).

Sunset Crater Scoria Cone

Sunset Crater is a nearly symmetrical cone, composed dominantly of black scoria, that is about 1,000 ft (300 m) in height and 1 mi (1.6 km) in base diameter. The symmetry of the cone is lowered only by the west-of-center location of the main crater and a gentle recess in the east side of the cone above the presumed extrusion point of the Kana-a flow. Older volcanoes that were partially buried by Sunset Crater form large rounded mounds at the base on the northeast, southeast, and southwest sides.

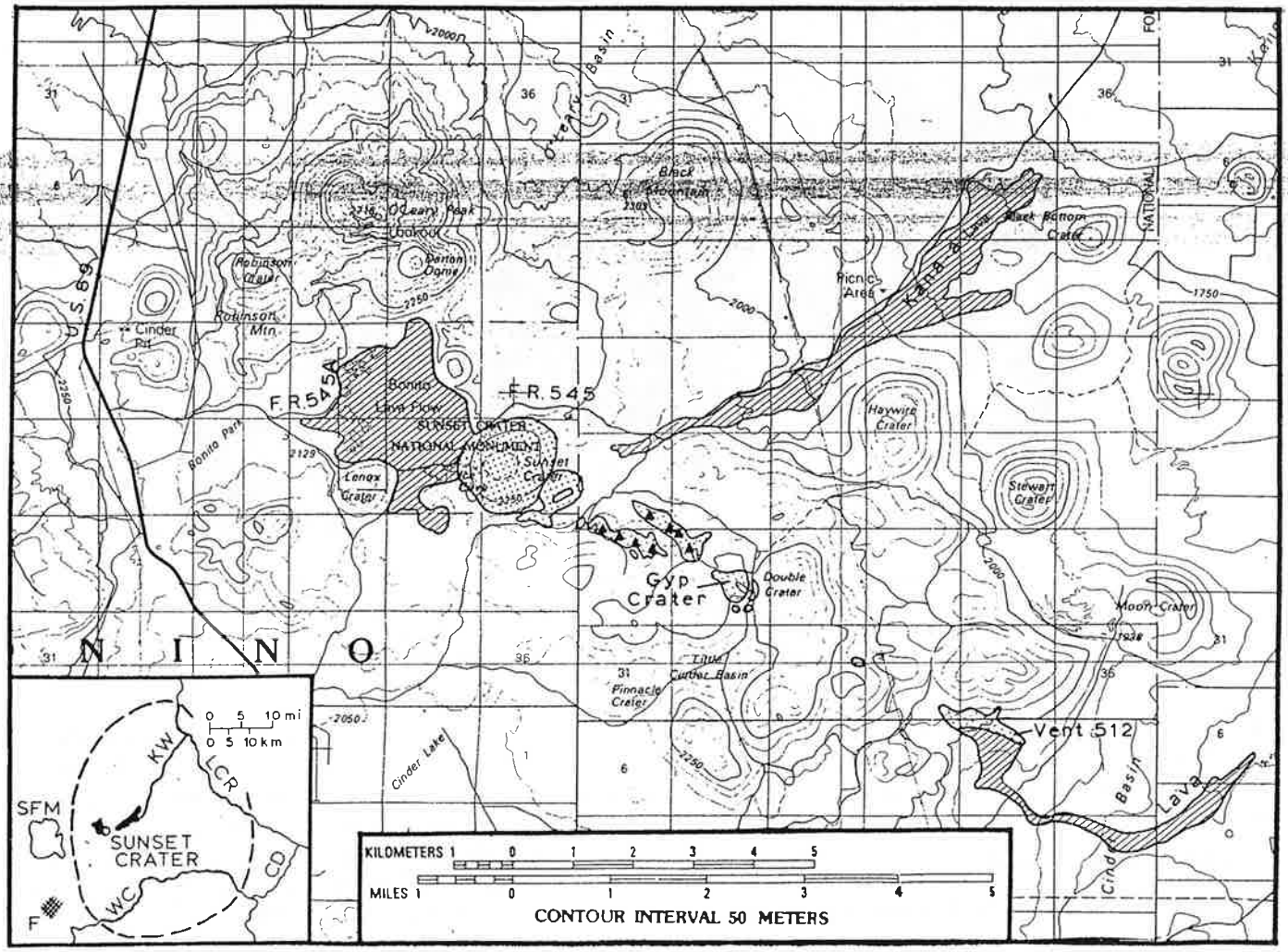

Figure 2. Map showing distribution of vent deposits (*dot pattern*) and lava flows (*lines*) of the Sunset Crater eruption (from Moore and Wolfe, 1976); some of the small scoria cones southeast of Sunset Crater are shown with *filled triangles.* Small scale map shows original distribution (*dashed line*) of the Sunset Crater tephra blanket (from Colton, 1932); *F,* Flagstaff; *SFM,* San Francisco Mountain; *WC,* Walnut Creek; *KW,* Kana-a Wash; *LCR,* Little Colorado River; *CD,* Canyon Diablo.

At the summit of Sunset Crater a rim encloses the main crater, which is more than 400 ft (120 m) deep, and a small crater on the east side of the larger that is about 160 ft (50 m) deep. The rim is highest on its eastern side, which probably is a reflection of the prevailing wind direction during the eruption, but prominent notches in the rim on its eastern and western sides above the extrusion points of the Kana-a and Bonito flows suggest that disruption of the original shape of the rim occurred by partial collapse events. Planar bedded deposits of red scoria on the crater rim were cemented by sublimation of silica, gypsum, and iron oxide from fumarolic vapors, which give the summit its distinctive red, pink, and yellow colors. The cemented beds on the rim dip outward around the main crater, but display inward dips around the smaller crater. Welded spatter and agglutinate deposits occur only in a few loose blocks up to 3 ft (1 m) in diameter in local areas on the upper surface of the cone. Unconsolidated black lapilli and bombs overlie the red summit scoria around the small crater and on the outer north slope of the main crater. Particles ranging in size from fine ash to spheroidal bombs up to 3 ft (1 m) in diameter mantle the slopes of the cone. Although granulometric data have not been obtained, the most common pyroclast size appears to be fine lapilli, but ash is also conspicuous in its abundance.

The Sunset Crater eruption produced a mantling blanket of black scoriaceous lapilli and ash, originally covering more than 800 mi^2 (2,100 km^2), that extended in a broad ellipse generally to the east of the volcano (Colton, 1932; Fig. 2). Amos and others (1981) noted the large size of this deposit compared to those from other Strombolian events and suggested that eruption columns may have been at least several hundred ft (m) high. Fluvial and eolian erosion has removed and locally redeposited much of the tephra, and today it covers an area of only about 122 mi^2 (315

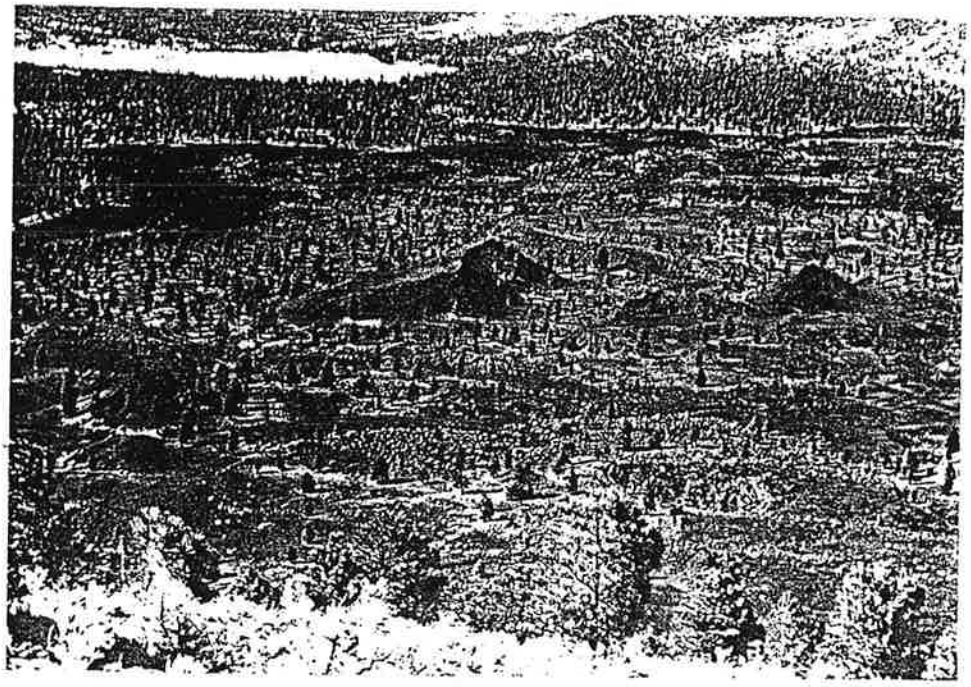

Figure 3. Photograph of the Bonito lava flow; view is to the west from the summit of Sunset Crater. The early scoria-mantled part of the flow has a smoother, lighter surface, whereas the later scoria-free margin is dark. In the foreground are a pit crater and several hornitos. The large mounds in the middle of the flow are agglutinate deposits rafted from an early cone of Sunset Crater. Scoria-covered islands of the early Bonito flow are surrounded by scoria-free zones in the upper right corner.

km^2; Moore, 1974). Near Sunset Crater the tephra blanket is several decimeters to over a meter thick, and it covers parts of the Bonito and Kana-a flows as well as agglutinate deposits to the east-southeast at Gyp Crater and vent 512.

Lava Flows From Sunset Crater

Bonito Flow. The Bonito lava flow was extruded at 2 or more points in a zone along the western to northwestern base of Sunset Crater. The lava spread northwesterly and ponded in an intercone basin bounded by Sunset Crater and older volcanic deposits. Low areas between older cones were inundated, and on the south side of the basin the lava overtopped a low divide and flowed into the crater of an older, extensively eroded scoria cone. Exposures around the periphery of the flow demonstrate that it is on top of black scoria of the Sunset Crater tephra blanket. The lava flow covers an area of 1.79 mi^2 (4.63 km^2) to a depth of around 6 ft (2 m) locally along its margin to perhaps more than 100 ft (30 m) in the center (Moore, 1974).

Many flow units and a wide variety of flow structures create a highly complicated appearance of the Bonito flow. Although the flow is dominantly slab pahoehoe, massive, ropy, festoon, and shelly surface structures occur locally, and aa clinkers are common around the flow's margin. Chains of hornitos, 3 ft to 50 ft (1 m to 15 m) high, and a few tumuli dot the top of the flow, presumably above lava tubes, and an impressive pit crater 320 ft (100 m) long is almost 50 ft (15 m) deep (Fig. 3).

The most conspicuous features of the Bonito lava flow are mounds of crudely stratified spatter, welded spatter, agglutinate, and rootless flows on the top of the flow (Fig. 3), and large fissures that break its crust. The mounds of welded pyroclasts are strung out like beads in a chain in a north-northwesterly direction for about 3,700 ft (1,130 m) from the base of Sunset Crater; the mounds appear to be near-vent deposits from an earlier, and now buried, cone of Sunset Crater that were rafted away when the Bonito flow was extruded from the base and caused partial collapse of the earlier cone. The fissures, up to 2,900 ft (880 m) long and 24 ft (7 m) deep occur in most areas of the flow, although they are most numerous near and in the margins; many of the fissures contain elongated squeeze-ups marked with vertical grooves, but some are gaping, open cracks with steep walls. The fissures were opened as the flow's molten interior continued to spread outward, and many are located in subsided areas where the interior lava drained away.

Most of the central and southeastern part of the Bonito flow is mantled with black scoria about 1 ft (several decimeters) to 3 ft (a meter) or more thick; locally, on the tops of mounds that may be small tumuli or lava blisters, fumarolic vapors emitted from the flow's interior oxidized the scoria to reddish colors. The scoria mantle is probably an air-fall blanket from Sunset Crater. Flow units exposed in the pit crater, fissures, and tumuli in the southeastern part of the flow commonly contain thin interbeds of scoria, which demonstrate concurrent extrusion of the early portions of the Bonito flow and eruption of scoria from Sunset Crater's vent.

62

Late Cenozoic Alkalic Basaltic Magmas in the Western Colorado Plateaus and the Basin and Range Transition Zone, U.S.A., and Their Bearing on Mantle Dynamics

M. G. BEST
W. H. BRIMHALL } *Department of Geology, Brigham Young University, Provo, Utah 84601*

ABSTRACT

Late Cenozoic volcanism along the eastern margin of the Basin and Range province in northern Arizona and Utah has created a suite of essentially alkalic basaltic lavas similar to those occurring in other regions of recent uplift, extensional tectonism, and high heat flow. The lavas were derived from a series of partial melts of the mantle, modified to varying degrees by polybaric fractionation of olivine and possibly plagioclase and clinopyroxene during ascent to the surface. Basanite and alkali olivine basalt melts originated at depths of at least 65 km and possibly as much as 95 km (20 to 30 kb) by variable but generally small degrees of partial melting. More voluminous hawaiite magmas originated at shallower depths by a somewhat greater degree of partial melting and were more substantially modified by crystal fractionation prior to extrusion.

Magmas parental to the lava extrusions became increasingly divergent in composition with time, reflecting a broadening depth interval of partial melting in the mantle. Concurrent eruptive activity and block faulting generally shifted eastward with time at a rate of approximately 1 cm/yr. These time-space-composition variations, in combination with the observed essentially marginal localization of basaltic volcanism for the whole Basin and Range province, are explained in terms of upper mantle dynamics. We envisage upwelling mantle or plume activity beginning sometime in the middle to late Cenozoic in the core area of the Basin and Range province and causing progressive thinning or "erosion" of the lithosphere. Erosion ultimately produced a steep, keellike asthenosphere-lithosphere boundary beneath the Colorado Plateaus and the Basin and Range transition zone. Eastward-flowing mantle peridotite from the core of the plume was throttled against this keel, causing localized shear heating. This heat enhanced partial melting so that sufficient liquid was created to separate from the refractory residuum and to rise to the surface. Diapiric uprise of magma, or partially melted mantle in the uppermost mantle, or injection of a swarm of dikes into the lower crust, might have weakened and attenuated the overlying brittle crust, causing concurrent faulting. Eastward erosion of the keel and site of partial melting as time progressed allowed eruptive and fault activity to also migrate.
Key words: igneous petrology, Cenozoic, basalt, magma, mantle.

INTRODUCTION

Much attention has been devoted to the late Mesozoic to mid-Tertiary calc-alkalic igneous rocks in the western United States because of their great volume, economic importance, and significance to models of plate tectonics activity. Fields of basaltic lavas have received less attention, even though they should provide valuable insight into plate tectonics processes in late Cenozoic time. Leeman and Rogers (1970), in a reconnaissance study, drew attention to the nature of the basaltic lavas in the Basin and Range province and related their origin to high surface heat flow, crustal extension, and certain seismic properties typical of this unusual continental area. Christiansen and Lipman (1972) noted the transition from calc-alkalic magmatism, associated with subduction of the Farallon plate, to basaltic and minor rhyolitic magmatism in late Cenozoic time, but reached no definite conclusions regarding the relation of this basaltic magmatism to continental-scale tectonism. McKee (1971) documented the hiatus in magmatic activity about 18 m.y. ago in the western Basin and Range province that marked the calc-alkalic to basaltic transition; he ascribed the initiation of basaltic magmatism to the westward drift of the North American plate over the extension of the East Pacific Rise.

We have obtained chemical and mineralogical data on a small, relatively isolated field of late Cenozoic basaltic lavas that covers an 18,000-km area in the western Grand Canyon region of northwestern Arizona and adjacent Utah (Fig. 1). The region lies in the transition zone between the western Colorado Plateaus and the Basin and Range province, and volcanism has been concurrent with major block faulting and regional uplift.

The transition from undeformed, flat-lying Paleozoic and Mesozoic sedimentary rocks of the Colorado Plateaus to the faulted blocks of deformed rocks of the Basin and Range province occurs within the western Grand Canyon region and is marked by a series of north-striking, normal fault systems (Hamblin, 1970a). Three major fault systems — Grand Wash, Hurricane and Toroweap — have displacements of up to 5,000 m each with the west block down; they extend northward into Utah and southward into Arizona so that the total length of a single fault system may reach 500 km. Although Paleozoic-Mesozoic strata between these faults in Arizona are essentially undeformed (in the Shivwits and Uinkaret Plateaus, Fig. 2), in Utah they are locally folded. Geophysically, the transition from east to west is marked by a thinning of the crust, from 40- to 30-km (Pakiser and Zietz, 1965) thickening of the low-velocity zone so its top is at the base of the crust (Scholz and others, 1971),

Geological Society of America Bulletin, v. 85, p. 1677–1690, 11 figs., November 1974

that typically have relatively greater concentrations of P_2O_5. Omission of these constituents is, however, counterbalanced by the assumption of a Fe_2O_3/FeO ratio, which undoubtedly reflects a significant degree of postextrusion oxidation — the lower ratios in rapidly quenched Kilauean basalt pumice reported in Richter and others (1964), and the extensive oxidation of Fe-Ti oxide phases at submagmatic temperatures in lava flows whose silicate phases manifest no unusual oxidation (Embree, 1970). The degree to which extruded lavas are oxidized is seldom precisely determinable and constitutes a source of uncertainty in any classification scheme based on the norm.

The lavas are classified following the recommendations of Macdonald and Katsura (1964) and of Coombs and Wilkinson (1969) into two major groups (hawaiite and basanite), constituting more than three-fourths of the Grand Canyon lavas, plus the following five minor groups (Fig. 3):

1. Hawaiite: An 40 to 52 percent, ne and hy <5 percent for most samples but hy equal to 14 percent in some. These are the Grand Wash, Hurricane, and Craig's Ranch basalts of our previous reports (Best and Brimhall, 1970).
2. Basanite: An >50 percent, ne >5 percent, modal analcime. These are the Uinkaret basalts of previous reports.
3. Alkali olivine basalt: An >50 percent, ne <5 percent. Although passing transitionally into basanite, these lavas have properties appropriate to the name and are so indicated.
4. Ankaramite: An and ne as in basanite but strongly porphyritic with abundant (~70 percent) modal olivine and calcic clinopyroxene in the whole rock. These are the Washington basalts of previous reports.
5. Sodic hawaiite: An <40 percent, ne 0 to 7 percent. One sample has an = 29.5 and is, strictly speaking, a mugearite.
6. Analcime hawaiite: 13 percent ne with modal analcime.
7. Quartz-bearing basaltic andesite: conspicuous embayed quartz crystals interpreted as high pressure phenocrysts. These are the Middleton basalts of previous reports.

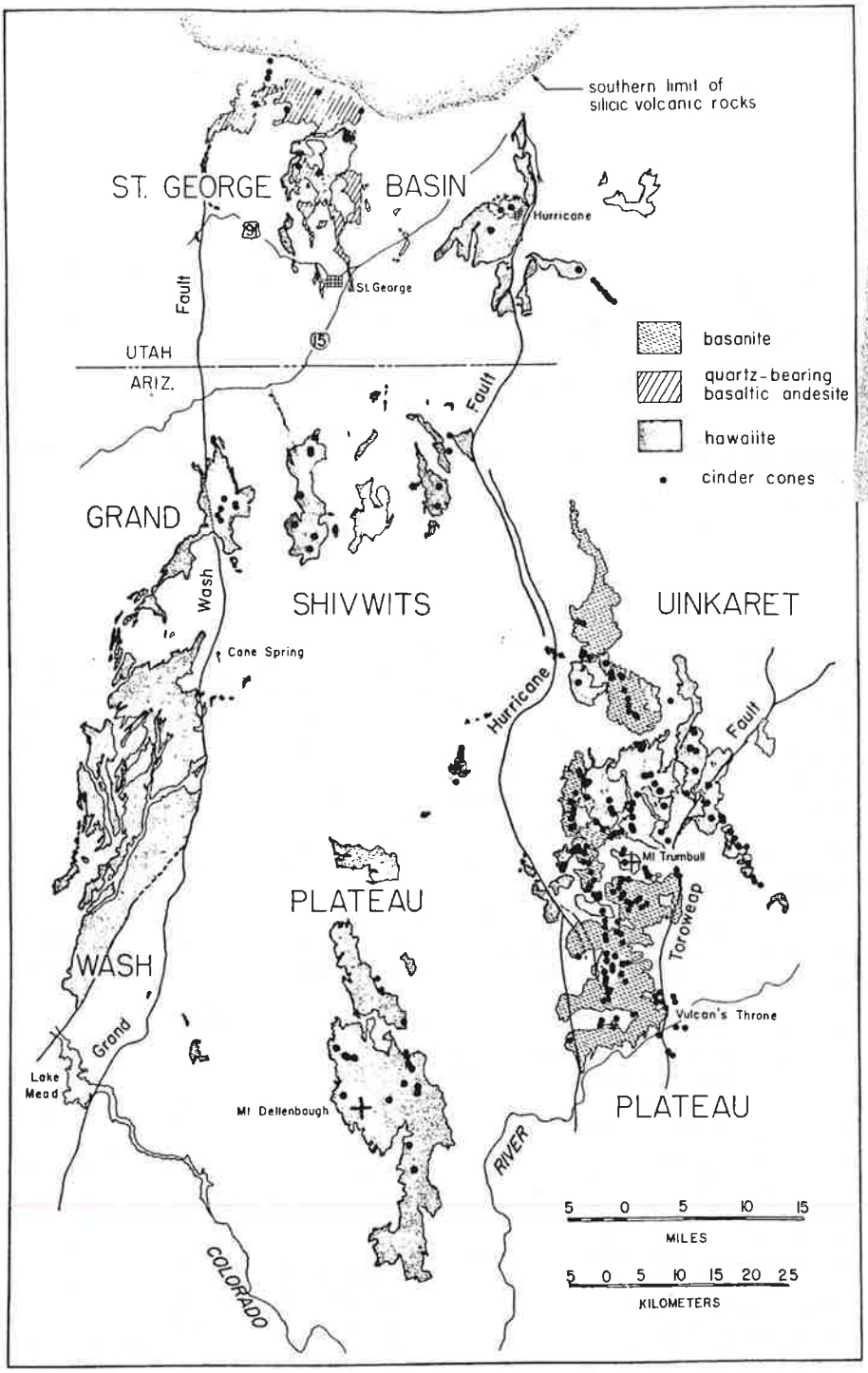

Figure 2. Generalized geologic map of western Grand Canyon region showing distribution of more extensive types of basaltic rocks and major fault systems. Alkali olivine basalts are included with basanite.

Hawaiite

These flows are the most widespread in space and time of any basalt type in the western Grand Canyon region. They occur in every lava field and in all stages, but are particularly voluminous as the plateau-forming lava flows of stage I. At one time these thick (up to 100 m) sequences of numerous (as many as 40) flows likely covered most of the southern Uinkaret and Shivwits Plateaus, as well as a large area extending from the Grand Wash northeastward across the northern Shivwits Plateau. Younger stage II, III, and IV flows occur locally in all parts of the region. Similar hawaiite lava flows have also been found in a reconnaissance of west-central Arizona.

The matrix is medium gray and, though somewhat variable texturally, is most commonly aphanitic, pilotaxitic to intergranular, and locally intersertal. Although some flows are aphyric, olivine phenocrysts are usually present and, in the older flows especially, are partially replaced by iddingsite. Phenocrysts of bytownite and augite, locally combined into glomeroporphyritic clots, appear in many flows. The most strongly porphyritic rocks are found in

San Francisco Mountain: A late Cenozoic composite volcano in northern Arizona

Richard F. Holm, Department of Geology, Northern Arizona University, Flagstaff, Arizona 86011

LOCATION AND ACCESS

San Francisco Mountain, about 6 mi (10 km) north of Flagstaff, Arizona (Fig. 1), is a composite volcano in the San Francisco volcanic field of northern Arizona; the volcano is situated on the southern Colorado Plateau about 31 mi (50 km) north of the escarpment that forms its topographic edge. Flagstaff, the major city in the volcanic field, is at the junction of I-40, U.S. 180, and U.S. 89, the latter two highways passing San Francisco Mountain on its west and east sides, respectively. Access to the mountain is by unpaved U.S. Forest Service roads, most of which are passable by low-clearance vehicles; a few primitive roads require 4-wheel-drive vehicles.

A ski resort on the west side of the mountain normally operates its chairlift during the summer months, providing easy access to the 11,600 ft (3,512 m) level on Agassiz Peak. Hiking restrictions are in effect on Agassiz and Humphreys Peaks, and the designation of the upper part of San Francisco Mountain as the Kachina Peaks Wilderness Area imposes wilderness area restrictions. The Inner Basin is reached by foot or with a vehicle permit from the U.S. Forest Service. The Elden Ranger District office in Flagstaff should be consulted in planning a back-country trip.

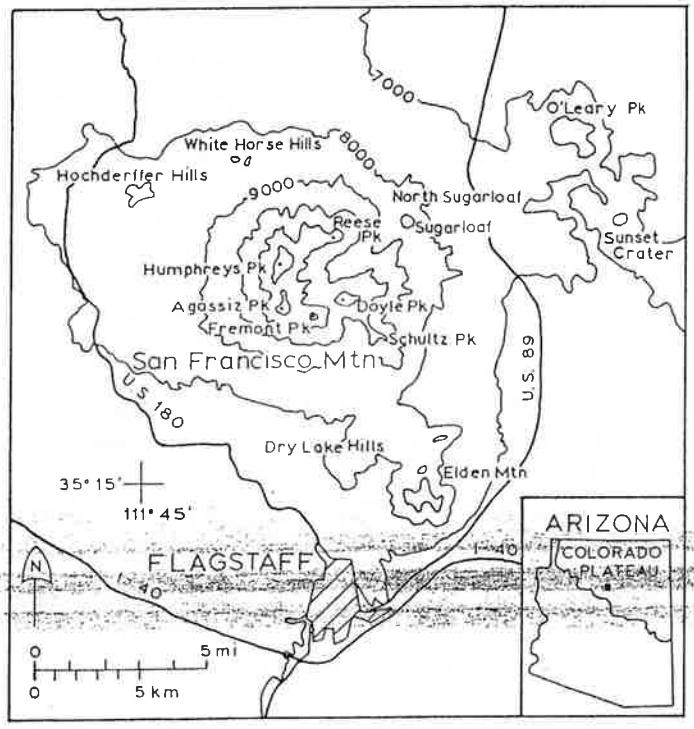

Figure 1. Index map of San Francisco Mountain. Contours are in feet above mean sea level.

Topographic maps available from the U.S. Geological Survey include the Humphreys Peak and Sunset Crater West quadrangles of the 7½-minute series (1:24,000), the San Francisco Mountain map at 1:50,000, and the Flagstaff, Arizona map of the 30- × 60-minute series (1:100,000); a planimetric map of the Coconino National Forest (scale ½-inch = 1 mile) is available from the U.S. Forest Service.

SIGNIFICANCE

Rising to an elevation of 12,633 ft (3,850 m), San Francisco Mountain is the most prominent geomorphic and volcanic structure in the San Francisco volcanic field, a late Miocene to Holocene volcanic province approximately 1,935 mi^2 (5,000 km^2) in area overlying eroded strata of Permian and locally Triassic age typical of the Colorado Plateau in northern Arizona. The volcanic field is dominated by basalt lava flows; more than 600 vents, basaltic to rhyolitic in composition, have been identified. Basaltic scoria cones are scattered throughout the field, whereas the intermediate-to-silicic rocks are localized in a few structurally controlled centers (Luedke and Smith, 1978). San Francisco Mountain, the only composite volcano in the southwestern part of the Colorado Plateau, displays well-preserved examples of a variety of features of volcanism and glaciation; a complete spectrum of lithologies from low-silica andesite to alkali rhyolite is present as lava flows, lava domes, pyroclastic deposits, and hypabyssal plutons. A large valley that breaches the core and northeast flank of the mountain provides exceptional exposures of the volcano's internal structure and stratigraphy, and affords relatively easy access to its interior.

VOLCANIC GEOLOGY

Morphology. In most profiles, San Francisco Mountain presents smooth, concave-up slopes that rise more than 3,900 ft (1,200 m) above the Colorado Plateau to culminate in several peaks over 11,100 ft (3,400 m) in elevation (Fig. 2). The individual peaks are erosional remnants of a compound composite volcano that predates the Inner Basin, a large bowl-shaped valley (caldera) that occupies the central part of the mountain. Nearly encircling the Inner Basin, the peaks form a horseshoe-shaped ridge open to the northeast where the Interior Valley breaches the mountain's flank. In plan, the volcano is slightly elliptical along a northeast-southwest axis parallel to the valley. The generally smooth slopes are interrupted locally where silicic domes were erupted low on the mountain's flanks; these include North Sugarloaf, Sugarloaf, and Schultz Peak. Centers of silicic domes peripheral to San Francisco Mountain are Hochderffer Hills, White Horse Hills, O'Leary Peak, Elden Mountain, and Dry Lake Hills.

Figure 2. Photograph of San Francisco Mountain viewed toward the southwest from O'Leary Peak. Humphreys Peak is the highest peak on the right, Agassiz Peak is in the middle, and Fremont Peak is on the left. The Interior Valley, Inner Basin, and Core Ridge are behind Sugarloaf, a small rhyolite dome in the middle distance with excavation scars on its lower slopes. North Sugarloaf underlies the treeless slope to the right of Sugarloaf.

San Francisco Mountain has the appearance of being extensively dissected, but calculations based on geologic mapping indicate that only about 7 percent of the original volume of the volcano has been removed. Most of the displaced material constitutes nine large debris fans that were deposited radially about the base of the volcano and contribute significantly to its classic profile. Fluvial erosion has cut deep ravines on the mountain's slopes, but the amount of material eroded is a very small part of the original mass (Robinson, 1913). Steep slopes and cliffs in the Inner Basin resulted largely from glacial erosion, and well-preserved cirques and moraines, along with other glacial features, are evident in the Inner Basin, Interior Valley, and in local areas on the outer slopes (Updike, 1977).

Occupying the southwest part of the Inner Basin is Core Ridge, together with a smaller ridge on its southeast side, trending northeast parallel to the Interior Valley. These ridges are formed by erosion-resistant hypabyssal plutons of the volcano's central conduit system.

Structure. San Francisco Mountain was constructed on a platform of late Miocene, and possibly younger, basalt lava flows that unconformably cover Paleozoic and Triassic strata. Basalt lavas and pyroclastic deposits from peripheral vents that were active during and after the growth of San Francisco Mountain locally interfinger with and overlie lavas and deposits erupted from the central volcano. Regional structures of the Colorado Plateau on northeast, north-south, and northwest trends controlled the locations and orientations of some vents, dikes, and peripheral silicic centers, and may even have influenced the location of San Francisco Mountain; the regional structures possibly contributed in the development of the Interior Valley as well.

Complexly related lava domes, radially outward-dipping lava-tuff sequences, and hypabyssal plutons comprise the composite volcano. Dacite and rhyolite domes that were buried by younger lavas and tuffs are exposed on the south and northeast sides of the Inner Basin, and partly buried dacite domes occur on the outer slopes of Humphreys, Fremont, and Doyle Peaks. A water well intersects a deeply buried rhyolite and obsidian dome on the lower west flank of Humphreys Peak. Stratified lavas and pyroclastic deposits of andesite and dacite form an impressive 3,300-ft (1,000-m)-thick section in the north wall of the Inner Basin below Humphreys Peak, and similar deposits form the upper slopes of the other major peaks. The absence of young lavas on Agassiz Peak imply that it is the eroded remnant of an early stratovolcano cone that blocked the southwestward flow of younger dacite and andesite lavas capping all of the other peaks and presumably erupted from central vents on a late stratovolcano cone constructed to the northeast of Agassiz.

Core Ridge and the adjacent ridge to the southeast consist of lava flows, tuffs, tuff breccias, flow breccias, intrusion breccias, breccia pipes, agglomerates, agglutinates, and small plutons that were deposited in and intruded into the central vent and conduit system of the volcano. Intracone dikes of andesite and dacite in the walls of the Inner Basin are arranged radially, converging on Core Ridge. Tuffisite dikes on the north side of the Inner Basin, a large, complex quartz monzodiorite dike along and near the crest of Core Ridge, and a large andesite dike in the valley between the two core ridges strike northeast parallel to the Interior Valley and appear to be related to regional structures beneath the volcano. Plugs of pyroxene diorite underlie the central part of the smaller core ridge.

Petrology. Volcanic rocks of San Francisco Mountain and its five peripheral silicic centers constitute a coherent and continuous suite of lithologies from low-silica andesite to alkali rhyolite (comendite); the suite forms a compositional continuum with hawaiite and transitional- to alkali-basalt lavas of the surrounding volcanic field (Fig. 3). The compositions of the rocks define a sodium-rich, mildly alkaline series. Correlations of phenocrysts with geochemical variation diagrams suggest that the lavas are related by processes of magmatic differentiation; this conclusion is supported by trace element studies (Wenrich-Verbeek, 1979), but field and petrographic observations demonstrate that crustal contamination and magma mixing also were involved in their origin, although only to minor extents. It is unlikely, however, that all of the lavas are comagmatic from a single magma chamber.

In San Francisco Mountain, the andesites are dark- to medium-gray lavas containing phenocrysts of plagioclase, augite, hypersthene, and olivine; pigeonite occurs locally and hornblende appears in medium- to high-silica andesites. The dacites are dark to light gray or pink, depending on the content of glass and degree of oxidation; commonly they carry phenocrysts of plagioclase, hypersthene, hornblende, biotite, and, in the low-silica dacites, augite. Some dacites, however, lack hydrous minerals, a few contain phenocrysts of quartz, and some have microphenocrysts of olivine. Rhyolites are light gray to light bluish-gray; locally they have lenses and bands of black obsidian. Characteristic pheno-

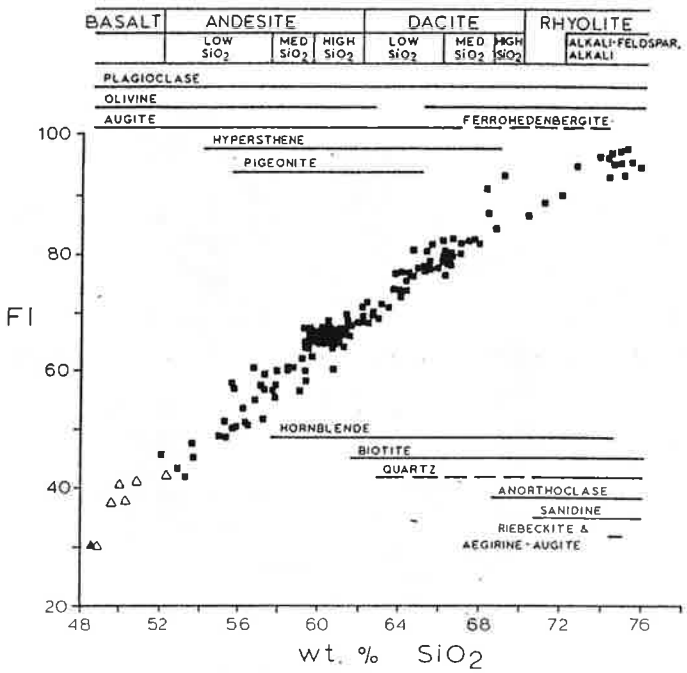

Figure 3. Silica vs. fractionation index (FI=Q + or + ab + ac + ns) for 169 chemical analyses of rocks from San Francisco Mountain, its peripheral silicic centers (squares), and seven basalts from the San Francisco volcanic field (triangles); the Bonito lava flow at Sunset Crater is identified with a filled triangle. Included are the ranges of phenocrysts and microphenocrysts relative to silica, and the petrographic classification of the rocks; dash lines indicate sparse occurrence.

Figure 4. Map of San Francisco Mountain showing distribution of rocks erupted during 5 stages of growth. Names of peaks are shown on Figure 1.

crysts and microphenocrysts in alkali-feldspar rhyolite are anorthoclase, quartz, sanidine, oligoclase-albite, biotite, hornblende, and locally olivine; alkali rhyolite, on the other hand, contains quartz, sanidine, aegirine-augite, riebeckite, and aenigmatite. Magnetite occurs throughout the suite as microphenocrysts.

Volcanic Development. The growth and development of San Francisco Mountain occurred during the late Pliocene and Pleistocene by the eruption of approximately 26 mi^3 (110 km^3) of lava and pyroclastic material. Estimated volumes of the lithologic types in the central volcano are andesite, 22 mi^3 (93 km^3), dacite, 3 mi^3 (13 km^3), and rhyolite, 0.24 mi^3 (1 km^3); erosion has removed 0.72 mi^3 (3 km^3) of unclassified rocks and 1.2 mi^3 (5 km^3) of identifiable units. The volume of andesite probably is overestimated and that of dacite and rhyolite underestimated because the buried portions of the volcano that could not be interpreted to be dacite or rhyolite were assumed to be andesite; nevertheless, the calculations indicate that San Francisco Mountain is an andesitic volcano. The explosive index of the volcano is about 20, suggesting that most of the magmas were relatively dry.

Reconstruction of the volcano's history is possible based on geologic mapping and K-Ar ages by P. E. Damon (written communication, 1977) and E. H. McKee (written communication, 1973). Five stages of growth that are characterized by distinctive styles of volcanism and lithologies are illustrated in Figure 4. Early in stage 1, lava domes of dacite (North Sugarloaf) and rhyolite (Inner Basin), 2.78 ± 0.13 Ma and 1.82 ± 0.16 Ma, respectively, were extruded after which an andesitic stratovolcano (about 12 mi^3) that rose over 5,600 ft (1,700 m) in height was constructed. The lavas and pyroclastic deposits of this early cone are exposed low only on the north and south sides of the Inner Basin, and at the north end of Schultz Peak where they were uplifted during stage 2. Stage 2 began with extrusion of rhyolite and dacite lava domes and flows; resumption of andesitic stratovolcano construction in stage 2 increased the volume to 23 mi^3 (95 km^3) and the height to about 6,900 ft (2,100 m). Agassiz Peak is an eroded remnant of the stage 2 cone, and an excellent section through its flank is well exposed in the steep slopes and cliffs on the north side of the Inner Basin; the entire section below Humphreys Peak has normal magnetic polarity and has been assigned to the Brunhes chronozone (T. Onstott, oral communication). In stage 3, the structure of the andesitic stratovolcano was disrupted, but 1 mi^3 (4 km^3) was added to its volume by a plinian eruption of rhyolite to dacite pumice and the emplacement of dacite lava domes on the northeast flank at Reese Peak and on the south flank between Doyle and Fremont Peaks. Stratovolcano construction during stage 4 shifted northeast relative to the stage 2 cone, and increased the volcano's height to 8,200 ft

(2,500 m) and its volume to about 26 mi^3 (108 km^3). Central eruptions produced stage 4 lavas of dacite and andesite that flowed down all flanks of the cone except toward the southwest where they were blocked by the stage 2 cone of Agassiz Peak. A flank eruption on the west slope of Agassiz Peak early in stage 4 extruded andesite lava similar in composition to lavas of stage 2. Parasitic eruptions of andesite and dacite lava flows on the northeast side during stage 5 added 0.5 mi^3 (2 km^3), but may have initiated events that led to the development of the Interior Valley that breaches the volcano's flank. Sugarloaf rhyolite dome, extruded 0.22 ± 0.02 m.y. ago in the mouth of the Interior Valley, concluded stage 5 and was the last known eruptive activity on San Francisco Mountain.

Origin of the Inner Basin and Interior Valley. The origin of the Inner Basin and Interior Valley has attracted interest for over 70 years (Robinson, 1913), and several processes have been suggested to account for their existence; these include: 1) erosion, 2) explosion, 3) collapse, with downward displacement, and 4) collapse, with outward displacement. Although all four mechanisms may have contributed, the latter is most consistent with available information. The distribution of stage 4 lavas indicates that San Francisco Mountain must have had a complete, if not perfectly symmetrical, cone by 0.43 ± 0.03 m.y. ago, the age of the youngest andesite lava flow on top of Humphreys Peak. The eruption of Sugarloaf dome in the mouth of the Interior Valley implies that it, as well as the Inner Basin, was in existence by 0.22 ± 0.02 m.y. ago, restricting their period of development to approximately 210,000 years.

Lavas and pyroclastic deposits that once formed the upper portion of the San Francisco Mountain composite volcano now reside in debris fans about its base (Fig. 5). The estimated volume of 1.1 mi^3 (4.4 km^3) in nine debris fans that were deposited distally and on the lower flanks of San Francisco Mountain plus 0.8 mi^3 (3.4 km^3) of debris buried by younger volcanic deposits northeast of the mountain compares very favorably with the 2 mi^3 (8.0 km^3) volume of the Inner Basin and Interior Valley (0.8 mi^3) and the restored cone (1.2 mi^3).

San Francisco Mountain still had a complete stratovolcano cone after early stage 5 parasitic eruptions of dacite on the northeast flank. Subsequent failure and collapse may have occurred after the cone became gravitationally unstable as a result of structural displacements due to magma intrusion and extrusion or tectonic faults in the volcano related to regional northeast-trending fractures in the platform below. Explosive eruptions or even an earthquake may have caused the unstable cone to collapse into debris avalanches and debris flows that formed the fans around the mountain's base. More than one collapse event is indicated by cuttings from a water well that penetrates a buried debris fan on Sunset Crater National Monument (Fig. 5); however, a late stage 5 dacite lava flow that partially covers the debris fan on the northeast side of the mountain implies that the Inner Basin originated in a fairly short period of time. Final sculpting of the volcano has been by glacial and ongoing fluvial processes.

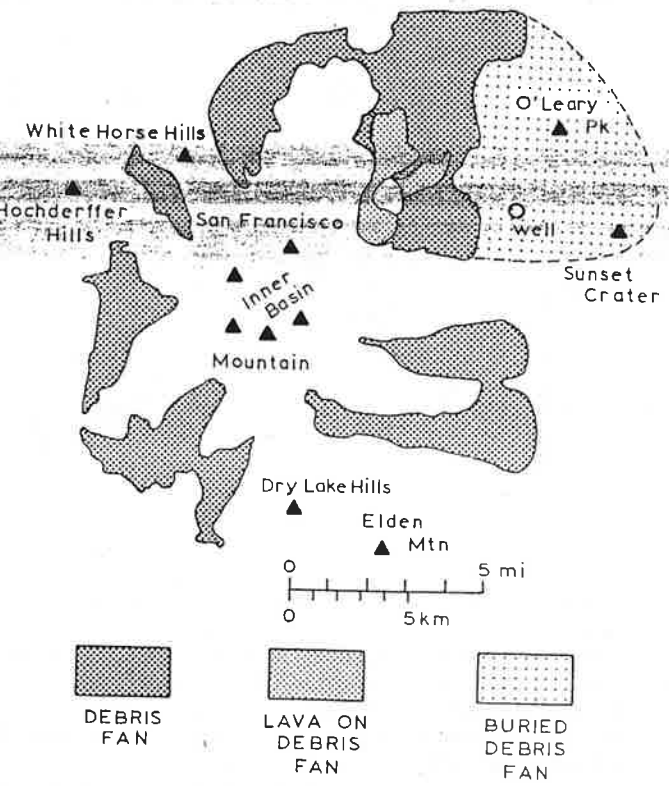

Figure 5. Map showing the distribution of debris fans around San Francisco Mountain; uncertain boundary is dashed. The water well that penetrates the buried debris fan is the Sunset Crater No. 2. (A-23-8) 21 aab 3.

REFERENCES CITED

Luedke, R. G., and Smith, R. L., 1978, Map showing distribution, composition, and age of late Cenozoic volcanic centers in Arizona and New Mexico: U.S. Geological Survey, Map I-1091-A, scale 1:1,000,000.

Robinson, H. H., 1913, The San Franciscan volcanic field, Arizona: U.S. Geological Survey, Professional Paper 76, 213 p.

Updike, R. G., 1977, The Geology of the San Francisco Peaks, Arizona [Ph.D. thesis]: Tempe, Arizona, Arizona State University, 423 p.

Wenrich-Verbeek, K. J., 1979, The petrogenesis and trace-element geochemistry of intermediate lavas from Humphreys Peak, San Francisco volcanic field, Arizona: Tectonophysics, v. 61, p. 103–129.

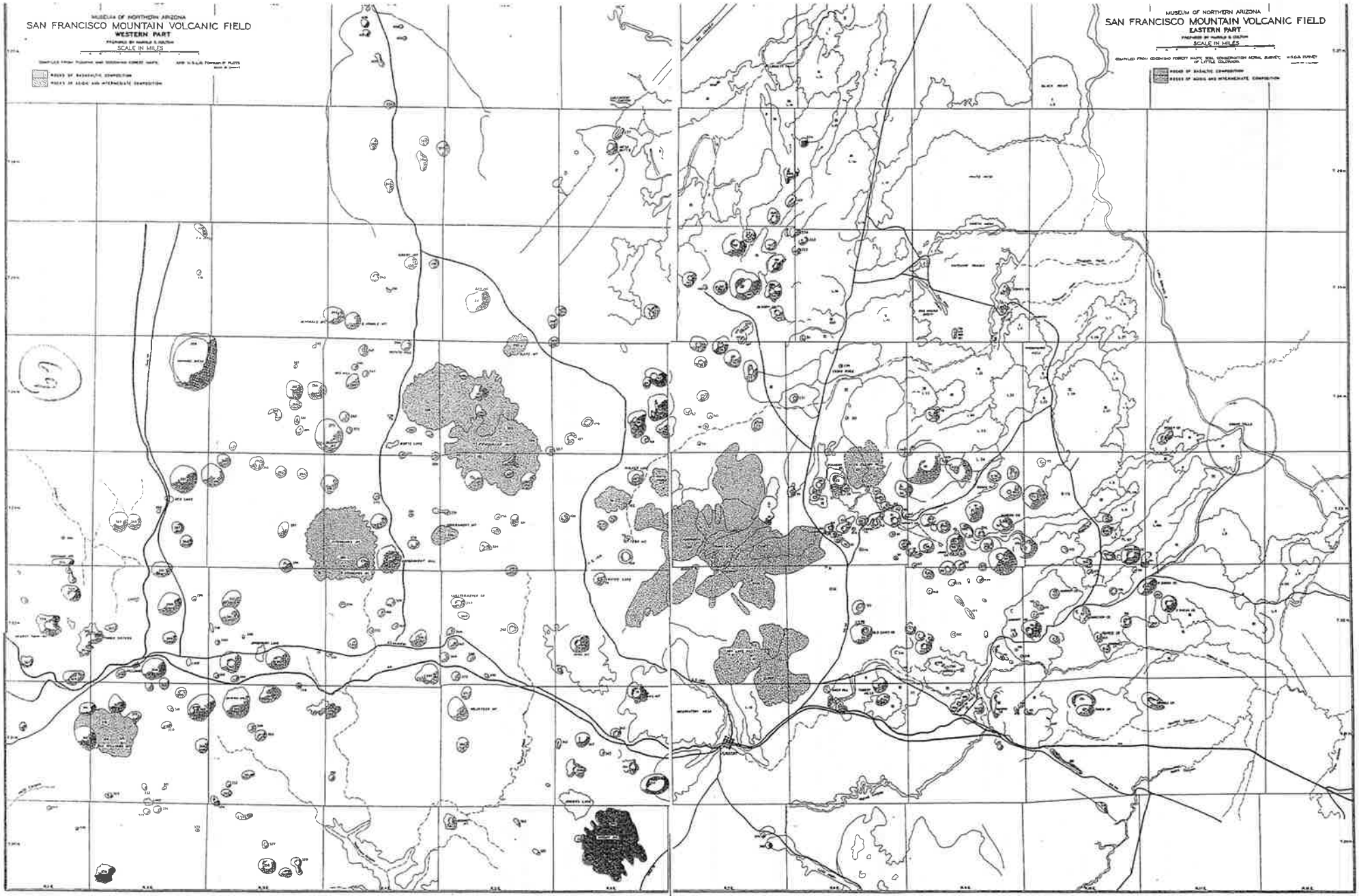
MUSEUM OF NORTHERN ARIZONA
SAN FRANCISCO MOUNTAIN VOLCANIC FIELD
WESTERN PART
SCALE IN MILES
MUSEUM OF NORTHERN ARIZONA
SAN FRANCISCO MOUNTAIN VOLCANIC FIELD
EASTERN PART
SCALE IN MILES

Lava River Cave

This mile-long lava tube cave was formed roughly 700,000 years ago by molten rock that erupted from a volcanic vent in nearby Hart Prairie. The top, sides and bottom of the flow cooled and solidified first, after which the insides of the lava river continued to flow emptying out the present cave.

Ample evidence of how the tube was born is written in the rocks of which it is formed. Small wave-like undulations in the floor are the remains of ripples frozen in the last trickle of molten rock that flowed from the cave. Stone icicles hanging from the ceiling show where a final blast of volcanic heat caused the rock to partially re-liquefy and drip.

Dress appropriately when you come to visit, with warm clothes and sturdy shoes. The cave is as cool as 42° even in summer, and you may even find some ice inside. The rocks are always sharp and slippery, too. Bring two or three sources of light, in case one happens to fail, it can be very dark one mile from the nearest light source.

Portions of the cave which were defaced by graffiti, have been recently cleaned up. Today's more environmentally aware visitors take better care of such a unique resource and report vandals when they see them.

Location: About 14 miles north of Flagstaff on paved highways and graveled Forest Roads. Travel time is about 45 minutes.

Access: Drive 9 miles north of Flagstaff on US 180 and turn west (left) on FR 245 (at milepost 230). Continue 3 miles to FR 171 and turn south 1 mile to where FR 171B turns left a short distance to Lava River Cave.

Season: You can visit Lava River Cave the year-round though you may need to ski to it in winter. Temperatures inside the cave remain roughly the same summer and winter. (between 35° and 45° Fahrenheit).

Attractions: Cool cave, Lava flow, Scenic drive, Wildlife viewing

Facilities: Interpretive sign

Notes:
Wear warm clothes and sturdy shoes.
Bring two or three light sources
Please don't deface cave surfaces, but do report anyone who does. Call 526-0600.

For more information contact:
Peaks Ranger Station, 5075 N. Highway 89, Flagstaff, Arizona 86004, (928) 526-0866

70

LAVA RIVER CAVE

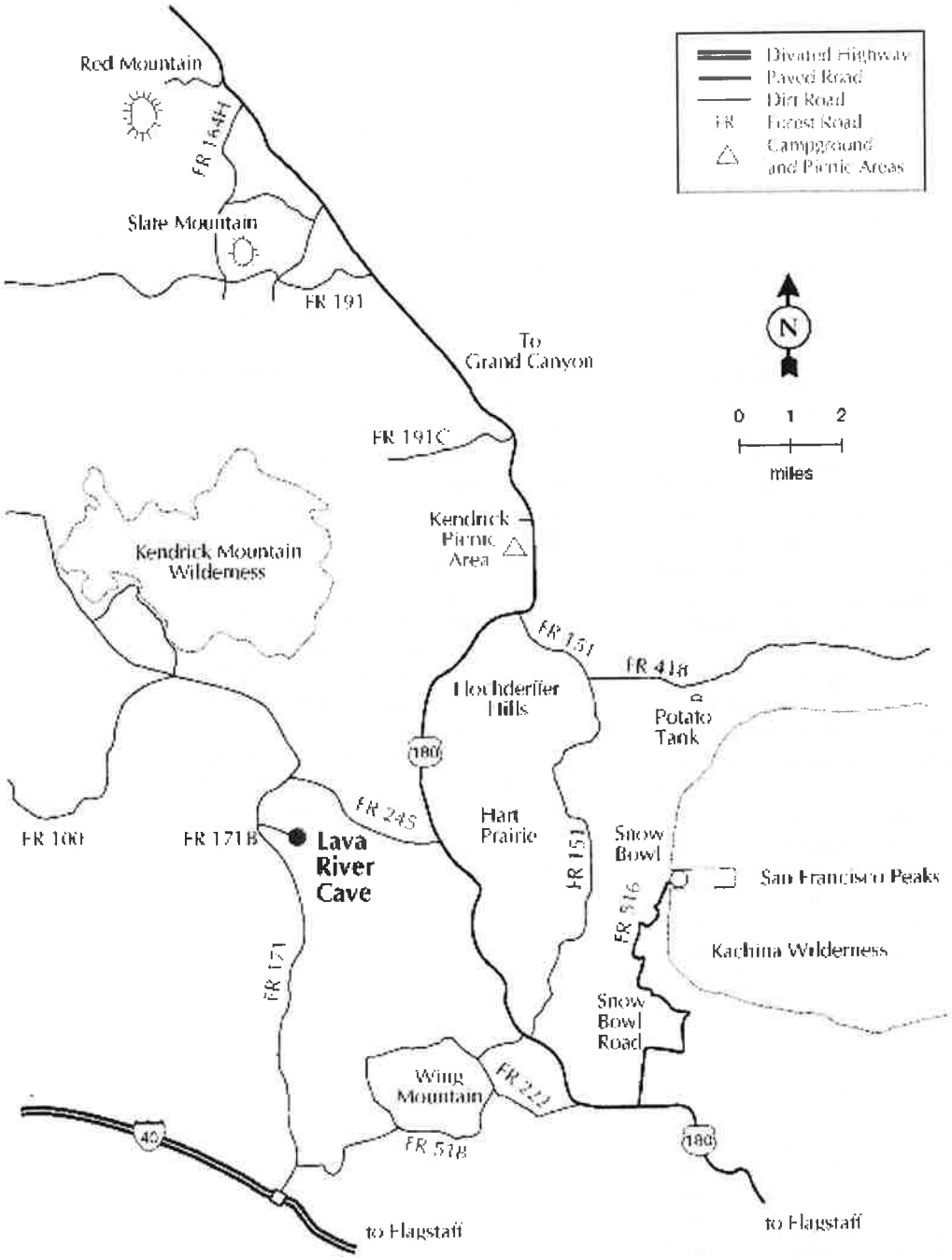

71

Meteor Crater, Arizona: Geology and Cultural History

Jeffrey S. Kargel *U.S. Geological Survey, Astrogeology Team, 2255 N. Gemini Dr., Flagstaff, AZ 86001*

Of all impact craters on Earth larger than 1 km across, Meteor Crater is the youngest and best preserved. Meteor Crater is a classic bowl-shaped "simple crater," similar in structure to craters of a similar size on the Moon, Mars, and other planetary bodies. It was formed 49,000 years ago in the layered sedimentary succession of the southern Colorado Plateau by the impact, at around 15 km per second, of an iron-nickel asteroid perhaps 50 meters across. The kinetic energy released by the impact was equivalent to that of a massive hydrogen bomb with a yield somewhere between 20 and 40 megatons of TNT. The most dramatic result was of course the crater, 1200 meters across, formed by the vaporization, melting, fragmentation, and ejection of the sedimentary formations. Besides the crater, a variety of geologic evidence testifies to the enormous shock effects produced by this impact. Quartz was transformed into shocked polymorphs, including coesite and stishovite. Impact melting and admixture of silicate material with molten droplets of partly oxidized meteoritic metal yielded geochemically peculiar magnetic melt lapilli, which later rained onto the surface of the ejecta blanket. Eugene Shoemaker showed that the ejecta itself is a stratigraphically inverted sequence of rubble derived from the three major rock formations penetrated by the bolide. The interior wall of the crater exhibits sharply uplifted (folded and faulted) strata, where the beds dip radially away from the center of the crater, caused by the continuous release of energy along the path of the penetrating mass.

As interesting as the crater itself are the physical remains of the efforts by Daniel M. Barringer, at the turn of this century, to exploit buried meteoritic material for its commercial value of contained nickel and platinum. Some have called Barringer's efforts heroic, others consider him to have been stubborn. In fact he was both - Barringer was the first human to attempt the mining of an asteroid, albeit one that had experienced its final planetary encounter. Barringer failed in his attempt for lack of full appreciation of the violence and energy of the impact event and the consequences for the integrity of the meteor - most of the impacting mass vaporized, melted, and/or was blown to smithereens in solid form. And so, all we have of the original bolide are relatively small fragments of the Canyon Diablo meteorite and microscopic metallic inclusions embedded within impactite glass. What remains of Barringer's efforts are his writings and correspondence with others, and his mine shafts, tailings, drill stems, and other artifacts.

Meteor Crater is about 65 km (40 miles) east of Flagstaff, Arizona, 10 km south of Interstate 40, on private land owned by the Barringer family. The crater's north rim is accessible by paved road. This 6-7-hour field excursion (including transit time to the crater) will start and stop at the Visitors' Center and take participants by foot completely around the rim on a crude trail, a short distance below the rim (off trail), and onto the ejecta blanket (off trail). A series of stops will allow participants to inspect geological features and historical cultural artifacts, both in situ and from the vantage of a museum at the Visitors' Center. Participants should bring sun screen, a hat, hiking boots or sturdy tennis shoes, a water bottle, and of course a camera with film! A simple box lunch, transportation between Flagstaff and the crater, and free admission will be provided.

72

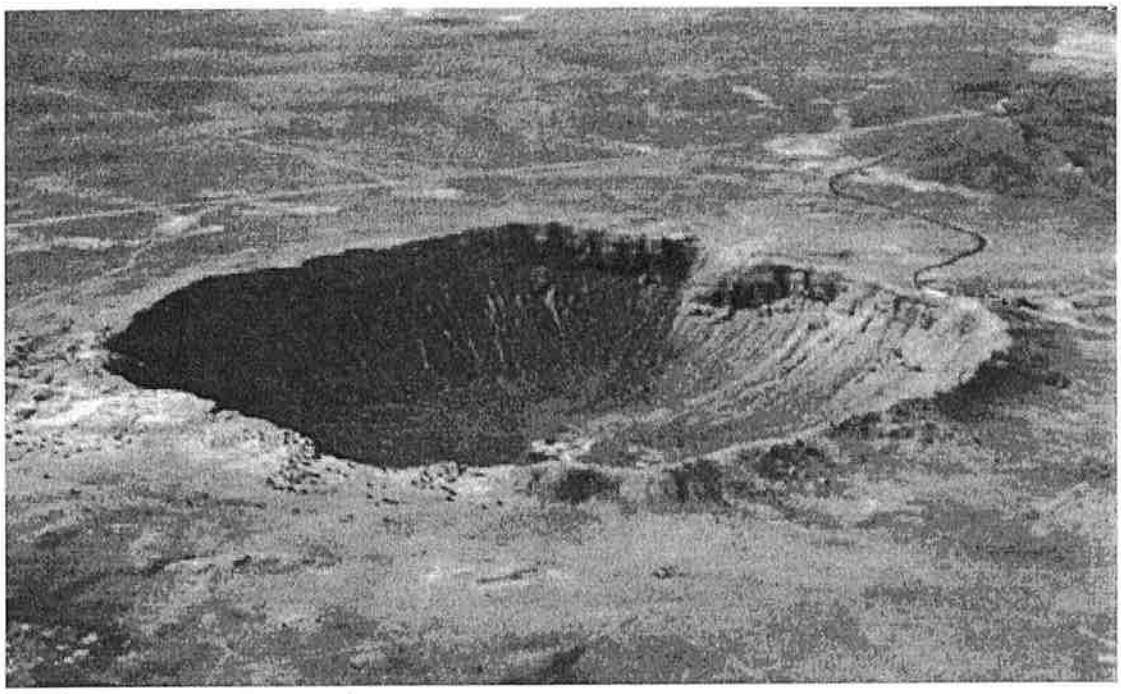

Barringer Meteor Crater, Arizona

Meteor Crater is one of the youngest and best-preserved impact craters on Earth. The crater formed roughly 50,000 years ago when a 50-meter-wide iron-rich meteor weighing 100,000 tons struck the Arizona desert at an estimated 20 kilometers per second. The resulting explosion exceeded the combined force of today's nuclear arsenals and created a 1.1-kilometer-wide, 200-meter-deep crater. Meteor Crater is a simple crater since it has no central peak or rim terraces. The crater formed in layered sedimentary rocks, some of which are exposed in the nearby Grand Canyon. These rocks have been uplifted and in some cases overturned at the crater's raised rim. Debris sliding and subsequent erosion have partially filled the bottom of the crater with minor amounts of rim material and sediment.

The heavily cratered history of the Moon indicates that Earth also experienced many impact events early in its history. The processes of erosion and plate tectonics have combined to erase nearly all Earth's craters. To date, only about 150 impact craters have been identified on Earth, and most of those are severely eroded or buried by later rock units. This aerial view shows the dramatic expression of the crater in the arid landscape.

- **Credit: D. Roddy, U.S. Geological Survey**

and these scattered across the plains to the west.

At the moment of impact, a shock wave was generated downward into the rock and upward through the meteorite. The crater produced was small at first, about the size of the meteorite itself. The meteorite and impacted rock were subjected to enormous pressures at the instant

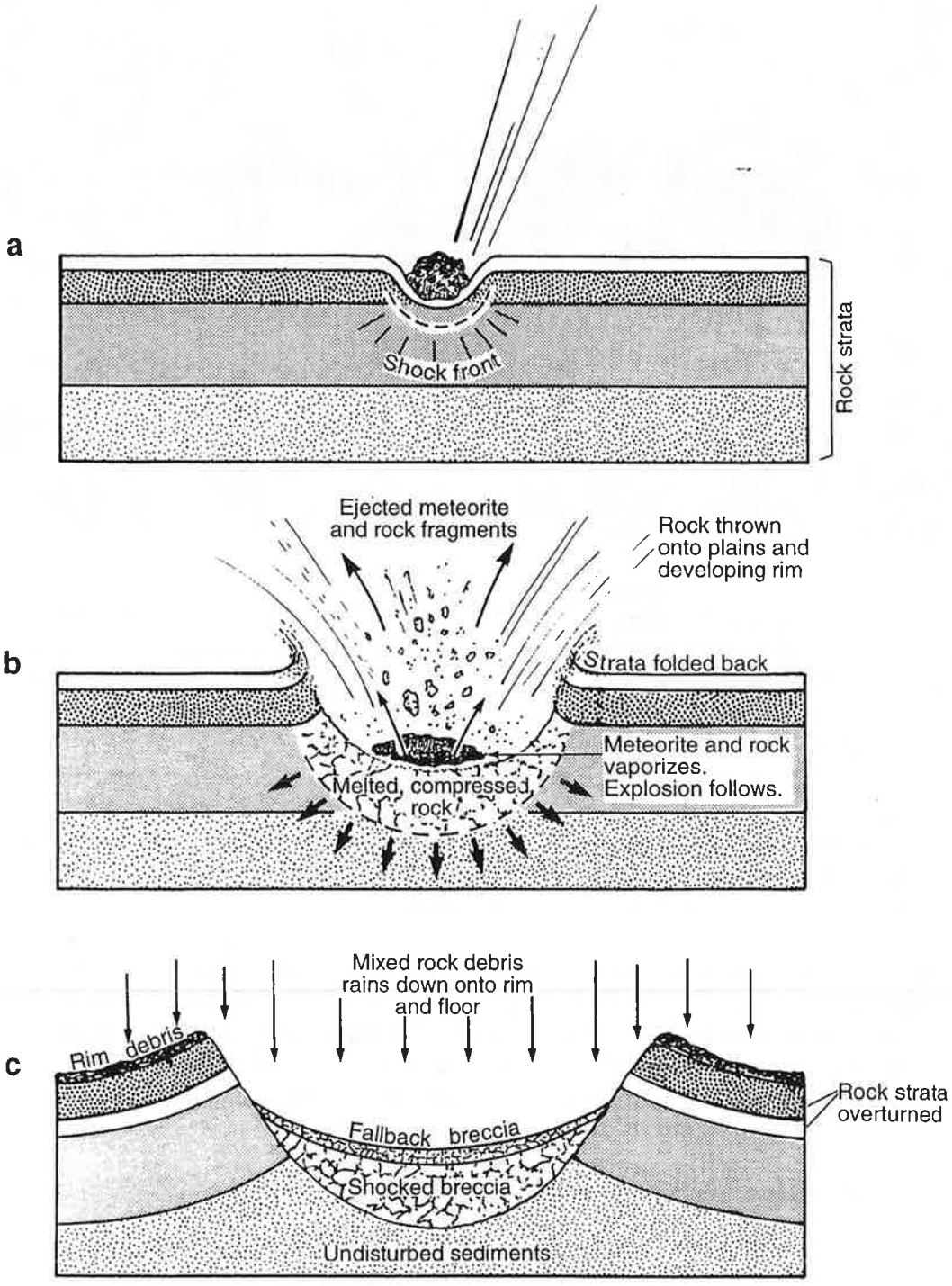

Sequential stages leading to the formation of Meteor Crater. a: Meteorite penetrates surface and sends shock wave through rock layers. b: Decompression wave displaces rock outward onto rim and plains. Shock wave traveling from front to back of meteorite expels meteorite fragments. Remaining meteorite explosively vaporizes. c: Rock and meteorite debris from dust cloud rain down on crater and surrounding plain.

74

desert that existed long before the sea covered the area in the late Permian period. Its thickness is more than 700 feet at the crater, placing the Coconino beds both in the crater walls and beneath its floor. This rock layer is broken into a breccia hundreds of feet below the crater floor, attesting to the shock of impact.

Finally, beneath the Coconino lie undisturbed red shales of the Supai group, marking the end of the impact-modified layers. The modification and rearrangement of these layers provided Barringer with the evidence he needed to prove the crater meteoritic.

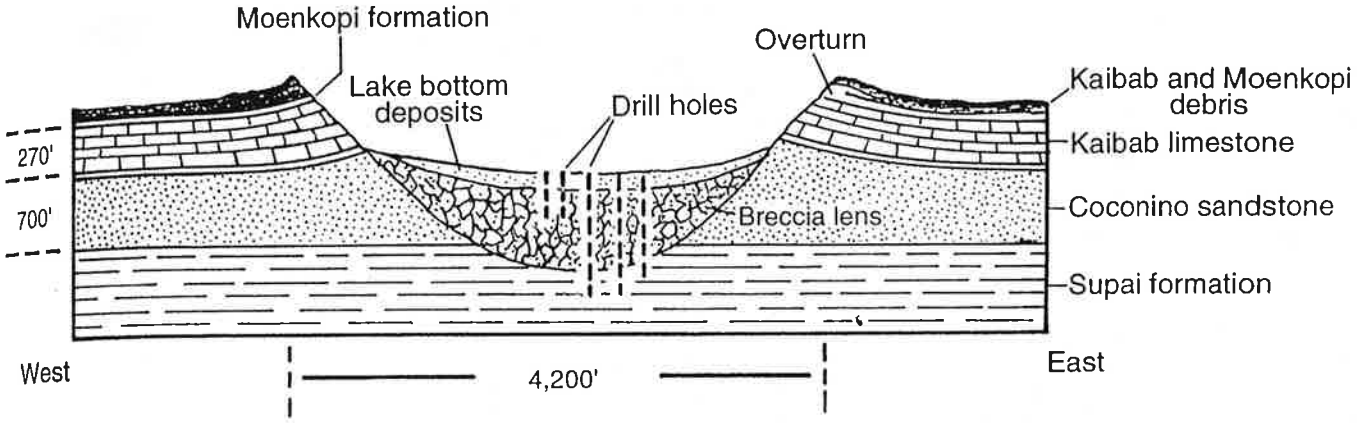

Cross section of Meteor Crater looking north shows the rock layers into which the crater intruded. Rock on the rim has been overturned, appearing in reverse order.

75

Drilling Operations

Barringer's first visit in 1905 was in earnest. He came prepared to determine the crater's origin. He drilled a total of twenty-eight test holes in the center. The cores showed that the rock had been badly fractured and pulverized to a fine powder, presumably by a crushing impact and explosion. He recognized that the "rock flour," as he called it, was actually Coconino sandstone. The grains of silica sand had been finely pulverized.

Bits of meteoritic iron oxide containing nickel were brought up from a depth of nearly 500 feet, from the pulverized layer. Undisturbed strata were finally encountered at about 1,300 feet.

Huge blocks of Kaibab limestone were lifted out of the crater as it was forming at the time of impact and were deposited on the rim and around the plains. Meteorites were found under the rim debris and beneath large boulders on the plain, proving that the meteorites landed at the same time the crater formed. Also, distribution of the meteorites

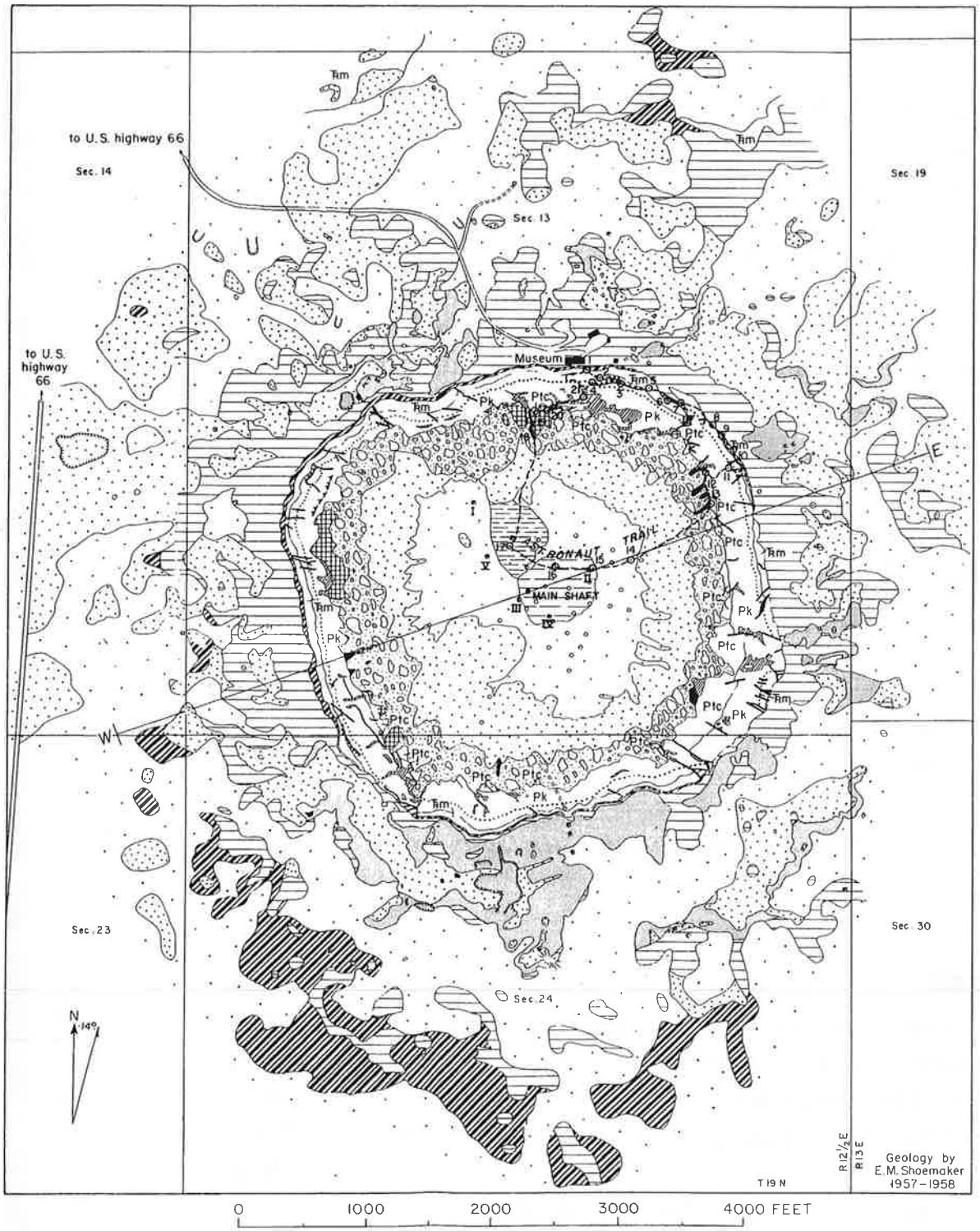

EXPLANATION

Recent
- Alluvium
- Playa beds

UNCONFORMITY

Pleistocene
- Alluvium
- Lake beds
- Talus

UNCONFORMITY

- Mixed debris from Coconino, Toroweap, Kaibab, and Moenkopi formations; includes lechatelierite and meteoritic material
- Debris from Coconino sandstone and Toroweap formation
- Debris from Kaibab limestone
- Debris from Moenkopi formation

QUATERNARY

UNCONFORMITY

- Trm — Moenkopi formation

TRIASSIC

UNCONFORMITY

- Pk — Kaibab limestone; dotted line is sandstone bed
- Ptc — Toroweap formation and Coconino sandstone

PERMIAN

- Contact
- Faults, nearly vertical or normal
- Thrust fault; teeth are on side of upper plate
- Authigenic breccia; fragments not mixed; occurs mostly along faults
- Allogenic breccia; fragments mixed, includes lechatelierite and meteoritic material
- Shaft
- Adit
- Pit
- Dump
- Drill hole

GEOLOGIC MAP OF METEOR CRATER, ARIZONA

76

MAP SHOWING DISTRIBUTION OF METEORIC MATERIAL AROUND METEOR CRATER COCONINO CO. ARIZONA.

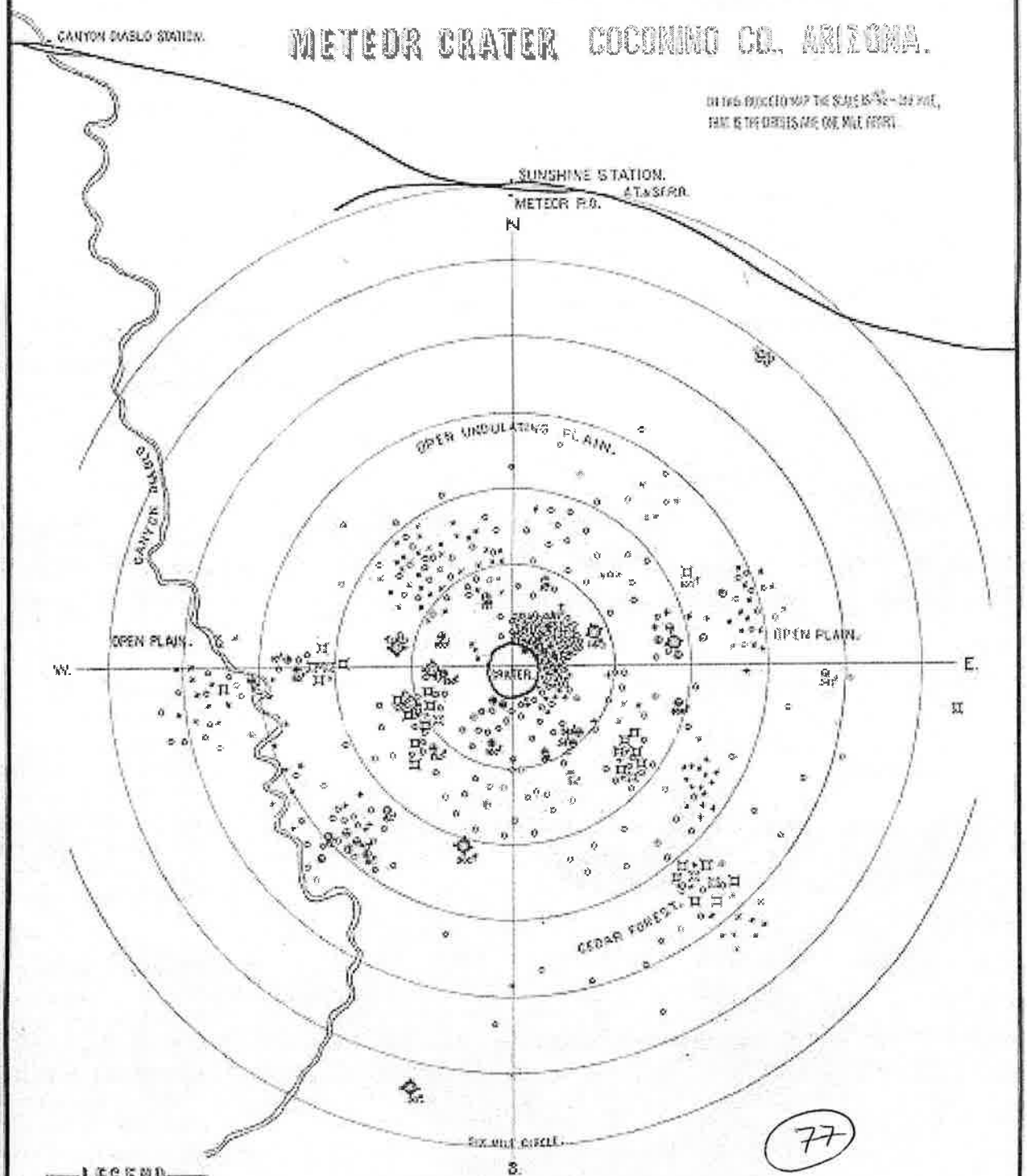

77

—LEGEND—

- ⊕ METEORIC IRONS (ORDINARY CANYON DIABLO SIDERITES) FROM 1/2 LB. TO 347 LBS. DISCOVERED BY STANDARD IRON COMPANY.
- ✧ " " FROM 10 LBS. TO 1010 LBS. DISCOVERED BY NEGROES EMPLOYED BY D.M. WOLZ ET AL. PREVIOUS TO ACQUISITION OF PROPERTY BY S.I.CO
- + " " SMALL. DISCOVERED BY S.I.CO. THOUSANDS OF THE SMALL IRONS FOUND. HENCE DISTRIBUTION ONLY APPROXIMATED. (THESE ARE GENERALLY ONLY A FEW GRAINS OR OUNCES IN WEIGHT, IRONS WEIGHING FROM ONE TO TEN POUNDS FOUND ONLY OCCASIONALLY.)
- ◈ LARGE IRREGULAR MASSES OF METEORIC IRON KNOWN AS LARGE "SHALE BALLS" FROM 100 LBS. TO 300 LBS. IN WEIGHT, DUE TO INCLUSION OF METEORIC IRON RICH IN CHLORINE AND SULPHUR OR SHALE BALL IRON.
- ▷ SMALL BROKEN FRAGMENTS OF METEORIC IRON KNOWN AS "IRON SHALE" (A FEW GRAINS OR OUNCES, RARELY A POUND IN WEIGHT.) THOUSANDS OF SUCH PIECES FOUND. HENCE DISTRIBUTION ONLY APPROXIMATED.

SURVEYED BY [illegible] NOVEMBER 1910

used melt and vapor scaling law is:

$$\frac{\text{mass of melt}}{\text{mass of projectile}} = 0.14\,\frac{v_i^2}{\epsilon_m} \text{ for } v_i \geq 12 \text{ km s}^{-1}$$

and

$$\frac{\text{mass of vapor}}{\text{mass of projectile}} = 0.4\,\frac{v_i^2}{\epsilon_v} \text{ for } v_i \geq 35 \text{ km s}^{-1}$$

where $\epsilon_m = 3.4 \times 10^6$ J kg^{-1} is the specific energy of melting and $\epsilon_v = 5.7 \times 10^7$ J kg^{-1} is the specific energy of vaporization of silicate rocks.

Since the masses melted and vaporized are independent of surface gravity, while the transient crater diameter decreases as gravity increases, the relative volume of melt to material excavated increases with increasing crater diameter, as shown in Figure I11. Very large craters may differ substantially in morphology from small ones because of this difference in relative melt volume. Similarly, craters

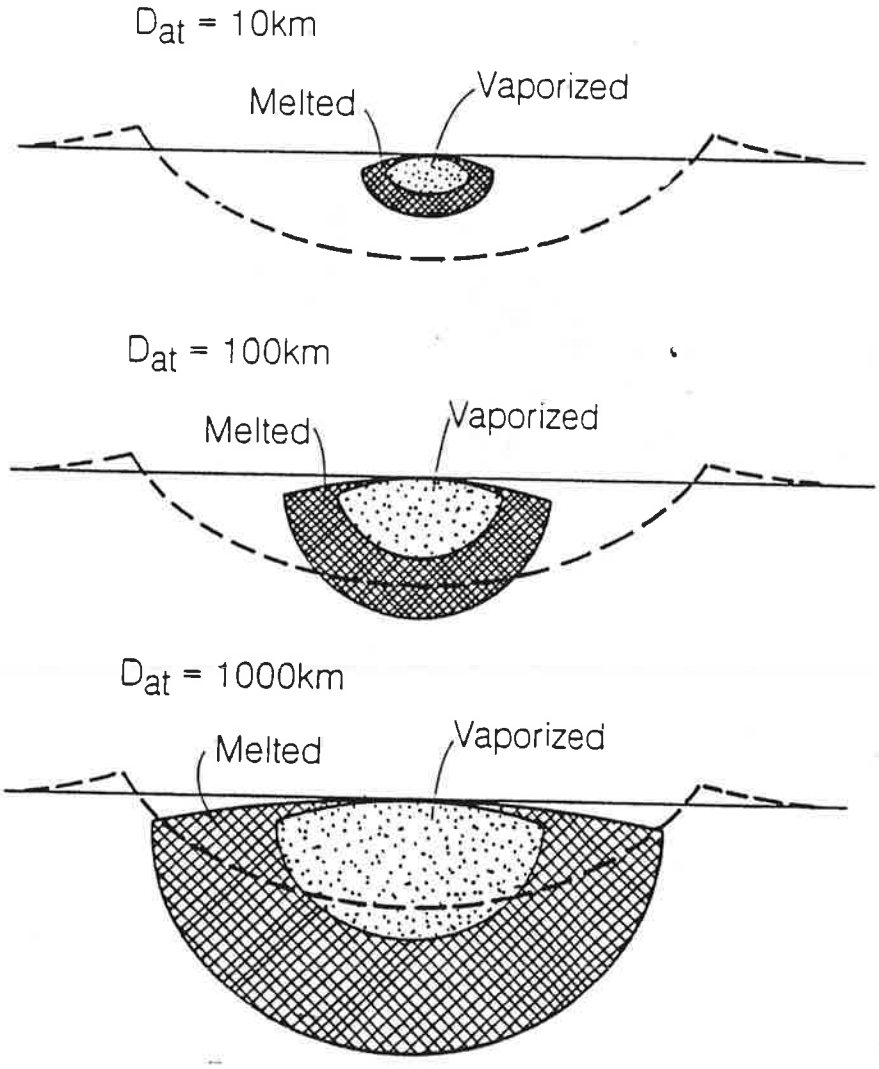

Figure I11 The different scaling laws for crater diameter and melt or vapor volume imply that as the crater diameter increases, the volume of melted or vaporized material may approach the volume of the crater itself. This figure is constructed for impacts at 35 km s^{-1} on the Earth.

kilometers per second. At s
objects were disruptive, wh
gravitational binding energy
struck them. Infalling planet
to the growing planets. In th
ure inside a growing planet inc
at the center to large values a
collision velocity as the plar
now seems probable that th
population was more evenly g
and that each growing plan
collisions with bodies up to
Such catastrophic collisions de
impacted body, wiping out ar
with increasing radius and m
planets rather stochastic (Me

The origin of the Moon is no
proto-Earth and a Mars-size
4.5×10^9 years ago. This the
classic theories of lunar origi
because only the giant impac
for the Moon's chemistry, as
Apollo. One view of this proce
(by jetting) a large quantity of
comparable quantity of the pr
projectile merged with the E
Earth: if the Earth was not
certainly was afterward), one
into dust in stable Keplerian
accumulated together to form t

Sometime after the Moon for
ago the inner planets and the
heavy bombardment', an era
orders of magnitude larger tha
period are preserved in the
terrains of Mars and Mercury.
age data from Apollo samples
cumulative crater density thro

$$N_{cum}(D > 4 \text{ km}) = 2.68 \times$$

where $N_{cum}(D > 4$ km) is the cur
of craters larger than 4 km diar
($T = 0$ is the present) and λ
different fits to the same data h
The current cratering rate on
with $D > 4$ km km^{-2} year^{-1}. O
estimated to be about 1.8×10
year^{-1}, which is comparable to t
different minimum sizes, sinc
$N_{cum}(D) \sim D^{-1.8}$. There is curre
ing rates, which might be uncert

The study of relative crater
planetary surfaces provides an i
ages of surface features. Since
occur randomly on a surface (
trailing edge cratering rate asyn
of the giant planets), the spati
information. However, older su